Structure-based discovery of a non-canonical prototype long-chain monoacylglycerol lipase through an endogenous catalysis intermediate complex

Nikos Pinotsis[1,#], Anna Krüger[2,#] , Nicolas Tomas[3], Spyros D Chatziefthymiou[1], Claudia Litz[1], Simon Arnold Mortensen[1], Mamadou Daffé[3], Hedia Marrakchi[3], Garabed Antranikian[2] and Matthias Wilmanns[1,4*]

[1] European Molecular Biology Laboratory, Hamburg Unit, Notkestrasse 85, 22607 Hamburg, Germany

[2] Hamburg University of Technology, Kasernenstrasse 12, 21073 Hamburg, Germany

[3] Institut de Pharmacologie et de Biologie Structurale, IPBS, Université de Toulouse, CNRS, UPS, Toulouse, France

[4] University Hamburg Clinical Center Hamburg-Eppendorf, Martinistrasse 52, 20251 Hamburg, Germany

[#] Equal contribution

ABSTRACT

The identification and characterization of enzyme function is lacking behind the rapidly increasing availability of large numbers of sequences and associated high-resolution structures. This often hampered by lack of knowledge on *in vivo* relevant substrates. Here, we present a case study where the high-resolution structure of an unusual orphan lipase in complex with an endogenous C18 monoacyl catalysis intermediate allowed its functional characterization as long-chain monacylglycerol lipase. Different from most other lipases, this enzyme uses a minimal helix–β-hairpin–helix lid domain that positions the substrate through a hydrophobic tunnel directly to the enzyme's active site. Knowledge about the molecular details of the substrate binding site and hydrolysis allowed us to boost the enzymatic activity by adjusting protein/substrate interactions. This enzyme serves as a prototype for non-conventional esterases and lipases that share similar helix–β-hairpin–helix lid domains of variable size. Taken together, our data provide crucial insight to advance our knowledge of unusual esterases and lipases, facilitating future biotechnology applications.

INTRODUCTION

The annotation of relevant enzyme function under physiological conditions remains a major challenge, despite the availability of millions of protein sequences and experimentally determined or predicted molecular structures associated with them [1-2]. Enzymes often have different and broader substrate profiles within their natural cellular environment than experimentally accessible under *in vitro* conditions or by using purified protein samples. Hence, albeit powerful tools have been developed to predict enzymatic function, options to prove them *in vivo* remain limited [3-8]. High-resolution structural biology allows the direct visualization of enzyme-ligand complexes at atomic detail and thus presents a highly attractive tool for enzyme function discovery, but it requires the availability of pure compounds for structural analysis. Alternatively, enzyme structures could also be determined in the presence of endogenous substrates or catalysis intermediates taken up from their cellular environment for direct evidence of enzyme-substrate relationships, but successful instances have remained rare to date [9]. This requires conditions where substrate turnover is inhibited by genetic modification of enzyme targets or experimental conditions that lead to lack of catalytic activity. In this study, we demonstrate the power of an endogenous catalysis intermediate uptake for structural and subsequent functional characterization of an orphan enzyme with putative lipase/esterase activity, which otherwise would not have been accessible due to lack of solubility.

Lipases are enzymes that reversibly catalyze the hydrolysis and synthesis of a large variety of glycerol esters [10-12]. Knowledge about these enzymes has allowed the development of numerous lipase-catalyzed processes in medical biotechnology, detergent industry, organic synthesis, biodiesel production, agrochemical industry, flavor and aroma industry, and food production [13-15]. In contrast to many other carboxyl ester hydrolases, lipases are active mainly at water-lipid interfaces, a process known as interfacial activation [16-17]. In essence, long-chain glycerol esters are delivered in non-monomeric emulsions rather than water-soluble substrates. Interfacial activation of lipases is thought to require an additional α-helical domain referred to as “lid” that contains several hydrophilic residues in the vicinity of the active site [18]. In contrast to the catalytic domain (CD), there is only little sequence conservation of the lid. Available structural data on lipases show highly diverse lid topology and structure, suggesting variable mechanisms to promote active site opening for access of acyl substrates and rendering precise prediction of enzymatic substrate specificity challenging [19-21].Lipases from extremophilic microorganisms are of superior interest for applications in industrial processes since demanding conditions such as high temperature or high salt concentration do not impair their activity [22-24].

Most of the previous molecular activity studies have been limited to isolated or recombinant lipases. Given that quantitative lipase activity measurements are generally hampered by the limited solubility of long-chain glycerol esters under those experimental conditions it is plausible to assume that the substrate profile differs under cellular conditions.

Based on turnover measurements with a broad spectrum of substrates, an enzyme from the thermophilic anaerobic bacterium *Thermoanaerobacter thermohydrosulfuricus (Tth)* was tentatively assigned as a lipase [25]. As this enzyme revealed a remarkable level of robustness against a variety of solvents and temperatures, it represents an attractive target for potential biotechnology applications. However, underlying molecular mechanisms explaining the enzyme's activity properties and substrate promiscuity remained unknown, defining the aim of this study. Structure determination of the enzyme revealed an unexpected long-chain C18 monoacyl ester intermediate bound to the active site, which was taken up from its expression host. Its distal part is embedded by a tunnel formed by an unconventional lid domain with minimal α-helix-β-hairpin-α-helix (HBH) topology. In cell extracts that overexpress the enzyme, we found high levels of C16/18 fatty acid (FA) products, in agreement with our structural data, demonstrating that the *Tth* enzyme functions as a long-chain monoacylglycerol lipase (MGL). *Tth* MGL prototypes a new lipase/esterase family with HBH lid domains comprising sequences inserted into the HBH β-hairpin that are highly divergent in length and structure. Our findings demonstrate a powerful example of using high-resolution structural biology where complex formation with an endogenous catalysis intermediate has become achievable to elucidate its function.

EXPERIMENTAL SECTION

Tth MGL was expressed in E. *coli* and purified for biochemical, biophysical and structural characterization. Enzymatic activity was determined by monitoring cleavage of p-nitrophenyl monoacyl esters using Michaelis-Menten kinetics. Cellular *Tth* MGL activity was determined by analysis of *E. coli* lipid cell extracts. The biophysical properties of *Tth* ML were characterized by nano differential scanning fluorimetry and circular dichroism. *Tth* MGL was crystallized in the presence and absence of PMSF, and the respective structures were determined by X-ray crystallography. *Tth* MGL crystal content was analyzed by MALDI–TOF mass spectrometry. Further details are found in the Supplement.

RESULTS AND DISCUSSION

The Tth MGL structure reveals an α/β hydrolase fold with a minimal helix–β-hairpin–helix lid domain.

To provide insight into the *Tth* MGL active-site topography and shed light on its unique substrate promiscuity, we characterized the enzyme structurally and functionally. Purified *Tth* MGL elutes as a dimer (Figure 1A). Its fold melting temperature measured by nano differential scanning fluorimetry (nanoDSF) is at 77°C, which is within expectation in light of the thermophilic origin of *Tth* (Figure 1B, Supplementary Table S1). Next, we determined its high-resolution crystal structure, both in the presence and absence of the covalent active site serine protease inhibitor phenylmethylsulfonyl fluoride (PMSF) (Figures 2-3, Supplementary Table S2). The overall fold of *Tth* MGL can also be reliably modeled using the AlphaFold2 and MMseqs2 package (Supplementary Figure S1) [26-27]. However, as there are significant differences in the areas of the bound ligands and the dimeric interface, in the remaining contribution we refer to our experimental structures only.

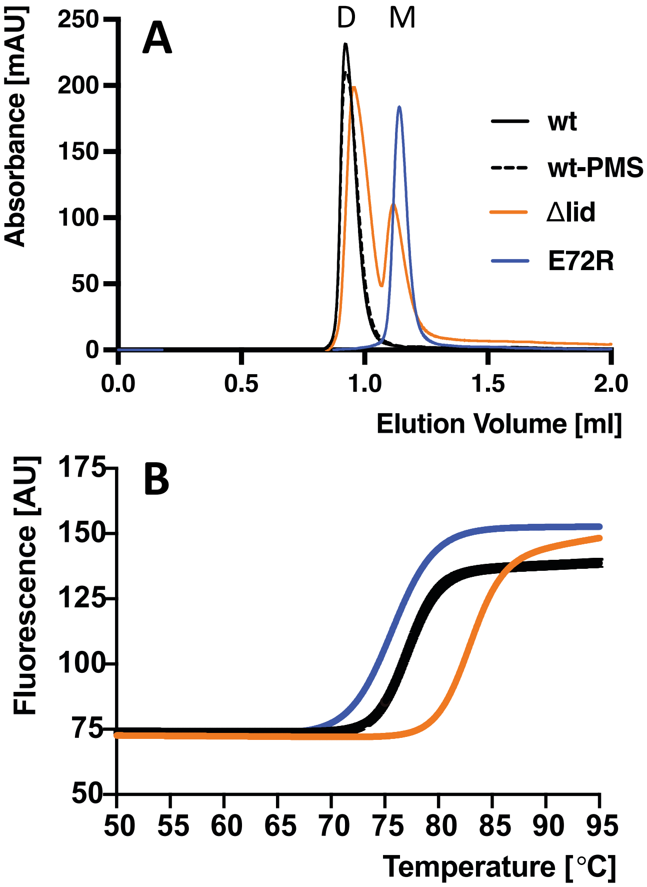

Figure 1. Biophysical of *Tth* MGL. A, Size exclusion chromatograms indicating dimeric (D) and monomeric (M) fractions and B, nano differential scanning fluorimetry profiles of selected *Tth* MGL variants. For further analysis, see Supplementary Table S1.

Both *Tth* MGL structures – the active and phenylmethylsulfonyl (PMS)-inhibited – reveal a two-fold symmetric dimer, in agreement with its dimeric assembly in solution (Figure 1A & Figure 2). The *Tth* MGL dimer is formed by an almost flat interface area which represents about 10 % of the total solvent accessible area (Figure 2D). The interface is established through an intricate network of charged interactions involving residues from both domains, with the majority of the interactions originating from residues of the CD (Figure 2B & D, Supplementary Figure S2). It forms a large cleft that connects the two active sites of the two protomers (Figure 2C). Converting the charge of one of the most central interface residues (E72R) renders a monomeric version of the protein, confirming that the interface observed in the structure is relevant (Figure 1A).

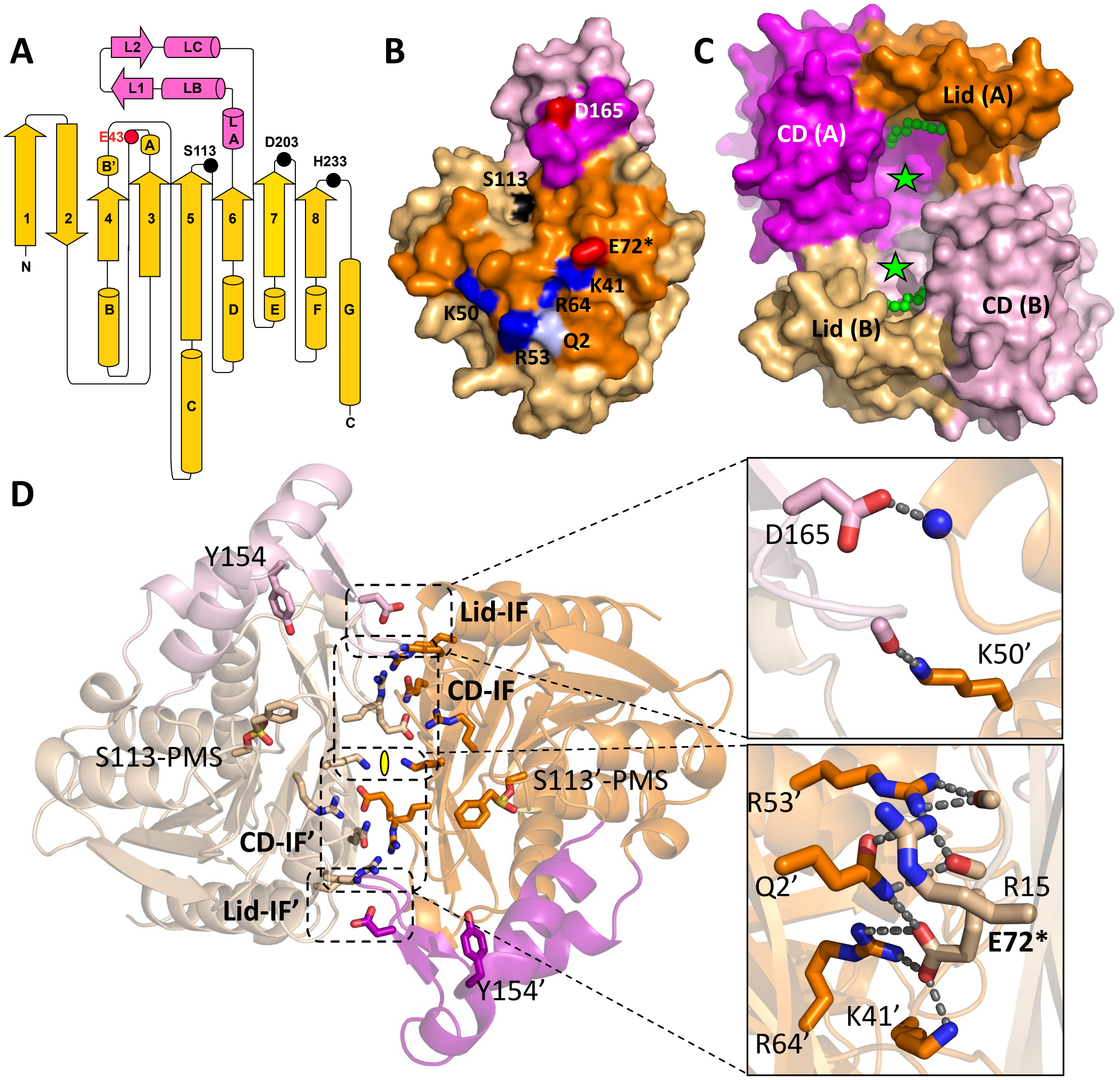
A
L2
LC
L1
LB
L
A
E43
A
B'
S113
D203
H233
1
2
4
3
5
6
7
8
N
B
C
D
E
F
G
C
B
D165
S113
E72*
K41
R64
K50
Q2
R53
C
Lid (A)
CD (A)
CD (B)
Lid (B)
D
Y154
Lid-IF
CD-IF
S113-PMS
S113'-PMS
CD-IF'
Lid-IF'
Y154'
D165
K50'
R53'
Q2'
R15
E72*
K41'
R64'

Figure 2. Structural properties of *Tth* MGL. A, topology diagram of the molecular structure of the *Tth* MGL protomer. CD, yellow; lid domain, pink. Secondary structural elements are in proportion to their length and are labeled. The positions of key active site residues (*cf*. Supplementary Figure S2) are highlighted. The active site glycerol interacting residue Glu43 is shown in red. While in the text three-letter codes were used for residue specifications, for the reason of clarity one-letter codes were used in all figures. B, surface presentation of *Tth* MGL protomer, with the dimeric interface surface highlighted in stronger colors. Polar residues that contribute to specific interactions to the dimeric interface are shown in red (glutamate, aspartate), blue (arginine, lysine), and pale blue (glutamine), and are labeled. Glu72, which was mutated into an arginine for probing the dimeric interface, is highlighted by an asterisk. The surface of the active site residue Ser113 is shown in black, as point of reference for locating the active site. C, *Tth* MGL dimer in surface presentation. The catalytic domains (CD) and lid domains of each protomer are labeled and colored separately. The two *Tth* MGL protomers form a large joint substrate binding site, as indicated by the bound C18 monoacyl ligands (Figure 3A) and two asterisks in green. D, two-fold symmetric dimeric interface of *Tth* MGL,

as indicated by a yellow symbol in the two-fold symmetry center, with the majority of specific interactions originating from the two-fold repeated central CD interface labeled CD-IF and CD-IF', and a smaller number of interactions originating from the two-fold repeated distal lid domain interface labeled Lid-IF and Lid-IF'. Zoom-in of the interfaces are shown on the right indicating specific hydrogen bonds (*cf.* panel B, Supplementary Figure S2). As the PMSF-inhibited *Tth* MGL structure is shown, Ser113-PMS is labeled in both protomers, to approximately locate the two active sites. The position of Tyr154, which was used for mutational analysis, is also labeled. Each *Tth* MGL molecule comprises a two-domain structure (Figure 2). The larger CD is assembled by two sequence segments (residues 1-140 and 184-259), which form a well-established α/β-hydrolase fold comprising a central eight-stranded superhelical twisted β-sheet and six α-helices positioned on both sides of the sheet (Figure 2A & D) [28]. In the PMSF-inhibited *Tth* MGL structure, a covalent PMS-adduct with the catalytic Ser113 is formed, thus blocking the active site from further enzymatic reaction ligands (Figure 3B). In agreement with other lipase structures, *Tth* MGL Ser113 is located at the nucleophilic elbow directly after strand β5 to act as a catalytic residue adopting a strained ε-conformation (Figure 2A, Figure 3A-C, Supplementary Figure S3) [29]. This position is part of the catalytic triad, which also includes Asp203 and His233 (Figure 2A, Figure 3A-B, Supplementary Figure S2). In both structures an active oxyanion hole is formed by Phe37 and Met114 by orienting their main chain amido groups towards the MGL active site (Figure 3B).

A minimal lid domain comprising the residues 141-183 is inserted between strand β6 and helix αE on top of the CD active-site area (Figure 2). Different from most other lipases, in which the lid is generally formed by a bundle of α-helices [18, 21], in *Tth* MGL this domain is compact. It is formed by two small α-helices, followed by a β-hairpin and an additional α-helix, referred to as α-helix-β-hairpin-α-helix (HBH) (Figure 2). In both *Tth* MGL structures, the orientation of the HBH lid to the CD is basically identical (Figure 3D-E), dismissing any large-scale opening/closing mechanisms previously shown for other lid domain-containing lipases [18, 21]. Despite the presence of the lid domain, the MGL active site remains largely accessible (Figure 2C).

Long chain monoacyl ester intermediate is held by a hydrophobic Tth MGL lid tunnel.

In the active site of both *Tth* MGL structures, with and without PMS, we observed literally identical density of a glycerol molecule, presenting one of the two final products of esterase/lipase catalysis (Figures 3A-B and 4). The glycerol molecule tightly interacts via its two C2 and C3 hydroxyl groups with the carboxylate group of a non-conserved active-site residue Glu43, specific to *Tth* MGL (Figure 3B, Supplementary Figure S2A). As di- and triacylglycerol esters would require linkages through these two hydroxyl groups, only monoacylglycerol ester binding via the C1 hydroxyl group of the glycerol backbone is sterically possible.

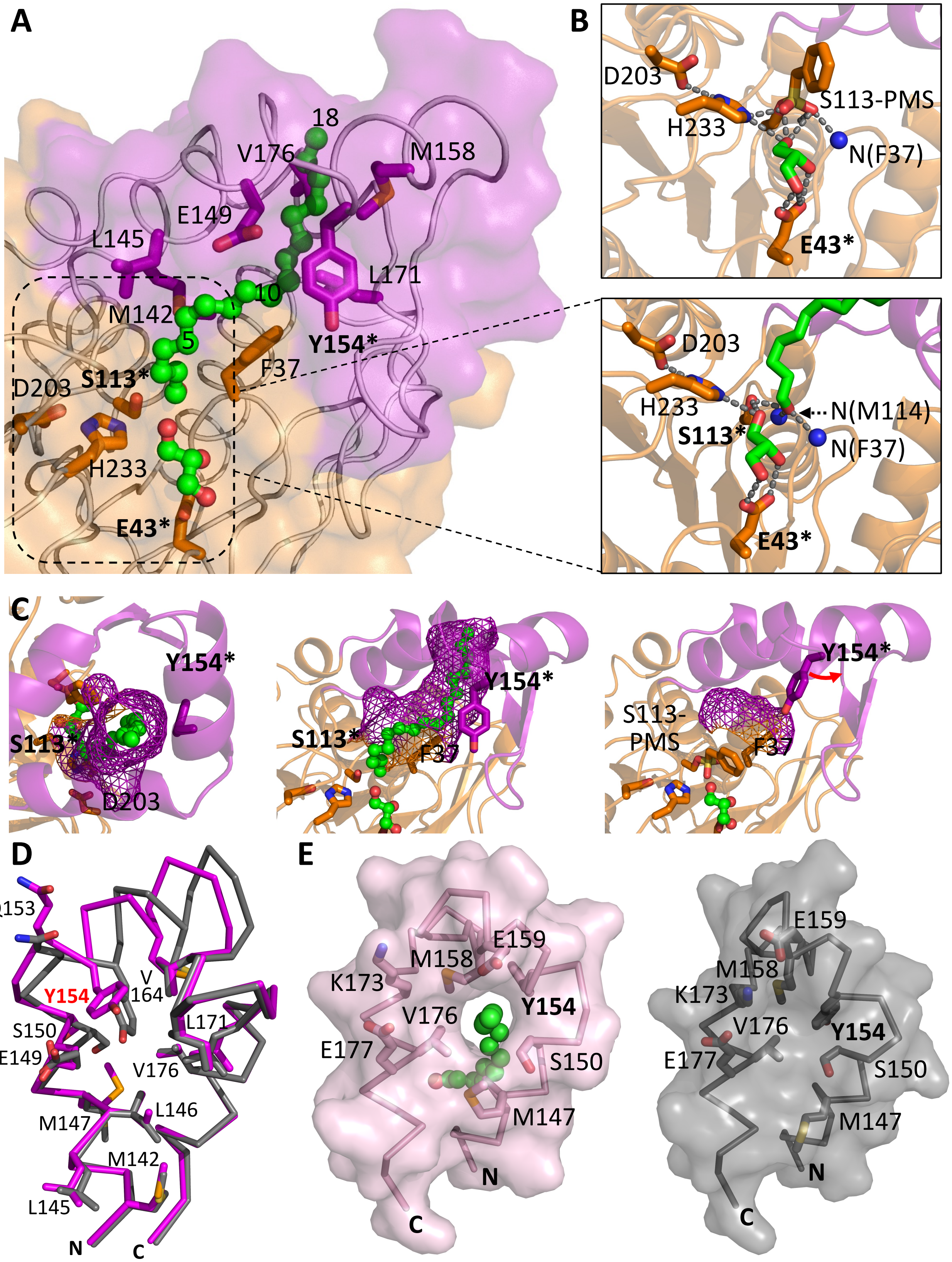
A
18
V176
M158
E149
L145
L171
10
M142
5
Y154*
S113*
F37
D203
H233
E43*
B
D203
S113-PMS
H233
N(F37)
E43*
D203
H233
N(M114)
S113*
N(F37)
E43*
C
Y154*
S113*
D203
Y154*
S113*
F37
Y154*
S113-
PMS
F37
D
Q153
V
164
Y154
S150
L171
E149
V176
L146
M147
M142
L145
N
C
E
E159
M158
K173
Y154
V176
E177
S150
M147
N
C
E159
M158
K173
Y154
V176
E177
S150
M147
N
C

Figure 3: *Tth* MGL active site and lid domain tunnel for long chain FA mono-acyl esters. A, Hybrid cartoon /

semi-transparent surface presentation of the *Tth* MGL active site and long-chain FA mono-acyl binding site, in part generated by a tunnel across the lid domain. Bound C18 mono-acyl FA and glycerol products are shown in green. Atom-specific colors are used for oxygen (red) and nitrogen (blue). Every fifth methylene group of the C18 monoacyl ester intermediate is numbered. Those parts of the C18 monoacyl ligand that are sequestered by the lid domain tunnel (C11-C18) appear to be darker due to the semi-transparent *Tth* MGL surface. Side chains of key residues contributing to ligand binding and the *Tth* active site are shown and labeled. Residues used for probing function are labeled with an asterisk. The central part of the active site is zoomed in a box to the right, indicating specific polar interactions of the glycerol product with *Tth* MGL Glu43. B (upper inlet), active site of the PMSF-inhibited *Tth* MGL structure for comparison. C, mesh surface representation of the C18 monoacyl lid domain tunnel from the top of the lid domain, indicating that it is open at the most distal end (left panel), side view of the lid tunnel (central panel) similar to the orientation in A. Right panel: for comparison, part of the surface generated by residues Phe37 from the CD and Tyr154 from the lid domain is shown for the distinct conformation of the PMSF-inhibited *Tth* MGL structure, due a conformational change of Tyr154, as indicated by a red arrow. This change leads to blockage of the lid tunnel found in the *Tth* MGL structure without PMSF. D, superposition of *Tth* MGL lid domain structures, without (violet) and with PMSF (grey). E, semi-transparent surface presentation of *Tth* MGL lid domain structures, without (violet, left panel) and with PMSF (grey, right panel). Residues involved in the formation of the proximal lid substrate tunnel opening and polar residues forming an outer half-ring wrapping the substrate tunnel exit are labeled. The proximal end of the C18 monoacyl ligand bound to the *Tth* MGL structure without PMSF is shown in green. Comparison of the two conformations shows that the lid tunnel is only opened in the *Tth* MGL structure without PMSF, when C18 monoacyl ligand is present. For reasons of optimizing illustration of the lid tunnel the orientation is different from the one in panel B.

The dihedral conformation of this residue is in an energetically less favored area of the Ramachandran plot in both *Tth* MGL structures (Supplementary Figure S3), suggesting that its role in glycerol binding may supersede any other lower energy conformation.

In both protomers of the active *Tth* MGL structure, we found additional extended ligand electron density pointing away from the active site crossing through a 15 Å long tunnel formed by the HBH lid domain (Figure 3). As we did not add any substrate to the crystallization buffer, bound ligands can only originate from the *Escherichia (E.) coli* expression host FA pool. To independently identify the ligand, we analyzed the protein crystals by liquid chromatography–mass spectrometry followed by reverse phase chromatography. A single peak found in the elution diagram corresponded to the glycerol monostearate (2,3-dihydroxypropyloctadecenoate) (Supplementary Figure S4A), suggesting that under the given sample preparation and crystallization conditions *Tth* MGL products cannot be released. Based on these data, we modeled a C18 monoacyl ligand into the electron density of the active *Tth* MGL structure (Figure 3A, Supplementary Figure S4B). In both *Tth* MGL:glycerol:C18 monoacyl ternary complexes, unrestrained refinement of the interactions of the C1 FA carbon atom with the γ-hydroxyl oxygen of Ser113 and the O1 oxygen of the glycerol moiety produced distances in the range of 2.4-2.5 Å, supporting the presence of a loosely coordinated tetrahedral monoacylester intermediate (Figure 3A-B & Figure 4) [10, 30-31].

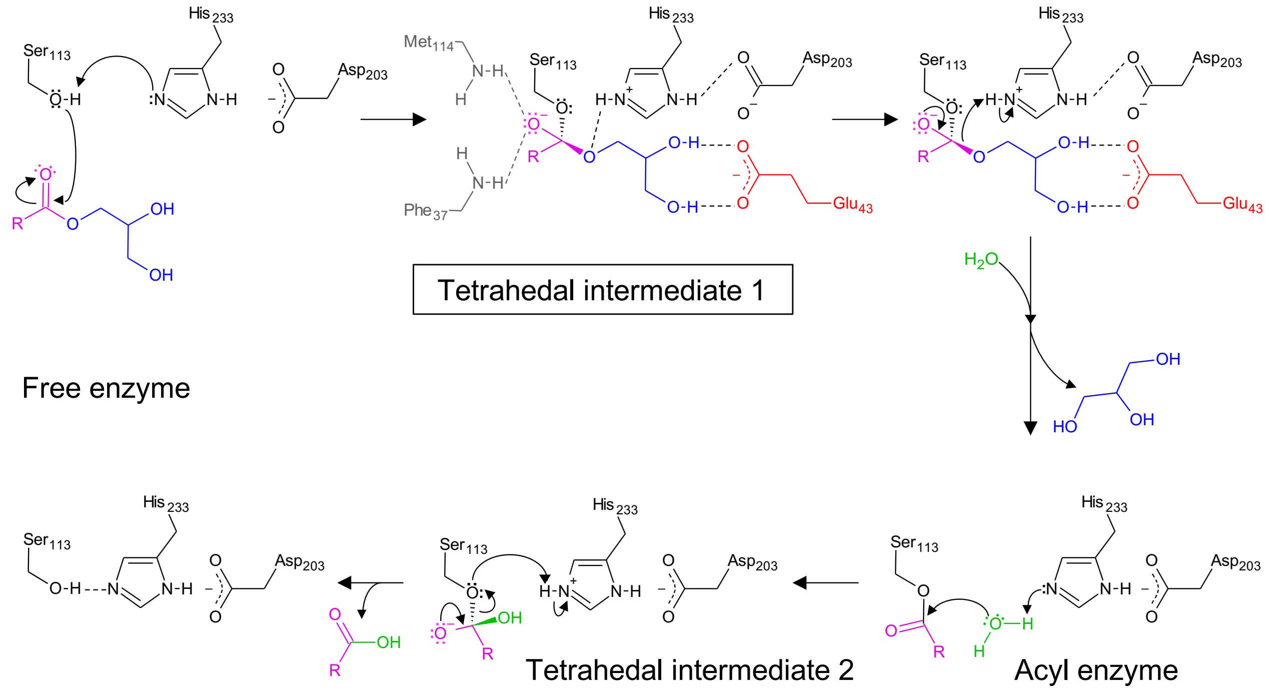

Figure 4: *Tth* MGL reaction scheme. Reaction intermediates are indicated. Color codes: acyl group, pink; glycerol group, blue; reactive water, green; side chain of Glu43, red. The C18 monoacyl ester intermediate found in the *Tth* MGL structure active site is closest to the tetrahedral transition intermediate 1 (boxed).

The distal part of the C18 monoacyl ester intermediate involving carbon atoms C11 to C18 is held by a hydrophobic tunnel across the *Tth* MGL HBH lid domain (Figure 3A & C). In the C18- monoacyl bound *Tth* MGL structure the lid tunnel is open at both ends (Figure 3E). Whereas the proximal opening towards the *Tth* MGL active site can be viewed as an extension of the active site area (Figure 3A), the distal lid tunnel exit is exposed and defined by a ring-like structure of side chains from hydrophobic residues (Figure 3D-E). In the presence of the C18 monoacyl ester intermediate, there are significant alterations in the packing arrangement of several residues within the lid core when comparing to the PMSF-inhibited structure (Figure 3D-E). The largest spatial deviations are found in the N-terminal part of the lid domain, which includes the first two lid helices α-LA and α-LB (Figure 3D, Supplementary Figure S5). In the *Tth* MGL ternary complex structure these two helices are separated by a short loop, whereas in the PMSF-inhibited structure both merge into one long helix (residues 142-161) with a sharp kink at residue Gln153 (Figure 3D). As a result, in the PMSF-inhibited structure the side chains of Ser150 and Tyr154 next to the kink block the formation of the lid tunnel (Figure 2C, Figure 3E). In the presence of the C18 monoacyl ligand, the aromatic ring plane of Tyr154 becomes part of the lid tunnel surface (Figure 3C & E). In conclusion, our structural data are strongly suggestive of the hydrophobic lid tunnel to be crucial for positioning long-chain monoacylglycerol esters to allow efficient turnover by lipase hydrolysis.

Mechanism for variable length monoacyl ester turnover by Tth MGL.

For quantitative characterization of *Tth* MGL *in vitro* activity, we employed a spectrophotometric mono p-nitrophenyl ester assay at an elevated temperature of 40°C [25, 32]. We used monoacyl FA esters ranging from C2 to C18, which is equivalent to the monoacyl ester intermediate we found in the *Tth* MGL structure (Figure 3A, Figure 5). We observed a skewed activity profile for C2-C18 esters, with the highest activities found for C4-C8 esters (Figure 6A, left panel; Supplementary Table S3). For C16 and C18 esters, there was only residual activity at a level where quantitative significance estimates were not possible.

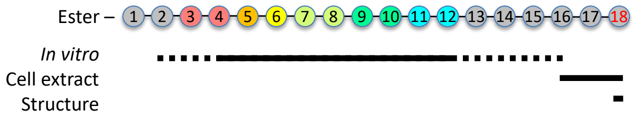

Figure 5: *Tth* MGL activities for FA monoacyl glycerol esters of variable length. Coloring scheme of esters characterized *in vitro* assays (Figure 6A-C). FA monoacyl glycerol esters found in cell extracts (Figure 6D) and by structural data (Figure 3) are also indicated, demonstrating complementarity of different experimental approaches.

We then screened a number of *Tth* MGL mutants for quantitative analysis with C6 FA ester, as representative high activity substrate (Figure 6A, central panel; Supplementary Table S3). As expected, virtually no activity was found for the S113A active-site mutant, which was subsequently used as negative control. Testing the (Δ140-183) *Tth* MGL mutant without the lid domain also resulted in no measurable activity even for short FA esters, suggesting a role in *Tth* MGL activity regulation in addition to its crucial role for distal long-chain monoacyl binding. The monomeric *Tth* MGL E72R mutant exhibited activity comparable to the wt enzyme, demonstrating that dimerization is not essential for *Tth* MGL activity. This is in agreement with our structural ligand binding data showing the same type of ternary glycerol:C18 monoacyl complex for each enzyme subunit (Figure 2D, Figure 3A & C). All *Tth* MGL variants were validated by circular dichroism to be properly folded as well as analyzed for thermal stability and dimeric assembly (Supplementary Table S1, Supplementary Figures S6 and S7).

We further removed the side chain functionality of two residues (Glu43, Tyr154), which we anticipated to be critical for *Tth* MGL catalytic activity. Unexpectedly, we found a more than four-fold activity increase for the E43A mutant, demonstrating gain-of-function by side chain removal (Figure 6A, central panel; Supplementary Table S3). Our data thus indicate that the unusual interaction by Glu43 with an active site glycerol molecule (Figure 3B) not only prevents binding of diacyl and triacyl FA esters but also has an inhibitory effect on its activity profile for monoacyl esters. To investigate whether any of the found effects are sensitive to monoacyl ester length, we analyzed *Tth* MGL variants with measurable activities against a broader spectrum of FA esters (C4-C10) with high *in vitro* activity (Supplementary Table S4). The data demonstrate that the activities were not significantly dependent on varying FA ester length, suggesting that the residues mutated had no major influence on preferred substrate length (Figure 6A, right panel; Supplementary Table S3).

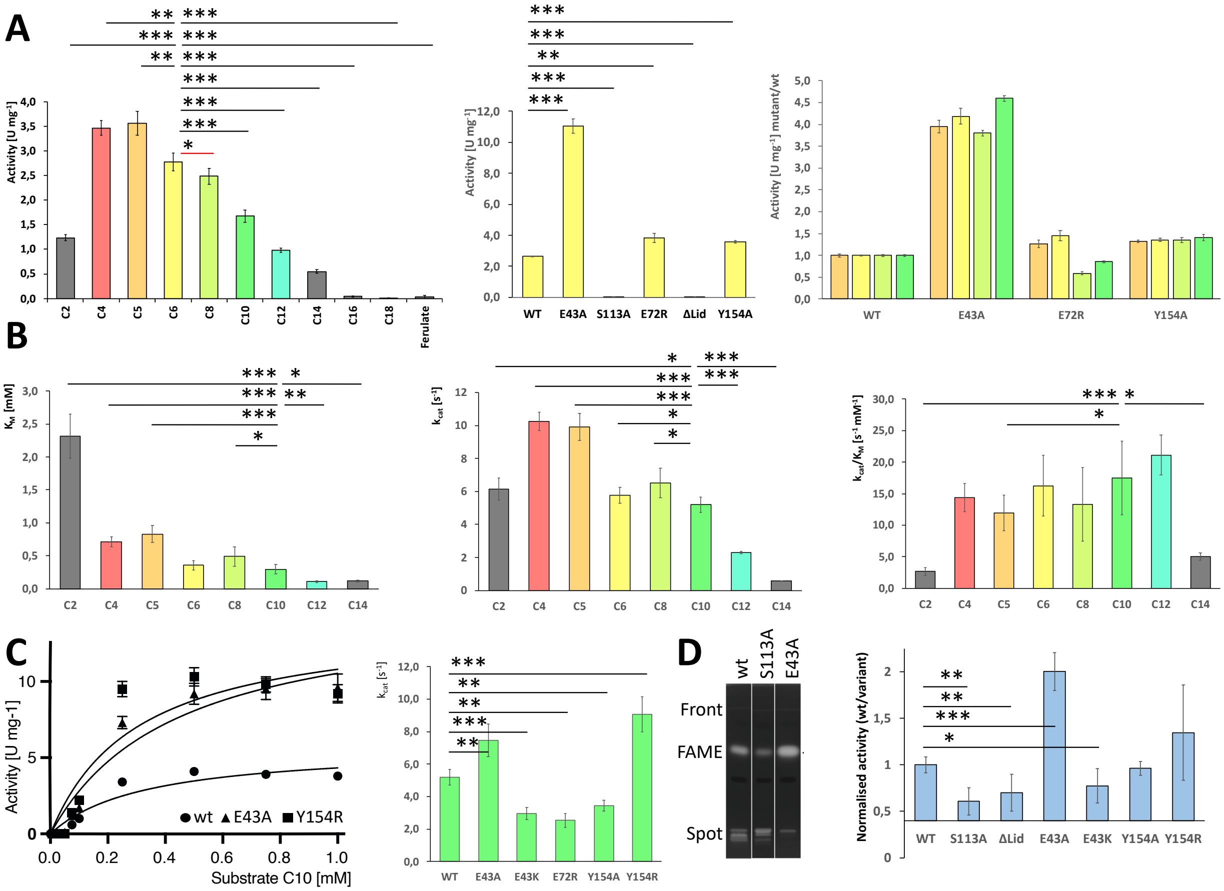

Figure 6: *Tth* MGL activities for FA mono-acyl esters. A, left panel: *in vitro Tth* MGL activity for several p-nitrophenylesters of mono-acyl C2-C18 FAs and ferulate, indicating a broad range of possible substrates. A, central panel: activity of *Tth* MGL variants for C6 mono-acyl FA ester, indicating gain-of-function for the E43A mutant. A, right panel: activity of selected *Tth* MGL variants for mono-acyl C4-C10 FA esters, indicating little dependence on specific FA ester length. Specific substrates used in subsequent experiments are colored: C4, pale red; C5, orange; C6, yellow; C8, yellow-green; C10; green; C12, turquoise (*cf*. Figure 5). B, steady-state Michaelis-Menten analysis for FA mono-acyl esters with quantifiable activity profiles. Left panel, apparent substrate binding affinities for C2-C14 mono-acyl FA esters measured by Michaelis constants KM, indicating increase of binding with increasing FA ester length; central panel, catalytic rates (kcat) for C2-C14 mono-acyl FA esters, showing an overall profile comparable to that measured for overall substrate turnover (central panel, *cf*. panel A, left); right panel, catalytic efficiencies kcat/KM for the same substrate spectrum, showing only minor variations for most of the FA mono-acyl esters used (C4-C12). C, left panel: experimental steady-state kinetic data of selected *Tth* variants (wt, Y154A, E43A)

to estimate Michaelis-Menten values for C6 mono-acyl esters; right panel, catalytic constants (kcat) for selected *Tth* MGL mutants, using C10 FA mono-acyl ester as representative substrate. The data indicate significant gain-of-function for *Tth* MGL variants E43A and Y154R. D, Fatty Acid Methyl Esters (FAMEs) analysis by high-performance thin-layer chromatography (HPTLC) of E. *coli* total lipid extracts (TLE) expressing *Tth* MGL. Left panel, 1, *Tth* MGL (wt); 2, *Tth* MGL (S113A); 3, *Tth* MGL (E43A). Right panel: FAMEs quantification for selected *Tth* MGL mutants, normalized to *Tth* MGL (wt).

At this point, we suspected that the established *Tth* activity profiles are largely convolutes of diverting FA ester length-dependent substrate binding affinities and catalytic turnover. To address this question, we employed steady-state Michaelis-Menten kinetics for quantitatively determining catalytic efficiency kcat/KM (Figure 6B-C; Supplementary Table S5). We found stronger binding affinities with increasing FA ester length in wt *Tth* MGL, ranging from residual C2 ester binding (> 2 mM) to substantially higher binding affinities of around 0.1 mM for the longest measurable FA esters (C12, C14) (Figure 4B, left panel). As expected, the catalytic rate constants (kcat) for C2-C14 FA esters show a similar profile as for overall activity turnover measurements (Figure 6B, central panel; Supplementary Table S5). As a result, the catalytic efficiencies for C4-C12 FA esters are all in the same range of 12-21 sec-1 mM-1, with insignificant differences of less than a factor of 2 (Figure 6B, right panel; Supplementary Table S5). The turnover efficiency was considerably less for the shortest substrate used in these experiments (C2) and medium- to long-chain FA esters (> C12), indicative that the catalytic efficiency of medium- to long-chain FA esters is hampered due to insufficient solubility under the given experimental conditions (Supplementary Table S4).

For subsequent catalytic efficiency experiments, we used C10 FA esters, representing a substrate with one of the highest turnover rates and acceptable solubility (Figure 6C, Supplementary Table S4). We expanded the set of *Tth* MGL variants by two additional mutants, where we – instead of removing – introduced new side-chain functionalities. We replaced Tyr154 by an arginine, as such side chain in the position of Tyr154 cannot adopt a substrate tunnel-inhibiting conformation as observed in the wt *Tth* MGL structure with a PMS-Ser113 adduct for steric reasons (Figure 6B, right panel). This variant showed a two-fold increased gain-of-function for catalytic turnover (Figure 6C, Supplementary Table S5), demonstrating that changes in the remote tunnel segment of the *Tth* MGL lid domain do have effects on the turnover especially of longer FA ester substrates, in support with our structural data in terms of long-chain FA monoacyl ester binding.

Finally, we investigated the release of FAs by different *Tth* MGL variants expressed in cells (E. *coli*) through the analysis of their respective fatty acid methyl esters (FAMEs). When analyzing the FA composition using gas chromatography–mass spectrometry (GC-MS), wt and S113A mutant *Tth* MGL as well as void vector displayed the same composition with mostly hexadecanoic (palmitic) acid (C16:0), cis-

Δ11-octadecenoic (cis-vaccenic) acid (C18:1) and smaller contributions of ethylenic/cyclopropanic acids (17:1 and 19:1) (Supplementary Figure S8). Further, we used high performance thin layer chromatography (Figure 6D, left panel; Supplementary Figure S8) to assess the FAMEs released in MGL variants. When comparing the data from wt *Tth* MGL with the S113A negative control variant, wt *Tth* MGL displayed about two-fold higher FA amounts, demonstrating the enzyme's ability to turn over the respective acyl esters under cellular conditions (Figure 6D, right panel; Supplementary Table S6). Consistently with our *in vitro* monoacyl FA turnover data, the *Tth* MGL E43A variant showed a two-fold increase of FA turnover with respect to wt *Tth* MGL. In agreement with our *in vitro* data as well, expression of the (Δ140-183) *Tth* MGL variant without the lid domain led to only residual level of FA turnover, similar to the S113A control mutant. Interestingly, the *Tth* MGL Y154R variant showed a tendency for increased FA turnover, similar to our *in vitro* data.

Tth MGL is a minimal prototype for helix–β-hairpin–helix lid domain-containing esterases and lipases.

Moving beyond the specific functional properties of *Tth* MGL, we wondered about the enzyme's relations to other previously characterized lipases and esterases. A search against the UniProtKB50 protein sequence data base revealed the top scoring 1000 sequence families to be almost exclusively from bacterial and archaeal phyla (Supplementary Figure S9A, Supplementary Table S7). Amongst these sequences were only two with known 3D structures: cinnamoyl esterase from *Lactobacillus johnsonii* (UNIPROT code D3YEX6, PDB code 3S2Z, plus additional codes of the same sequence), and feruloyl esterase from *Butyrivibrio proteoclasticus* (UNIPROT code D2YW37, PDB code 2WTM, plus additional codes of the same sequence). Cinnamoyl and feruloyl esters are found as CoA ester intermediates in phenylpropanoids metabolic pathways [33]. Even though these enzymes share a high degree of similarity with *Tth* MGL minor active site sequence differences can explain the inability of *Tth* MGL to hydrolyze phenylpropanoid FA ester substrates (for further details, see Supplement).

Next, we searched for more distantly related esterase/lipase sequences by exploiting available structural data. The structure-based identities of all 16 selected target sequences (except those from L. johnsonii and B. proteoclasticus with closer relations) are in the range of 15-23 % and the root mean square deviation values of the superimposed structures are between 1.9 and 2.2 Å, suggesting their relations to be distant with uncertain phylogenetic relations (Supplementary Figure S9B, Supplementary Table S8). Invariant residue positions are confined to the active site including the catalytic triad and four glycine positions (Gly71, Gly111, Gly115, Gly116), which also contribute to the active site oxyanion hole, another hallmark of α/β hydrolases (Supplementary Figure S2) [21, 34].

Remarkably, we found an accumulation of esterase/lipase sequences with non-canonical HBH lid domains (Figure 7, Supplementary Table S8, Supplementary Figure S2). Comparison of these HBH lid structures showed that the terminal helices and adjacent loops function as flexible hinges, even in structures of the same sequence with different ligands (Figure 5B) [18, 21]. On the other hand, the hydrogen bond pattern found in the conserved lid β-hairpin provides an additional element of local fold rigidity, which is not found in other more generic lid domains that are formed from α-helices only. While the small antiparallel β-hairpin motif is conserved in HBH lid-containing esterases/lipases, there is substantial divergence with respect to the length of inserted sequences (Figure 7A-B). Different from the short hairpins found in the *Tth* MGL and the most closely related esterases from *L. johnsonii* and *B. proteoclasticus,* in other more remotely related sequences there are various levels of extensions, allowing to cover extensive surface areas of the CD active site. The most extreme case is found in the hydrolase-1 domain-containing protein from *B. bassiana,* which contains an insert of 43 residues with a 12-residue helix and an extensive loop structure, allowing to shield the complete active site of this enzyme (PDB code 7D79) (Figure 7A, Supplementary Table S8).

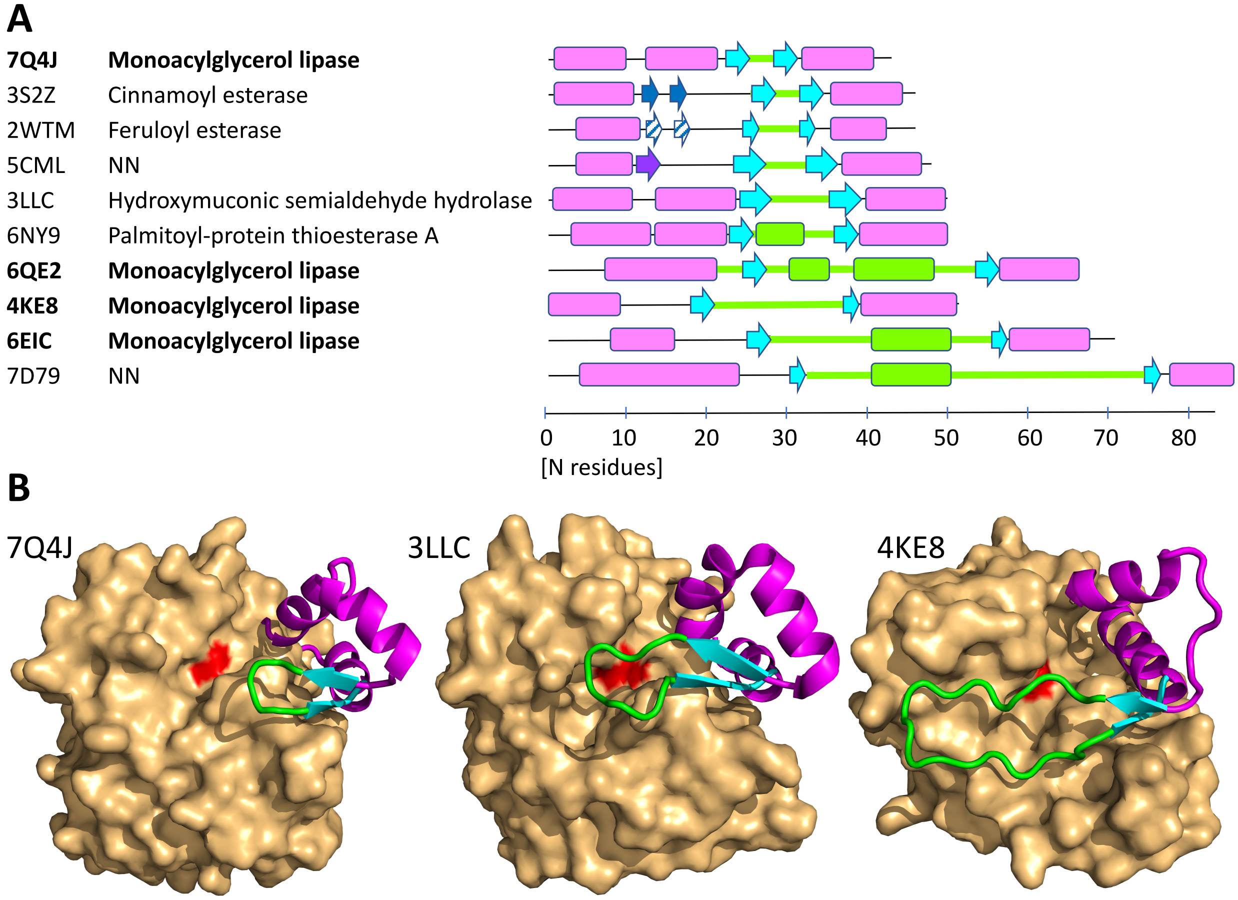
A
7Q4J **Monoacylglycerol lipase**
3S2Z Cinnamoyl esterase
2WTM Feruloyl esterase
5CML NN
3LLC Hydroxymuconic semialdehyde hydrolase
6NY9 Palmitoyl-protein thioesterase A
6QE2 **Monoacylglycerol lipase**
4KE8 **Monoacylglycerol lipase**
6EIC **Monoacylglycerol lipase**
7D79 NN
0
10
20
30
40
50
60
70
80
[N residues]
B
7Q4J
3LLC
4KE8

Figure 7: Sequence, structural and functional relations of esterase/lipases with divergent HBH lid domains. A, Scheme of HBH lid domain sequences related to *Tth* MGL (Figure 2) with secondary structural elements indicated proportional to sequence length. The two-stranded HBH lid β-hairpins are in cyan, sequence and secondary structural

elements inserted between strands βL1 and βL2 are in green. The additional two-stranded β-hairpin structure hovering over the active site in the esterase from *L. johnsonii* (PDB code: 3S2Z) is shown in dark blue. The related β-hairpin-like structure in the esterase from *B. proteoclasticus* (PDB code: 2WTM) is shown in the same color with a diagonal stripe pattern. The lid structure of the Osmotically inducible protein C from *R. marinus* (PDB code: 5CML) comprises an additional third β-strand colored in dark violet, which interacts with the first β-strand of the HBH β-hairpin. B, HBH lid structures of three representative esterase/lipases with their PDB codes indicated (Supplementary Figure S9B), demonstrating common elements (N- and C-terminal α-helices, two-stranded β-hairpin) and diversity of the inserted sequences in terms of length and structure. The CDs of these structures are shown by surface presentation in light orange, and the HBH domains are illustrated by cartoon presentation. The surface covered by the catalytic triad serine (Ser113 in *Tth* MGL) is shown in red, as a point of reference to locate the active site.

We finally investigated to what extent esterase/lipases with a HBH lid domain may resemble properties we observed in the structure of *Tth* MGL. Remarkably, none of the structures with a short HBH lid domain (Figure 7A), except for *Tth* MGL, reveals any tunnel-like structure across the lid domain. This is in accordance with data indicating most efficient substrate turnover for esters of small organic compounds with additional polar groups, as well demonstrated for hydroxycinnamic acid family esterases [35-36]. In contrast, HBH lid tunnels are observed in at least two structures with long HBH lid domains (6QE2, 4KE8/4KE9), which both have been annotated as long-chain MGLs (Supplementary Table S8). In one of these structures of the monoglyceride lipase from *Bacillus sp.* (4KE9), the distal end of a 16-carbon monoglyceride analogue binds through a short tunnel of its HBH lid domain [20], with some resemblance of the HBH lid path found in the structure of *Tth* MGL. A more detailed structural comparison is not possible as there is only very little conservation of residues contributing to long-chain monoglyceride binding.

Taking the data together, HBH lid domains seem to play a crucial role in esterase/lipase function. Supported by our *Tth* MGL structural and functional data, they promote binding of especially long chain monoacylglycerol substrates. MGL binding and turnover is promoted by a toolbox of specific lid domain features: largely varying levels of extensive substrate-shielding areas as demonstrated by vastly diverting HBH β-hairpin sequence inserts, and the formation of lid domain tunnels to hold especially the distal part of long-chain monoacylglycerol esters. Ultimately, our structural data on *Tth* MGL demonstrate that unlike previous thoughts in the literature [18, 21, 37], the presence of a minimal HBH lid domain is sufficient to allow turnover of long-chain monoacylglycerol esters. Thus, the structure of *Tth* MGL presents a minimal prototype for a growing number of esterases and lipases with HBH lid domains of different length. HBH lid lipases with the ability for tunnel formation may offer opportunities for additional evolvement to recognize promiscuous lipidic substrates of variable length, which may even be extracted directly from lipid membranes [17, 38].

CONCLUSION

This study presents a rare case where a high-resolution enzyme structure in the presence of an endogenous long-chain lipid catalysis intermediate led to its functional annotation as an MGL. This or related compounds would not be accessible for structural and functional studies when directly added to purified protein due to lack of solubility in aqueous solution. We attribute the opportunity of capturing such complex to the extremophilic properties of its natural host *Tth*, which are sufficiently different from the growth conditions of the target enzyme's heterologous expression host (*E. coli*). Due to the high level of lid diversity and dynamics, which is a signature of lipases requiring interfacial activation for substrate turnover, homology modeling tools successfully advocated for various other discoveries of enzymatic function [1-2] would have failed, as the closest related enzymes with known structures to *Tth* MGL have specific phenylpropanoid FA esterase activities. Ultimately, this study highlights the strength of high-resolution structural biology to identify and characterize unexplored enzymatic functions under physiological conditions that allowed effective inhibition of substrate turnover. It may inspire future investigations of enzyme function by systematically searching for suitable conditions, under which endogenous substrates or catalysis intermediates could be directly captured.

ACKNOWLEDGEMENTS

We acknowledge the technical support by the Sample Preparation and Characterization facility of the EMBL Hamburg Unit. We also acknowledge the contributions of Marina Royter during the early phase of the project, as well as the technical contributions of Anke Peters and Barbara Klippel, all from the Hamburg University of Technology, as well as Lucie Spina and Marie-Antoinette Laneelle from the IPBS, University of Toulouse, CNRS, UPS, for contribution in methodology.

ASSOCIATED CONTENT

Supporting Information

The Supporting Information is available free of charge.

It includes experimental details on protein expression and purification, *Tth* MGL crystallization and analysis of crystal content, X-ray data collection and structure solution, *in vitro* assay to determine lipolytic enzyme activity, cellular *Tth* MGL activity by cell extract analysis, nano differential scanning fluorimetry, circular dichroism; additional results on structural comparison of *Tth* MGL with known cinnamoyl and feruloyl esterases; additional Tables on the thermostability of *Tth* variants (S1), X-ray structure determination and refinement (S2*), in vitro* activity data (S3), water solubility of p-nitrophenyl FA esters used for *Tth* MGL activity measurements (S4), steady-state kinetics of *Ttl* MGL variants with p-nitrophenyl substrates of different chain lengths (S5), FAME data (S6), sequences producing significant alignments with *Tth* MGL (S7), *Tth* MGL sequence/structure relations to other α/β hydrolases (S8); additional Figures on Alpha Fold 2 predicted structures of dimeric *Tth* MGL (S1), alignments of CD and HBH lid sequences, for which an overall structure-based alignment was possible (S2), Ramachandran plot of *Tth* MGL structures (S3), evidence for the presence of active site-bound C18 monoacylester intermediate and glycerol in the *Tth* MGL (S4), dynamic substrate tunnel opening in the Tth MGL lid domain (S5), analytic SEC profiles of all *Tth* MGL variants investigated (S6), CD spectra for all MGL *Tth* variants investigated (S7), A, schematic workflow of sample preparation and lipid cell-based data analysis and B, representative gas chromatogram used for FAME analysis structure without PMSF (S8), A, taxonomic analysis 496 sequence groups most closely related to *Tth* MGL and B, phylogenetic tree presentation of sequences with known 3D structures and distant relations to *Tth* MGL (S9), structural comparison of the ligand bound HBH lid domains and active site area for *Tth* MGL (S10).

Accession Codes: 7Q4H, 7Q4J contain the crystallographic data of the paper. These data can be obtained free of charge via https://www.rcsb.org/

AUTHOR INFORMATION

Corresponding author

Matthias Wilmanns – European Molecular Biology Laboratory, Hamburg Unit, Notkestrasse 85, 22607 Hamburg, Germany; University Hamburg Clinical Center Hamburg-Eppendorf, Martinistrasse 52, 20251 Hamburg, Germany; ORCID: 0000-0002-4643-5435; Email: matthias.wilmanns@embl-hamburg.de

Authors

Nikos Pinotsis* – European Molecular Biology Laboratory, Hamburg Unit, 22607 Hamburg, Germany; ORCID 0000-0002-5096-257; Present address: Birkbeck College, London WC1E 7HX, United Kingdom.

Anna Krüger* – Hamburg University of Technology, 21073 Hamburg, Germany; ORCID 0000-0001-8007-4955; Present address: Authority for the Environment, Climate, Energy and Agriculture in Hamburg, 21109 Hamburg, Germany.

Nicolas Tomas – IPBS, University of Toulouse, CNRS, UPS, 31077 Toulouse, France; ORCID 0000-0001-7688-4453; Present address: Toulouse White Biotechnology, 31400 Toulouse, France.

Spyros D Chatziefthymiou – European Molecular Biology Laboratory, Hamburg Unit, 22607 Hamburg, Germany; ORCID 0000-0001-7569-5474; Present address: Deutsches Elektronen-Synchrotron, Notkestraße 85, 22607, Hamburg, Germany.

Claudia Litz – European Molecular Biology Laboratory, Hamburg Unit, 22607 Hamburg, Germany; ORCID 0000-0002-7527-0633.

Simon Arnold Mortensen – European Molecular Biology Laboratory, Hamburg Unit, 22607 Hamburg, Germany; ORCID 0000-0001-9013-1802.

Mamadou Daffé – IPBS, University of Toulouse, CNRS, UPS, 31077 Toulouse, France; ORCID 0000-0002-6248-3824.

Hedia Marrakchi – IPBS, University of Toulouse, CNRS, UPS, 31077 Toulouse, France. ORCID 0000-0003-2749-5966.

Garabed Antranikian – Hamburg University of Technology, 21073 Hamburg, Germany; ORCID 0000-0001-6934-5603.

* Equal contribution

REFERENCES AND FOOTNOTESs

1. Jacobson, M. P.; Kalyanaraman, C.; Zhao, S.; Tian, B., Leveraging structure for enzyme function prediction: methods, opportunities, and challenges. *Trends Biochem Sci* **2014,** *39* (8), 363-71.

2. Mills, C. L.; Beuning, P. J.; Ondrechen, M. J., Biochemical functional predictions for protein structures of unknown or uncertain function. *Comput Struct Biotechnol J* **2015,** *13*, 182-91.

3. Bastard, K.; Smith, A. A.; Vergne-Vaxelaire, C.; Perret, A.; Zaparucha, A.; De Melo-Minardi, R.; Mariage, A.; Boutard, M.; Debard, A.; Lechaplais, C.; Pelle, C.; Pellouin, V.; Perchat, N.; Petit, J. L.; Kreimeyer, A.; Medigue, C.; Weissenbach, J.; Artiguenave, F.; De Berardinis, V.; Vallenet, D.; Salanoubat, M., Revealing the hidden functional diversity of an enzyme family. *Nat Chem Biol* **2014,** *10* (1), 42-9.

4. Calhoun, S.; Korczynska, M.; Wichelecki, D. J.; San Francisco, B.; Zhao, S.; Rodionov, D. A.; Vetting, M. W.; Al-Obaidi, N. F.; Lin, H.; O'Meara, M. J.; Scott, D. A.; Morris, J. H.; Russel, D.; Almo, S. C.; Osterman, A. L.; Gerlt, J. A.; Jacobson, M. P.; Shoichet, B. K.; Sali, A., Prediction of enzymatic pathways by integrative pathway mapping. *Elife* **2018,** *7*.

5. Zhao, S.; Kumar, R.; Sakai, A.; Vetting, M. W.; Wood, B. M.; Brown, S.; Bonanno, J. B.; Hillerich, B. S.; Seidel, R. D.; Babbitt, P. C.; Almo, S. C.; Sweedler, J. V.; Gerlt, J. A.; Cronan, J. E.; Jacobson, M. P., Discovery of new enzymes and metabolic pathways by using structure and genome context. *Nature* **2013,** *502* (7473), 698-702.

6. Carter, M. S.; Zhang, X.; Huang, H.; Bouvier, J. T.; Francisco, B. S.; Vetting, M. W.; Al-Obaidi, N.; Bonanno, J. B.; Ghosh, A.; Zallot, R. G.; Andersen, H. M.; Almo, S. C.; Gerlt, J. A., Functional assignment of multiple catabolic pathways for D-apiose. *Nat Chem Biol* **2018,** *14* (7), 696-705.

7. Sévin, D. C.; Fuhrer, T.; Zamboni, N.; Sauer, U., Nontargeted in vitro metabolomics for high-throughput identification of novel enzymes in Escherichia coli. *Nat Methods* **2017,** *14* (2), 187-194.

8. Zhao, S.; Sakai, A.; Zhang, X.; Vetting, M. W.; Kumar, R.; Hillerich, B.; San Francisco, B.; Solbiati, J.; Steves, A.; Brown, S.; Akiva, E.; Barber, A.; Seidel, R. D.; Babbitt, P. C.; Almo, S. C.; Gerlt, J. A.; Jacobson, M. P., Prediction and characterization of enzymatic activities guided by sequence similarity and genome neighborhood networks. *Elife* **2014,** *3*.

9. Kim, J.; Xiao, H.; Bonanno, J. B.; Kalyanaraman, C.; Brown, S.; Tang, X.; Al-Obaidi, N. F.; Patskovsky, Y.; Babbitt, P. C.; Jacobson, M. P.; Lee, Y. S.; Almo, S. C., Structure-guided discovery of the metabolite carboxy-SAM that modulates tRNA function. *Nature* **2013,** *498* (7452), 123-6.

10. Jaeger, K. E.; Dijkstra, B. W.; Reetz, M. T., Bacterial biocatalysts: molecular biology, three-dimensional structures, and biotechnological applications of lipases. *Annu Rev Microbiol* **1999,** *53*, 315-51.

11. Labar, G.; Wouters, J.; Lambert, D. M., A review on the monoacylglycerol lipase: at the interface between fat and endocannabinoid signalling. *Curr Med Chem* **2010,** *17* (24), 2588-607.

12. Salhi, A.; Carriere, F.; Grundy, M. M. L.; Aloulou, A., Enzymes Involved in Lipid Digestion. In *Bioaccessibility and Digestibility of Lipids from Food*, Grundy, M. M. L.; Wilde, P. J., Eds. Springer International Publishing: Cham, 2021; pp 3-28.

13. Jaeger, K. E.; Eggert, T., Lipases for biotechnology. *Curr Opin Biotechnol* **2002,** *13* (4), 390-7.

14. Borrelli, G. M.; Trono, D., Recombinant Lipases and Phospholipases and Their Use as Biocatalysts for Industrial Applications. *Int J Mol Sci* **2015,** *16* (9), 20774-840.

15. Anobom, C. D.; Pinheiro, A. S.; De-Andrade, R. A.; Aguieiras, E. C.; Andrade, G. C.; Moura, M. V.; Almeida, R. V.; Freire, D. M., From structure to catalysis: recent developments in the biotechnological applications of lipases. *Biomed Res Int* **2014,** *2014*, 684506.

16. Reis, P.; Watzke, H.; Leser, M.; Holmberg, K.; Miller, R., Interfacial mechanism of lipolysis as self-regulated process. *Biophys Chem* **2010,** *147* (3), 93-103.

17. Aloulou, A.; Rodriguez, J. A.; Fernandez, S.; van Oosterhout, D.; Puccinelli, D.; Carriere, F., Exploring the specific features of interfacial enzymology based on lipase studies. *Biochim Biophys Acta* **2006,** *1761* (9), 995-1013.

18. Khan, F. I.; Lan, D.; Durrani, R.; Huan, W.; Zhao, Z.; Wang, Y., The Lid Domain in Lipases: Structural and Functional Determinant of Enzymatic Properties. *Front Bioeng Biotechnol* **2017,** *5*, 16.

19. Aschauer, P.; Rengachari, S.; Lichtenegger, J.; Schittmayer, M.; Das, K. M.; Mayer, N.; Breinbauer, R.; Birner-Gruenberger, R.; Gruber, C. C.; Zimmermann, R.; Gruber, K.; Oberer, M., Crystal structure of the Saccharomyces cerevisiae monoglyceride lipase Yju3p. *Biochim Biophys Acta* **2016,** *1861* (5), 462-70.

20. Rengachari, S.; Aschauer, P.; Schittmayer, M.; Mayer, N.; Gruber, K.; Breinbauer, R.; Birner-Gruenberger, R.; Dreveny, I.; Oberer, M., Conformational plasticity and ligand binding of bacterial monoacylglycerol lipase. *J Biol Chem* **2013,** *288* (43), 31093-104.

21. Bauer, T. L.; Buchholz, P. C. F.; Pleiss, J., The modular structure of α/β-hydrolases. *Febs j* **2020,** *287* (5), 1035-1053.

22. López-López, O.; Cerdán, M. E.; González Siso, M. I., New extremophilic lipases and esterases from metagenomics. *Curr Protein Pept Sci* **2014,** *15* (5), 445-55.

23. Salameh, M. A.; Wiegel, J., Purification and characterization of two highly thermophilic alkaline lipases from Thermosyntropha lipolytica. *Appl Environ Microbiol* **2007,** *73* (23), 7725-31.

24. Littlechild, J. A., Improving the 'tool box' for robust industrial enzymes. *J Ind Microbiol Biotechnol* **2017,** *44* (4-5), 711-720.

25. Royter, M.; Schmidt, M.; Elend, C.; Hobenreich, H.; Schafer, T.; Bornscheuer, U. T.; Antranikian, G., Thermostable lipases from the extreme thermophilic anaerobic bacteria Thermoanaerobacter thermohydrosulfuricus SOL1 and Caldanaerobacter subterraneus subsp. tengcongensis. *Extremophiles* **2009,** *13* (5), 769-83.

26. Mirdita, M.; Steinegger, M.; Söding, J., MMseqs2 desktop and local web server app for fast, interactive sequence searches. *Bioinformatics* **2019,** *35* (16), 2856-2858.

27. Jumper, J.; Evans, R.; Pritzel, A.; Green, T.; Figurnov, M.; Ronneberger, O.; Tunyasuvunakool, K.; Bates, R.; Žídek, A.; Potapenko, A.; Bridgland, A.; Meyer, C.; Kohl, S. A. A.; Ballard, A. J.; Cowie, A.; Romera-Paredes, B.; Nikolov, S.; Jain, R.; Adler, J.; Back, T.; Petersen, S.; Reiman, D.; Clancy, E.; Zielinski, M.; Steinegger, M.; Pacholska, M.; Berghammer, T.; Bodenstein, S.; Silver, D.; Vinyals, O.; Senior, A. W.; Kavukcuoglu, K.; Kohli, P.; Hassabis, D., Highly accurate protein structure prediction with AlphaFold. *Nature* **2021,** *596* (7873), 583-589.

28. Ollis, D. L.; Cheah, E.; Cygler, M.; Dijkstra, B.; Frolow, F.; Franken, S. M.; Harel, M.; Remington, S. J.; Silman, I.; Schrag, J.; et al., The alpha/beta hydrolase fold. *Protein Eng* **1992,** *5* (3), 197-211.

29. Arpigny, J. L.; Jaeger, K. E., Bacterial lipolytic enzymes: classification and properties. *Biochem J* **1999,** *343 Pt 1*, 177-83.

30. Holmquist, M., Alpha/Beta-hydrolase fold enzymes: structures, functions and mechanisms. *Curr Protein Pept Sci* **2000,** *1* (2), 209-35.

31. Reis, P.; Holmberg, K.; Watzke, H.; Leser, M. E.; Miller, R., Lipases at interfaces: a review. *Adv Colloid Interface Sci* **2009,** *147-148*, 237-50.

32. Winkler, U. K.; Stuckmann, M., Glycogen, hyaluronate, and some other polysaccharides greatly enhance the formation of exolipase by Serratia marcescens. *J Bacteriol* **1979,** *138* (3), 663-70.

33. Barros, J.; Serrani-Yarce, J. C.; Chen, F.; Baxter, D.; Venables, B. J.; Dixon, R. A., Role of bifunctional ammonia-lyase in grass cell wall biosynthesis. *Nat Plants* **2016,** *2* (6), 16050.

34. Nardini, M.; Dijkstra, B. W., Alpha/beta hydrolase fold enzymes: the family keeps growing. *Curr Opin Struct Biol* **1999,** *9* (6), 732-7.

35. Goldstone, D. C.; Villas-Bôas, S. G.; Till, M.; Kelly, W. J.; Attwood, G. T.; Arcus, V. L., Structural and functional characterization of a promiscuous feruloyl esterase (Est1E) from the rumen bacterium Butyrivibrio proteoclasticus. *Proteins* **2010,** *78* (6), 1457-69.

36. Lai, K. K.; Stogios, P. J.; Vu, C.; Xu, X.; Cui, H.; Molloy, S.; Savchenko, A.; Yakunin, A.; Gonzalez, C. F., An inserted α/β subdomain shapes the catalytic pocket of Lactobacillus johnsonii cinnamoyl esterase. *PLoS One* **2011,** *6* (8), e23269.

37. Riegler-Berket, L.; Leitmeier, A.; Aschauer, P.; Dreveny, I.; Oberer, M., Identification of lipases with activity towards monoacylglycerol by criterion of conserved cap architectures. *Biochim Biophys Acta Mol Cell Biol Lipids* **2018,** *1863* (7), 679-687.

38. Scalvini, L.; Piomelli, D.; Mor, M., Monoglyceride lipase: Structure and inhibitors. *Chem Phys Lipids* **2016,** *197*, 13-24.

Structure-based discovery of a non-canonical prototype long-chain monoacylglycerol lipase through an endogenous catalysis intermediate complex

SUPPLEMENT

MATERIAL AND METHODS

Protein expression and purification

Wild-type *Tth* MGL was expressed and purified as described elsewhere [1]. For production of the seleno-L-methionine (SeMet)-incorporated *Tth* MGL, the corresponding expression vector was used to transform the methionine auxotroph *E. coli* strain B834(DE3). A preculture grown in LB broth medium was used for the expression of the protein in 2L M9 minimal medium including trace elements. After a 3-hour starvation step a L-aminoacid mixture was added (40 mg/ml each except methionine) and SeMet (60 mg/ml). The culture was induced with 1 mM isopropyl-β-D-thiogalactopyranoside (IPTG) when entering the logarithmic growth phase and was further grown overnight. The SeMet protein was purified using the same protocol as native protein.

To generate different protein variants for *in vitro* assays we sub-cloned the gene encoding *Tth* MGL into pETM-14 (EMBL). For all single residue *Tth* variants used in this study, we performed PCR-based mutagenesis on wt *Tth* MGL. For the *Tth* MGL (Δ140-183) construct two primers were designed, the first one in forward orientation for the C-terminal segment of the catalytic domain expressing residues 183-259 and the second one in reverse orientation for the N-terminal segment of the catalytic domain expressing residues 1-140. Both primers generated a unique KpnI restriction site. PCR amplification followed by KpnI restriction and ligation yielded the *Tth* MGL (Δ140-183) construct. For expression of the constructs cloned in pETM-14, *E. coli* Rosetta (DE3) cells were transformed with respective constructs and grown at 37 °C in lysogeny broth (LB-Lennox) supplemented with kanamycin and chloramphenicol. Overexpression was induced by addition of 1 mM IPTG at an OD_{600} of 0.6-0.8 and cells were harvested after continuous shaking at 37 °C for 1 hour. For purification, the cells were resuspended in lysis buffer, containing 50 mM Tris-HCl (pH 8.0), 500 mM NaCl, 5-20 mM imidazole, sonicated and centrifuged at 40.000 g for 30 minutes at 4 °C. The supernatant was filtered and loaded onto nickel-nitrilotriacetic acid (Ni-NTA) beads, which had been equilibrated in lysis buffer. Each protein was further purified by size exclusion chromatography, using a Superdex 75 16/60 column (GE Healthcare). Prior to their usage for *in vitro* assays all purified proteins were dialyzed into 25 mM Tris-HCl (pH 8.0), 50 mM NaCl.

***Tth* MGL crystallization and analysis of crystal content**

Since we were not able to obtain diffracting crystals from unmodified *Tth* MGL, purified protein was concentrated to 5 mg ml^{-1} and for each 1 ml of enzyme solution, 20 µl 1 M dimethylaminoborane (DMAB) were added followed by 40 µl 1 M formaldehyde, as previously described [2]. DMAB and formaldehyde were added once more after 2 hours of incubation. After another 2 hours, another 10 µl 1 M DMAB were added and incubated for 18 hours. During the entire incubation time the sample was kept in the dark and at 4 °C. To terminate the reaction, DMAB and formaldehyde were removed via a three-step centrifugation buffer exchange to a 50 mM Tris-HCl pH 8.0 and 100 mM NaCl buffer using a filter with a 10 kDa molecular-weight cutoff. The purity of the methylated *Tth* MGL was analyzed by SDS-PAGE. Methylation of *Tth* MGL was verified via MALDI–TOF mass spectrometry.

Prior to setting up crystallization screens, the protein sample was concentrated to 20 mg ml^{-1}. Diffracting crystals were grown in 2.4 M ammonium sulfate and 0.1 M Tris buffer (pH 7.5). While the crystals of Se-Met *Tth* MGL substituted were grown in a large parallelepiped shape with dimensions of 50 x 50 x 100 µm, the native PMS-bound *Tth* MGL crystallized in long and very thin rods.

About 30 crystals of Se-Met *Tth* MGL were carefully washed with water and dissolved in 200 µl 1 M NaCl. A chloroform/methanol mixture of 250/500 µl was then added to the solution. After 10 minutes of intensive vortexing, 250 µl chloroform were added and the solution mixed for 1 minute. Then, 250 µl water were added and the solution mixed again for 1 minute. The mixture was centrifuged for 10 minutes at maximum speed and the upper water phase was carefully discarded. The organic phase was evaporated under vacuum centrifugation at room temperature and resuspended in 20 µl hexafluoroisopropanol. LC-MS measurements revealed a single peak eluted from the column, which in the MS spectrum gave a peak at 359 in positive ionization mode (358+1) (Supplementary **Figure S3A**).

X-ray data collection, structure solution, and validation

A single anomalous dispersion experiment using a SeMet-containing *Tth* MGL crystal was carried out on the tunable beamline BM14 (EMBL/ESRF, Grenoble, France) for structure determination. X-ray data of PMS-inhibited *Tth* MGL were also collected on the same beamline. Before data collection, the crystals were immersed in mother liquid containing 30 % (v/v) glycerol and flash cooled in liquid nitrogen. All data sets were integrated, scaled and merged using the HKL suite [3]. Selenium atoms were located using the SHELXD program and initial density modification was performed by SHELXE [4]. The correct heavy atom substructure was then used together with the anomalous data from HKL as input for the PHENIX AutoSol wizard, which recalculated the experimental phases and carried out density modification [5]. The density modified phases where then merged with the high resolution data-set from the same crystal using the program CAD and were then used as an input for model building by ARP/wARP [6-7]. The produced model was further improved by manual corrections and modifications in COOT [8]. ARP/wARP was used again for adding ordered solvent molecules. Additional ligands were added manually after inspecting the electron density maps in COOT. Refinement using molecular dynamics and TLS was performed by PHENIX [9]. The data collection and refinement statistics are reported in **Supplementary Table S2**.

A structure-based sequence alignment was computed by PDBeFold [10]**.** Figures of the 3D structural model were prepared using PYMOL (http://www.pymol.org/).

In vitro **assay to determine lipolytic enzyme activity**

The genes encoding wt *Tth*, E43A, E43K, E72R, Y154A, and Y154R were cloned into the pETM-14 expression vector, and for expression *E. coli* BL21-CodonPlus(DE3)-RIL cells (Agilent Technologies) were used. Cells were grown at 37 °C in lysogeny broth (LB-Lennox) supplemented with kanamycin and chloramphenicol. Cells were induced by addition of 0.5 mM IPTG at an OD_{600} of 0.6-0.8 and harvested after continuous shaking overnight at 18 °C. For purification, the cells were resuspended in lysis buffer (25 mM Tris-HCl (pH 8.0), 300 mM NaCl, 20 mM imidazole, and DNaseI), sonicated, and centrifuged at 40.000 g for 30 minutes at 4 °C. The supernatant was filtered and loaded onto Ni-NTA beads, which had been equilibrated in wash buffer (25 mM Tris-HCl (pH 8.0), 300 mM NaCl, 20 mM imidazole). After loading, beads were washed with wash buffer and eluted in elution buffer (25 mM Tris-HCl (pH 8.0), 300 mM NaCl, 500 mM imidazole). Each *Tth* variant was concentrated using an Amicon® Ultra concentrator with a 10 kDa cutoff (membrane - regenerated cellulose) and further purified by size exclusion chromatography, using a Superdex 75 10/300 column (GE Healthcare), equilibrated in 25 mM Tris-HCl (pH 8.0), 50 mM NaCl.

Cleavage of *p*-nitrophenyl monoacyl esters was determined as in previous studies [1]. The protein concentration of the purified enzyme variants was adjusted with sample buffer (25 mM Tris, pH 8.0 and 50 mM NaCl) to a suitable concentration ranging from 0.02 to 0.05 mg ml^{-1} to perform measurements in the linear range of the assay. The substrates **(Supplementary Table S4)** were dissolved in sample buffer additionally containing 1 mg ml^{-1} gum arabicum (Sigma Aldrich).

All values were determined in quadruplicates and corrected for autohydrolysis using the experimentally determined pH-dependent extinction coefficient of *p*-nitrophenyl in microtiter plates (ε = 9.3024 mL μmol^{-1}). The activity assay was performed at 40 °C in a semi-automated high-throughput setup in micro-scale. Applying a Freedom EVO® screening robot equipped with a Safire2 plate reader (Tecan Group Ltd.), *p*-nitrophenyl substrates were used at a final concentration of 0.9 mM and continuous measurements were performed at λ = 410 nm for 10 minutes in a total assay volume of 200 µl.

Tth MGL Michaelis-Menten kinetics were performed by quadruple measurements of enzyme activity with *p*-nitrophenyl esters at different substrate concentrations (0.005 mM, 0.0075 mM, 0.01 mM, 0.025 mM, 0.05 mM, 0.075 mM, 0.1 mM, 0.25 mM, 0.5 mM, 0.75 mM and 1 mM). The respective activity values were fitted to the Michaelis-Menten equation applying a non-linear regression tool in Prism version 9.1.2. Obtained K_M and v_{max} values of each Michaelis-Menten fit were then used to calculate averages and standard deviations of these basic kinetic parameters. Finally, k_{cat} and K_M yielded the catalytic efficiency, which was compared to wild-type *Tth* MGL for each of the analyzed mutants **(Supplementary Table S5)**.

Cellular *Tth* MGL activity by cell extract analysis

Wt *Tth* and Y154A were cloned into the pETBlue-1 vector, transformed into *E. coli* Tuner™ (DE3) pLacI cells and grown at 37 °C in lysogeny broth (LB-Lennox) supplemented with ampicillin and chloramphenicol. Cells were induced by addition of 1 mM IPTG at an OD_{600} of 0.6-0.8 and harvested after continuous shaking at 37 °C for 1 hour. Cell pellets were washed with PBS prior to lipid extraction.

Total lipid extracts (TLE) were obtained from wet *E. coli* cell pellets by three successive extractions using distinct chloroform/methanol mixtures (1:2, 1:1, and 2:1 v/v). The fractions were pooled, washed with water, and dried under air stream. For chromatography analyses, FAs were methylated using TMS-diazomethane (Sigma), purified on a florisil batch column and analyzed by thin layer chromatography (TLC) (Merck silica Gel 60) with dichloromethane as developing solvent.

For lipid semi-quantitative analysis, equivalent masses of total lipid fraction from each strain were spotted onto a high-performance TLC (HPTLC) silica gel 60 plate (Merck) with a Camag ATS4 apparatus. The plates were developed in dichloromethane using a Camag ADC2 device and stained by immersion using a Camag CID3 apparatus with 10 % primuline in acetone/water (84:16). Lipids were revealed and quantified by determining their relative percentage using the Chemidoc Imaging System and ImageLab software (Biorad) [11]**.** To determine FA composition, the FAMEs were analyzed by GC-MS (Thermo Scientific gas chromatograph, fitted with a 15 m x 0.25 mm TG1MS fused silica capillary column and connected to an ISQ single quadrupole mass spectrometer), and identified according to their retention time and their fragmentation pattern.

Nano differential scanning fluorimetry

Temperature-induced aggregation curves were measured using Prometheus NT.48 (NanoTemper Technologies GmbH) equipped with a scattering module. Proteins were prepared in 25 mM Tris-HCl (pH 8.0), 50 mM NaCl and measured in three technical replicates at a concentration of 1.5 mg ml^{-1}. Excitation power was pre-adjusted to get fluorescence readings above 2000 RFU for F330 and F350, and samples were heated from 15 °C to 95 °C with a slope of 1 °C per minute. The processed data were exported from the manufacturer's software (PR.ThermControl) and analysed with MoltenProt to obtain aggregation temperatures [12].

Circular dichroism

Far-UV CD spectrums for the *Tth* samples were recorded on a Chirascan Circular Dichroism Spectrometer upgraded with an Active Nitrogen Management System (Applied Photophysics). Measurements were performed at a controlled temperature of 20 °C in a 1 mm QS cuvette, between 280-190 nm using a bandwidth of 1 nm. The *Tth* samples were measured at a concentration of 0.25 mg ml^{-1} in 20 mM Tris-HCl (pH 8.0) in three technical replicates. Signal from buffer was subtracted for all measured samples.

RESULTS

Structural comparison of Tth MGL with cinnamoyl and feruloyl esterases

The relations of cinnamoyl esterase from *Lactobacillus johnsonii* (UNIPROT code D3YEX6, PDB code 3S2Z, plus additional codes of the same sequence) and feruloyl esterase from *Butyrivibrio proteoclasticus* (UNIPROT code D2YW37, PDB code 2WTM, plus additional codes of the same sequence) to the sequence and structure of *Tth* MGL are at a comparable level, as illustrated by rmsd values of 1.2–1.3 Å and structure-based sequence identities of 30-32 % **(Figure 7, Supplementary Figure S2, Supplementary Table S8)**. The lid domain in these three structures comprises a virtually identical two-stranded antiparallel β-hairpin (residues 163-165 and 170-172 in the *Tth* MGL), which is connected by a short hairpin motif of five or less residues **(Figure 2A, Figure 7A)**. This hairpin shields a highly conserved histidine-glycine-phenylalanine (HGF) motif within the catalytic domain loop connecting β-strand 3 and α-helix B (residues 35-37 in the *Tth* MGL structure) and the small α-helix B' (residues 77-79 in the *Tth* MGL structure) next to the active site **(Figure 7B, Supplementary Figure S2)**. Helix B' comprises a phenylalanine-serine-glutamate/aspartate (FSE/D) motif that is conserved in the sequences of the related esterases from *L. johnsonii, B. proteoclasticus,* and *T. siderophilus* (*Tth*) but not in other related esterase/lipases (**Supplementary Figure S2**). Phe37, Phe77 and Phe/Tyr175 from the C-terminal lid domain helix α-LC form a highly conserved aromatic residue cluster in these structures and play a crucial role in shaping the substrate-binding sites of the respective enzymes **(Figure 3A, Supplementary Figures S2 & S10).**

Based on these relations it is surprising that *Tth* MGL did not show measurable activity against phenylpropanoid FA ester substrates of the esterases from *L. johnsonii* and *B. proteoclasticus* **(Figure 6A)** [13-14]**.** Inspection of their structures revealed a plausible explanation of the distinct substrate specificities: First, in these esterases, there is an additional second small β-hairpin interaction following the first lid helix α-LA, which is not found in any other HBH esterase/lipase lid domains including the structure of *Tth* MGL **(Figure 7A, Supplementary Figure S10)**. This hairpin hovers over the central part of the active site of these two esterases to shield bound substrates and thereby further restricts the size of the substrate binding pocket. In the *Tth* MGL this hairpin structure is replaced by a second lid helix α-LB, which is more distal to the enzyme's active site **(Supplementary Figure S10, left panel)**. Secondly, there are two residues in the *Tth* MGL lid structure, Leu145 from the N-terminal lid helix α-LA and Phe175 from the C-terminal lid helix α-LC that are replaced by residues with functional polar groups, aspartate (Asp138, only in the sequence of the *L. johnsonii* esterase sequence) and tyrosine (Tyr169 in the *L. johnsonii* and *B. proteoclasticus* esterase sequences) respectively **(Supplementary Figure S10)**. Structures of the esterase from *L. johnsonii* in the presence of several ferulate derivatives (3PFB, 3PFC, 3S2Z) demonstrate the distinct roles of these residues in substrate binding, and removal of the polar side chain of Asp138 strongly impairs substrate turnover [14]**.** In conclusion, the absence of these functional residue groups in the *Tth* MGL well explains the lack of any measurable activity towards hydroxycinnamic esters.

Supplementary Table S3: Thermostability of *Tth* variants

***Tth* lipase variant**	**Tm (°C)**	**ΔT_m(°C)**
wt	77.2 ± 0.16	
wt-PMS	77.1 ± 0.04	- 0.1
ΔLid	82.8 ± 0.01	+ 5.6
E43A	76.1 ± 0.02	- 1.1
E43K	77.9 ± 0.21	+ 0.7
E72R	75.7 ± 0.05	- 1.5
S113A	81.8 ± 0.07	+ 4.6
Y154A	78.3 ± 0.14	+ 1.1
Y154R	78.3 ± 0.10	+ 1.1

Legend Supplementary Table S1: We did not detect significant changes in thermostability (< 2 degrees changes), except for a variant without the lid domain (Δ140-183) that revealed an increased melting temperature of 83 °C, which is 6 °C higher than one found for the wt Tth MGL **(Figure 1B)**. This was within the melting temperature of the wt *Tth* MGL **(Figure 1B)**. This was within expectation as the lid domain is highly exposed and presents the most dynamic part of the overall *Tth* MGL structure (**Figures 1 & 3).** Interestingly, we have also observed a similar level of thermal stabilization in the *Tth* MGL S113A active site mutant. The most plausible explanation is that a mutation of this active site residue could lead to a relieve of the high-energy ε-conformation of Ser113 found in both *wt* enzymes in the presence and absence of PMSF **(Supplementary Figure S3)**.

Supplementary Table S2: X-ray structure determination and refinement

	Se-Met peak	**SeMet inflection**	**PMSF derivative**
PDB identifier	7Q4J		7Q4H
Crystal data			
Space group	$P4_{3}2_{1}2$	$P4_{3}2_{1}2$	$P4_{3}22$
Unit cell parameters (Å)	a=b= 137.5, c=67.8		a=b= 85.8, c=157.5
Mosaicity (deg.)	0.25	0.25	0.90
Data collection			
Beam line	BM14, ESRF	BM14, ESRF	BM14, ESRF
Wavelength (Å)	0.97873	0.97903	0.95372
Resolution range	50.0-2.56 (2.60-2.56)	20.0-1.91 (1.94-1.91)	30.0-2.00 (2.05-2.00)
R_{sym} (%)	0.059 (13.1)	5.1 (64.2)	8.2 (51.4)
I/σ (I)	35.3 (19.3)	21.4 (2.03)	24.0 (1.65)
Reflections measured/unique	482,920/21,648	543,030/49,383	728,975/38930
Redundancy	10.4 (10.0)	3.3 (2.9)	5.1 (2.7)
Completeness (%)	99.7 (100.0)	97.1 (82.2)	98.1 (82.2)
Refinement			
Program		Phenix, TLS	Phenix, TLS
R / R_{free} (%)		17.09/19.93	18.72/24.72
Reflections (work/test sets)		46,554/1,457	38,285/1,200
Protein atoms		4,190	4,148
Ligands*		1 x STE, 1 x D10, 7 x GOL, 4 x SO_4^{2-}	1x OLC, 1 x Cl^-, 5 x GOL, 3 x SO_4^{2-}
Solvent molecules		303	157
r.m.s.d. bonds (Å)		0.007	0.017
r.m.s.d. angles (deg)		1.446	1.894
Average B values for main chain atoms ($Å^2$)		39.45	46.46
Average B values for side chain and solvent molecules ($Å^2$)		45.37	49.84
Model quality (Ramachandran plot)			
Most favored (%)		90.8	89.5
Additionally allowed (%)		8.3	9.2
Generously allowed (%)		0.9	0.9
Disallowed (%)		0.0	0.4

*STE: stearic acid; D10: decan; GOL: glycerol; OLC: (2R)-2,3-dihydroxypropyl (9Z)-octadec-9-enoate

Supplementary Table S3*:* *In vitro* activity data

Figure 6A, left panel

***Tth* MGL (wt) activity towards *p*NP substrate [U mg^{-1}]**

C2	C4	C5	C6	C8	C10
1.23 ± 0.06	3.46 ± 0.15	3.56 ± 0.24	2.77 ± 0.18	2.49 ± 0.16	1.67 ± 0.13

C12	C14	C16	C18	ferulate
0.98 ± 0.05	0.55 ± 0.04	0.04 ± 0.01	0.01 ± 0.01	0.03 ± 0.03

Figure 6A, central panel

***Tth* MGL variant activity towards *p*NP substrate [U mg^{-1}]**

	C5	C6	C8	C10	C14
wt	3.53 ± 0.13	2.64 ± 0.02	2.14 ± 0.05	1.50 ± 0.04	0.46 ± 0.02
E43A	13.94 ± 0.51	11.04 ± 0.47	8.13 ± 0.14	6.90 ± 0.10	0.62 ± 0.06
S113A	0.01 ± 0.02	0.01 ± 0.01	-0.01 ± 0.02	0.00 ± 0.01	-0.01 ± 0.02
E72R	4.47 ± 0.31	3.84 ± 0.30	1.26 ± 0.08	1.28 ± 0.04	0.01 ± 0.01
ΔLid	0.01 ± 0.02	0.01 ± 0.02	-0.02 ± 0.00	0.00 ± 0.00	0.00 ± 0.01
Y154A	4.67 ± 0.11	3.58 ± 0.08	2.88 ± 0.13	2.11 ± 0.11	0.59 ± 0.07

Supplementary Table S4: Water solubility of *p*-nitrophenyl FA esters used for *Tth* MGL activity measurements

Name	**Corresponding acid**	**Water solubility (mg ml^{-1})[1]**
4-Nitrophenyl acetate (*p*NP-C2)	Acetic/ethanoic acid	1160
4-Nitrophenyl butyrate (*p*NP-C4)	Butyric/Butanoic acid	24
4-Nitrophenyl valerate (*p*NP-C5)	Valeric/Pentanoic acid	9
4-Nitrophenyl hexanoate (*p*NP-C6)	Caproic/Hexanoic acid	15
4-Nitrophenyl octanoate (*p*NP-C8)	Caprylic/Octanoic acid	1.513
4-Nitrophenyl decanoate (*p*NP-C10)	Capric/Decanoic acid	0.1515
4-Nitrophenyl laurate (*p*NP-C12)	Lauric/Dodecanoic acid	0.01504
4-Nitrophenyl myristate (*p*NP-C14)	Myristic/Tetradecanoic acid	0.001481
4-Nitrophenyl palmitate (*p*NP-C16)	Palmitic/Hexadecanoic acid	0.0001449
4-Nitrophenyl stearate (*p*NP-C18)	Stearic/Octadecanoic acid	0.00001409

[1] Source: ChemSpider (http://www.chemspider.com/)

Supplementary Table S5: Steady-state kinetics of Ttl MGL variants with *p*-nitrophenyl substrates of different chain lengths

***p*NP-C2**	K_M [mM]	k_{cat} [s^{-1}]	k_{cat}/K_M [M^{-1} s^{-1}]	$(k_{cat}/K_M)_{variant}/_{wt}$
wt	2.3 ± 0.3	6.1 ± 0.7	2.7 ± 0.5 x 10^{3}	1.0
E43A	1.9 ± 0.3	1.7 ± 0.2 x 10^{1}	8.7 ± 1.5 x 10^{3}	3.3
E43K	6.3 ± 0.6 x 10^{-1}	1.0 ± 0.1	1.6 ± 0.2 x 10^{3}	0.6
E72R	7.1 ± 0.7 x 10^{-1}	4.2 ± 0.2	6.0 ± 0.6 x 10^{3}	2.2
Y154A	1.4 ± 1.1 x 10^{-1}	2.5 ± 1.8 x 10^{1}	1.8 ± 1.9 x 10^{3}	0.7
Y154R	2.0 ± 0.3	1.5 ± 0.2 x 10^{1}	7.5 ± 1.4 x 10^{3}	2.8

***p*NP-C4**	K_M [mM]	k_{cat} [s^{-1}]	k_{cat}/K_M [M^{-1} s^{-1}]	$(k_{cat}/K_M)_{variant}/_{wt}$
wt	7.1 ± 0.7 x 10^{-1}	1.0 ± 0.1 x 10^{1}	1.4 ± 0.2 x 10^{4}	1.0
E43A	6.7 ± 1.9 x 10^{-1}	1.7 ± 0.3 x 10^{1}	2.5 ± 0.8 x 10^{4}	1.7
E43K	8.2 ± 0.8 x 10^{-1}	4.6 ± 0.2	5.6 ± 0.6 x 10^{3}	0.4
E72R	1.4 ± 2.0	5.8 ± 5.4	4.0 ± 6.8 x 10^{3}	0.3
Y154A	3.4 ± 0.6	1.5 ± 0.2 x 10^{1}	4.5 ± 1.0 x 10^{3}	0.3
Y154R	7.2 ± 1.9 x 10^{-1}	1.4 ± 0.2 x 10^{1}	1.9 ± 0.6 x 10^{4}	1.3

***p*NP-C5**	K_M [mM]	k_{cat} [s^{-1}]	k_{cat}/K_M [M^{-1} s^{-1}]	$(k_{cat}/K_M)_{variant}/_{wt}$
wt	8.3 ± 1.3 x 10^{-1}	9.9 ± 0.8	1.2 ± 0.2 x 10^{4}	1.0
E43A	6.5 ± 1.6 x 10^{-1}	1.5 ± 0.2 x 10^{1}	2.3 ± 0.6 x 10^{4}	1.9
E43K	4.5 ± 0.8 x 10^{-1}	3.4 ± 0.3	7.6 ± 1.5 x 10^{3}	0.6
E72R	9.4 ± 3.3 x 10^{-1}	1.2 ± 0.2 x 10^{1}	1.2 ± 0.5 x 10^{4}	1.0
Y154A	1.4 ± 0.2	1.3 ± 0.1 x 10^{1}	9.6 ± 1.9 x 10^{3}	0.8
Y154R	8.8 ± 2.2 x 10^{-1}	1.6 ± 0.2 x 10^{1}	1.8 ± 0.5 x 10^{4}	1.5

***p*NP-C6**	K_M [mM]	k_{cat} [s^{-1}]	k_{cat}/K_M [M^{-1} s^{-1}]	$(k_{cat}/K_M)_{variant}/_{wt}$
wt	3.6 ± 0.8 x 10^{-1}	5.8 ± 0.5	1.6 ± 0.4 x 10^{4}	1.0
E43A	7.1 ± 3.0 x 10^{-1}	1.3 ± 0.3 x 10^{1}	1.8 ± 0.9 x 10^{4}	1.1
E43K	3.2 ± 0.9 x 10^{-1}	2.9 ± 0.3	9.1 ± 2.8 x 10^{3}	0.6
E72R	6.3 ± 3.4 x 10^{-1}	8.7 ± 2.3	1.4 ± 0.8 x 10^{4}	0.8
Y154A	4.8 ± 0.8 x 10^{-1}	6.7 ± 0.5	1.4 ± 0.3 x 10^{4}	0.9
Y154R	7.5 ± 3.6 x 10^{-1}	1.4 ± 0.3 x 10^{1}	1.8 ± 1.0 x 10^{4}	1.1

***p*NP-C8**	K_M [mM]	k_{cat} [s^{-1}]	k_{cat}/K_M [M^{-1} s^{-1}]	$(k_{cat}/K_M)_{variant}/_{wt}$
wt	4.9 ± 1.5 x 10^{-1}	6.5 ± 0.9	1.3 ± 0.4 x 10^{4}	1.0
E43A	5.2 ± 3.4 x 10^{-1}	1.2 ± 0.3 x 10^{1}	2.3 ± 1.6 x 10^{4}	1.7
E43K	4.6 ± 1.3 x 10^{-1}	3.7 ± 0.5	8.0 ± 2.5 x 10^{3}	0.6
E72R	5.1 ± 2.2 x 10^{-1}	6.7 ± 1.3	1.3 ± 0.6 x 10^{4}	1.0
Y154A	6.2 ± 2.3 x 10^{-1}	7.6 ± 1.4	1.2 ± 0.5 x 10^{4}	0.9
Y154R	8.2 ± 4.4 x 10^{-1}	1.3 ± 0.4 x 10^{1}	1.6 ± 1.0 x 10^{4}	1.2

***p*NP-C10**	K_M [mM]	k_{cat} [s^{-1}]	k_{cat}/K_M [M^{-1} s^{-1}]	$(k_{cat}/K_M)_{variant}/_{wt}$
wt	3.0 ± 0.7 x 10^{-1}	5.2 ± 0.5	1.7 ± 0.5 x 10^{4}	1.0
E43A	2,7 ± 1.0 x 10^{-1}	7.5 ± 1.0	2.7 ± 1.1 x 10^{4}	1.6
E43K	3.3 ± 1.1 x 10^{-1}	3.0 ± 0.4	8.9 ± 3.1 x 10^{3}	0.5
E72R	1.3 ± 0.7 x 10^{-1}	2.5 ± 0.4	1.9 ± 1.1 x 10^{4}	1.1
Y154A	2.2 ± 0.6 x 10^{-1}	3.4 ± 0.3	1.6 ± 0.5 x 10^{4}	0.9
Y154R	3.9 ± 1.1 x 10^{-1}	9.1 ± 1.1	2.3 ± 0.7 x 10^{4}	1.3

***p*NP-C12**	K_M [mM]	k_{cat} [s^{-1}]	k_{cat}/K_M [M^{-1} s^{-1}]	$(k_{cat}/K_M)_{variant}/_{wt}$
wt	1.1 ± 0.1 x 10^{-1}	2.3 ± 0.1	2.1 ± 0.3 x 10^{4}	1.0
E43A	1.0 ± 0.1 x 10^{-1}	3.4 ± 0.1	3.4 ± 0.5 x 10^{4}	1.6
E43K	5.3 ± 1.3 x 10^{-2}	1.0 ± 0.1	1.9 ± 0.5 x 10^{4}	0.9
E72R	1.7 ± 0.6 x 10^{-2}	4.1 ± 0.3 x 10^{-1}	2.5 ± 0.9 x 10^{4}	1.2
Y154A	6.4 ± 0.9 x 10^{-2}	1.3 ± 0.0	2.0 ± 0.3 x 10^{4}	0.9
Y154R	1.2 ± 0.2 x 10^{-1}	3.3 ± 0.1	2.8 ± 0.4 x 10^{4}	1.3

***p*NP-C14**	K_M [mM]	k_{cat} [s^{-1}]	k_{cat}/K_M [M^{-1} s^{-1}]	$(k_{cat}/K_M)_{variant}/_{wt}$
wt	1.2 ± 0.1 x 10^{-1}	5.9 ± 0.2 x 10^{-1}	5.0 ± 0.5 x 10^{3}	1.0
E43A	1.0 ± 0.1 x 10^{-1}	8.6 ± 0.2 x 10^{-1}	8.5 ± 0.8 x 10^{3}	1.7
E43K	4.3 ± 1.2 x 10^{-2}	1.8 ± 0.1 x 10^{-1}	4.1 ± 1.2 x 10^{3}	0.8
E72R	4.4 ± 1.4 x 10^{-2}	3.5 ± 0.3 x 10^{-1}	8.0 ± 2.7 x 10^{3}	1.6
Y154A	9.0 ± 1.3 x 10^{-2}	4.5 ± 0.2 x 10^{-1}	5.0 ± 0.8 x 10^{3}	1.0
Y154R	1.7 ± 0.7 x 10^{-1}	1.2 ± 0.2	7.3 ± 3.1 x 10^{3}	1.5

Supplementary Table S6: FAME data

Activity (mg FAMEs/g bacteria)

WT	Lid	E43A	E43K	S113A	Y154R	WT2	Y154A
0,4499	0,2568	0,8950	0,4008	0,2835	0,6647	2,6032	2,7885
0,4132	0,3726	0,8710	0,3757	0,2933	0,7022	2,4927	2,5948
0,4515	0,3500	0,7370	0,2559	0,1822	0,3148	3,4162	3,0043
0,4360	0,2076		0,2575				2,5359
0,3826	0,3964						
0,3663	0,2682						
	0,1863						

Normalized activity (Ratio mutant/WT)

WT	Lid	E43A	E43K	S113A	Y154R	WT2	Y154A
1,080	0,616	2,148	0,962	0,680	1,595	0,917	0,983
0,992	0,894	2,091	0,902	0,704	1,686	0,879	0,915
1,084	0,840	1,769	0,614	0,437	0,756	1,204	1,059
1,046	0,498		0,618				0,894
0,918	0,952						
0,879	0,644						
	0,447						

Normalized activity (Ratio mutant/WT)

WT	**Lid**	**E43A**	**E43K**	**S113A**	**Y154A**	**Y154R**
1,080	0,616	2,148	0,962	0,680	0,983	1,595
0,992	0,894	2,091	0,902	0,704	0,915	1,686
1,084	0,840	1,769	0,614	0,437	1,059	0,756
1,046	0,498		0,618		0,894	
0,918	0,952					
0,879	0,644					
	0,447					

Normalized activity (Ratio mutant/WT) REPORTED ON the GRAPH

1,000	0,699	2,003	0,774	0,607	0,963	1,346	**MEAN**
0,086	0,198	0,204	0,184	0,148	0,075	0,513	**SD**
	0,0055	< 0,0001	0,0288	0,0013	0,4985	0,1285	**p value vs WT**
	**	****	*	**	ns	ns	p value summary

Supplementary Table S7: Sequences producing significant alignments with *Tth* (UNIPROT code: I9KU82)

	Score	E Value	Phylum
UR50:UniRef50_G2MWQ3 Alpha/beta hydrolase fold containing protein ...	513	0.0	Clostridia
UR50:UniRef50_A0A1I5TFW2 Hydrolase_4 domain-containing protein n=1...	266	5,00E-87	Clostridia
UR50:UniRef50_A0A1M6CI71 Peptidase_S9 domain-containing protein n=...	263	2,00E-85	Firmicutes
UR50:UniRef50_A0A1W1X6Q3 Hydrolase_4 domain-containing protein n=5...	245	2,00E-78	Clostridia
UR50:UniRef50_UPI000B980ED8alpha/beta fold hydrolase n=1 Tax=Petr...	229	2,00E-72	Clostridia
UR50:UniRef50_A0A177ZKP7Alpha/beta hydrolase n=17 Tax=Firmicutes ...	228	7,00E-72	Firmicutes
UR50:UniRef50_A0A355RZC9Alpha/beta hydrolase n=1 Tax=Clostridiace...	223	4,00E-70	Clostridia
UR50:UniRef50_A0A0C2UJT1 Peptidase_S9 domain-containing protein n=...	221	6,00E-69	Cohnella
UR50:UniRef50_T0BRH7 Hydrolase_4 domain-containing protein n=40 Ta...	216	5,00E-67	Firmicutes
UR50:UniRef50_A0A353N5E8Alpha/beta hydrolase n=6 Tax=Firmicutes T...	216	6,00E-67	Firmicutes
UR50:UniRef50_A0A0A8X650Alpha/beta superfamily hydrolase n=3 Tax=...	214	2,00E-66	Firmicutes
UR50:UniRef50_A0A660RIT6Alpha/beta hydrolase n=4 Tax=Thermotogae ...	209	2,00E-64	Thermotogae
UR50:UniRef50_A0A660TFB6Alpha/beta hydrolase n=2 Tax=Spirochaetes...	209	3,00E-64	Spirochaetes
UR50:UniRef50_A0A285CSW9 Hydrolase_4 domain-containing protein n=5...	208	5,00E-64	Firmicutes
UR50:UniRef50_UPI000A26B42Dalpha/beta hydrolase n=1 Tax=Clostridi...	205	1,00E-62	Clostridia
UR50:UniRef50_A0A6N7M3G8Alpha/beta fold hydrolase n=3 Tax=root Ta...	201	3,00E-61	
UR50:UniRef50_D1CF13 Dienelactone hydrolase n=1 Tax=Thermobaculum ...	200	6,00E-61	Chloroflexi
UR50:UniRef50_A0A1M6M0X5 Hydrolase_4 domain-containing protein n=7...	200	6,00E-61	
UR50:UniRef50_A0A1G6GNU3 Hydrolase_4 domain-containing protein n=3...	200	8,00E-61	Firmicutes
UR50:UniRef50_A0A1I2SBI9 Hydrolase_4 domain-containing protein n=4...	197	7,00E-60	Firmicutes
UR50:UniRef50_A0A173U362 Acetoin dehydrogenase E2 subunit dihydrol...	194	2,00E-58	Firmicutes
UR50:UniRef50_A0A101IKX3 Hydrolase of the alpha/beta superfamily-l...	193	3,00E-58	Parcubacteria
UR50:UniRef50_H8XW45 Carboxylesterase n=8 Tax=Bacteria TaxID=2 Rep...	192	5,00E-58	

UR50:UniRef50_C7N773 Peptidase_S9 domain-containing protein n=29 T...	187	1,00E-55	Actinobacteria
UR50:UniRef50_A0A7C2XQZ5Alpha/beta fold hydrolase n=5 Tax=root Ta...	185	4,00E-55	
UR50:UniRef50_UPI0004788E77alpha/beta hydrolase n=1 Tax=Alicyclob...	183	4,00E-54	Firmicutes
UR50:UniRef50_A0A0S7X983 Peptidase_S9 domain-containing protein n=...	182	9,00E-54	Planctomycetes
UR50:UniRef50_A0A7C3MWS3Alpha/beta fold hydrolase n=1 Tax=Firmicu...	181	1,00E-53	Firmicutes
UR50:UniRef50_A0A2V9K2M2Alpha/beta hydrolase n=8 Tax=Acidobacteri...	180	4,00E-53	Acidobacteria
UR50:UniRef50_A0A350X132Alpha/beta hydrolase n=1 Tax=Firmicutes b...	179	7,00E-53	Firmicutes
UR50:UniRef50_A0A1F7FLL2 Hydrolase_4 domain-containing protein n=1...	178	3,00E-52	
UR50:UniRef50_A0A7C6UT48Alpha/beta fold hydrolase n=1 Tax=Firmicu...	177	5,00E-52	Firmicutes
UR50:UniRef50_A0A0L8F3E0 Hydrolase_4 domain-containing protein n=2...	176	8,00E-52	Clostridia
UR50:UniRef50_B8E2K8 Dienelactone hydrolase n=8 Tax=Dictyoglomus T...	177	8,00E-52	Firmicutes
UR50:UniRef50_X1B567 Peptidase_S9 domain-containing protein n=1 Ta...	173	7,00E-51	
UR50:UniRef50_A0A3Q9HNM1 Peptidase_S9 domain-containing protein n=...	174	1,00E-50	Firmicutes
UR50:UniRef50_A0A1W9SG40 Peptidase_S9 domain-containing protein n=...	174	2,00E-50	
UR50:UniRef50_A0A1F9X5K1 Peptidase_S9 domain-containing protein n=...	173	3,00E-50	Elusimicrobia
UR50:UniRef50_A0A1G9X0F9 Hydrolase_4 domain-containing protein n=3...	172	7,00E-50	Firmicutes
UR50:UniRef50_A0A660R9K6Alpha/beta hydrolase n=1 Tax=Thermotoga s...	172	7,00E-50	Thermotoga
UR50:UniRef50_B9E0E1 AB hydrolase-1 domain-containing protein n=6 ...	172	7,00E-50	Clostridia
UR50:UniRef50_A0A1T4P9G4 Peptidase_S9 domain-containing protein n=...	171	1,00E-49	Firmicutes
UR50:UniRef50_A0A1H8CGU1 AB hydrolase-1 domain-containing protein ...	171	2,00E-49	Firmicutes
UR50:UniRef50_A0A386H4I4Alpha/beta hydrolase n=2 Tax=unclassified...	171	2,00E-49	Clostridia
UR50:UniRef50_D7RU28 Ferulic acid esterase n=2 Tax=Lactobacillus b...	170	3,00E-49	Firmicutes
UR50:UniRef50_A0A1V6BNQ8 Non-heme bromoperoxidase BPO-A1 n=1 Tax=T...	169	9,00E-49	Tenericutes
UR50:UniRef50_A0A0G2ZFB4 Peptidase_S9 domain-containing protein n=...	165	2,00E-47	Thermotogae
UR50:UniRef50_A0A143WVC9 Putative aminoacrylate hydrolase RutD n=2...	162	2,00E-46	Clostridia

UR50:UniRef50_A0A7C6N4Z9Alpha/beta fold hydrolase n=1 Tax=Acholep...	162	2,00E-46	Firmicutes
UR50:UniRef50_A0A7C5K5D5Alpha/beta fold hydrolase n=2 Tax=Verruco...	163	3,00E-46	Verrucomicrobia
UR50:UniRef50_B1BZ56 Hydrolase_4 domain-containing protein n=54 Ta...	162	3,00E-46	Firmicutes
UR50:UniRef50_A0A3D6D8K7Alpha/beta hydrolase n=14 Tax=Thermotogae...	162	4,00E-46	Thermotogae
UR50:UniRef50_A0A7C5IFR0Alpha/beta hydrolase n=1 Tax=bacterium Ta...	162	6,00E-46	
UR50:UniRef50_A0A3M2F2U0Alpha/beta fold hydrolase n=1 Tax=Candida...	163	1,00E-45	
UR50:UniRef50_A0A0S8HFA0 Peptidase_S9 domain-containing protein n=...	161	1,00E-45	Planctomycetes
UR50:UniRef50_A0A2H5WXV4 2-succinyl-6-hydroxy-2, 4-cyclohexadiene-...	160	2,00E-45	
UR50:UniRef50_A0A6J4MJQ0 Peptidase_S9 domain-containing protein n=...	159	7,00E-45	Chloroflexi
UR50:UniRef50_A0A1F5UGK4 Uncharacterized protein n=1 Tax=Candidatu...	157	2,00E-44	
UR50:UniRef50_A0A1V4QWG9 Peptidase_S9 domain-containing protein n=...	157	2,00E-44	
UR50:UniRef50_A0A7C1E965Alpha/beta fold hydrolase (Fragment) n=1 ...	159	4,00E-44	Firmicutes
UR50:UniRef50_A0A1Y4GAT0 Peptidase_S9 domain-containing protein n=...	156	9,00E-44	Synergistetes
UR50:UniRef50_A0A399FFE0 Esterase EstD n=1 Tax=Meiothermus granati...	156	1,00E-43	Deinococcus
UR50:UniRef50_A0A1G9G1K1 Hydrolase_4 domain-containing protein n=1...	155	2,00E-43	Actinobacteria
UR50:UniRef50_A0A496ABF8Alpha/beta hydrolase n=7 Tax=Candidatus P...	155	4,00E-43	
UR50:UniRef50_C9Z377 AB hydrolase-1 domain-containing protein n=30...	153	1,00E-42	Actinobacteria
UR50:UniRef50_A0A2H5V4E2 2-succinyl-6-hydroxy-2, 4-cyclohexadiene-...	151	4,00E-42	
UR50:UniRef50_UPI000C1BB749alpha/beta fold hydrolase n=1 Tax=Mini...	150	2,00E-41	Miniphocibacter
UR50:UniRef50_A0A1H6TBQ8 Hydrolase_4 domain-containing protein n=5...	149	4,00E-41	Deinococcus
UR50:UniRef50_A0A1F9XBG6 Peptidase_S9 domain-containing protein n=...	149	4,00E-41	Elusimicrobia
UR50:UniRef50_C0CTE6 Hydrolase_4 domain-containing protein n=5 Tax...	147	3,00E-40	Actinobacteria
UR50:UniRef50_A0A1V5Z8D4 Phosphoribosylformylglycinamidine cyclo-l...	154	4,00E-40	
UR50:UniRef50_A0A4R2RPK9 Hydrolase_4 domain-containing protein n=5...	146	1,00E-39	Firmicutes
UR50:UniRef50_A0A3R7ASF0Alpha/beta fold hydrolase n=9 Tax=Candida...	145	2,00E-39	

UR50:UniRef50_A0A1F3XTK4 Peptidase_S9 domain-containing protein n=...	145	2,00E-39	Proteobacteria
UR50:UniRef50_S9UDC0 Hydrolase_4 domain-containing protein n=13 Ta...	145	2,00E-39	Firmicutes
UR50:UniRef50_A0A0Q3VY12 Hydrolase_4 domain-containing protein n=4...	144	6,00E-39	Firmicutes
UR50:UniRef50_A0A559IWC1Alpha/beta fold hydrolase n=3 Tax=Paeniba...	143	1,00E-38	Firmicutes
UR50:UniRef50_A0A410QE23Alpha/beta fold hydrolase n=2 Tax=Tissier...	142	2,00E-38	Firmicutes
UR50:UniRef50_A0A3D5RJW5 Hydrolase_4 domain-containing protein n=4...	142	3,00E-38	Actinobacteria
UR50:UniRef50_W4Q095 Peptidase S15 n=1 Tax=Bacillus wakoensis JCM ...	141	7,00E-38	Firmicutes
UR50:UniRef50_UPI000C2348F2alpha/beta fold hydrolase n=1 Tax=Baci...	141	8,00E-38	Firmicutes
UR50:UniRef50_S2ZQT5 Hydrolase_4 domain-containing protein n=65 Ta...	140	2,00E-37	
UR50:UniRef50_A0A511N521Alpha/beta hydrolase n=4 Tax=Deinococcus ...	139	2,00E-37	Deinococcus
UR50:UniRef50_E0SNK2 Dienelactone hydrolase n=3 Tax=Ignisphaera ag...	139	2,00E-37	
UR50:UniRef50_A0A6L3VAP3Alpha/beta hydrolase n=3 Tax=Bacillales T...	140	2,00E-37	Firmicutes
UR50:UniRef50_F7JM98 Hydrolase_4 domain-containing protein n=3 Tax...	139	3,00E-37	Firmicutes
UR50:UniRef50_A0A3R7AJM1Alpha/beta fold hydrolase n=1 Tax=Candida...	142	4,00E-37	
UR50:UniRef50_A0A6N7INW5Alpha/beta fold hydrolase n=2 Tax=Desulfo...	139	6,00E-37	Thermodesulfobacteria
UR50:UniRef50_UPI0009EC19CCalpha/beta fold hydrolase n=1 Tax=Limn...	139	6,00E-37	
UR50:UniRef50_A0A562QML1 Peptidase_S9 domain-containing protein n=...	138	1,00E-36	
UR50:UniRef50_A0A7C4YG41Alpha/beta fold hydrolase n=5 Tax=Bacteri...	137	2,00E-36	
UR50:UniRef50_A0A2D5YTE8 Peptidase_S9 domain-containing protein n=...	137	3,00E-36	Planctomycetes
UR50:UniRef50_A0A7C2Z7G5Alpha/beta fold hydrolase n=1 Tax=Armatim...	139	7,00E-36	Armatimonadetes
UR50:UniRef50_U6SV57 Peptidase_S9 domain-containing protein n=4 Ta...	135	9,00E-36	Firmicutes
UR50:UniRef50_A0A7C5W765Alpha/beta fold hydrolase n=1 Tax=Plancto...	135	9,00E-36	Planctomycetes
UR50:UniRef50_A0A1V5Y0E8Fermentation/respiration switch protein n...	134	3,00E-35	
UR50:UniRef50_A0A1W1VKA4 Hydrolase_4 domain-containing protein n=2...	133	5,00E-35	Deinococcus
UR50:UniRef50_X1UDA6 Peptidase_S9 domain-containing protein (Fragm...	133	5,00E-35	

UR50:UniRef50_UPI0009EB71D7alpha/beta fold hydrolase n=2 Tax=Lagi...	133	9,00E-35	Firmicutes
UR50:UniRef50_A0A7C6Y8R1Alpha/beta hydrolase n=1 Tax=Acholeplasma...	132	1,00E-34	Firmicutes
UR50:UniRef50_A0A517YSM1Fermentation/respiration switch protein n...	132	1,00E-34	Planctomycetes
UR50:UniRef50_L1PMY6 Hydrolase_4 domain-containing protein n=37 Ta...	132	2,00E-34	Bacteroidetes
UR50:UniRef50_A0A4S8QDR3Alpha/beta fold hydrolase n=1 Tax=Glycomy...	134	2,00E-34	Glycomyces
UR50:UniRef50_A0A2V9JLX7Alpha/beta hydrolase (Fragment) n=1 Tax=A...	128	4,00E-34	Acidobacteria
UR50:UniRef50_A0A090CYN4 Peptidase_S9 domain-containing protein n=...	132	4,00E-34	Chlamydiae
UR50:UniRef50_C2BEE5 Hydrolase, alpha/beta domain protein n=20 Tax...	130	1,00E-33	Clostridia
UR50:UniRef50_A0A0E2H8K7 Hydrolase_4 domain-containing protein n=2...	129	1,00E-33	
UR50:UniRef50_A0A7C6HYB2Alpha/beta hydrolase n=2 Tax=Acholeplasma...	129	2,00E-33	Firmicutes
UR50:UniRef50_A0A094YYJ9 Hydrolase_4 domain-containing protein n=4...	129	2,00E-33	Firmicutes
UR50:UniRef50_UPI000DC1D062alpha/beta fold hydrolase n=1 Tax=Meso...	129	3,00E-33	Thermotogae
UR50:UniRef50_A0A2S0UCN1 Hydrolase_4 domain-containing protein n=5...	130	3,00E-33	Firmicutes
UR50:UniRef50_UPI000854E465alpha/beta fold hydrolase n=1 Tax=Cand...	129	3,00E-33	
UR50:UniRef50_A0A6M2A136 Esterase FrsA n=1 Tax=Chlamydiae bacteriu...	129	4,00E-33	Chlamydiae
UR50:UniRef50_A0A2M7QX46 Peptidase_S9 domain-containing protein n=...	128	4,00E-33	
UR50:UniRef50_UPI0002F3A25Dalpha/beta fold hydrolase n=2 Tax=Anae...	128	8,00E-33	Clostridia
UR50:UniRef50_A0A2Z4Y4K2Alpha/beta superfamily hydrolase n=2 Tax=...	127	2,00E-32	
UR50:UniRef50_A0A5N7IN55Alpha/beta hydrolase n=1 Tax=Clostridium ...	124	2,00E-32	Clostridia
UR50:UniRef50_A0A0A0C164Alpha/beta hydrolase n=2 Tax=Cellulomonas...	127	2,00E-32	Actinobacteria
UR50:UniRef50_F0RJ91 Hydrolase, putative n=4 Tax=Deinococcus TaxID...	126	3,00E-32	Deinococcus
UR50:UniRef50_A0A2N2PNJ1 AB hydrolase-1 domain-containing protein ...	127	5,00E-32	
UR50:UniRef50_D6YWC6 Peptidase_S9 domain-containing protein n=2 Ta...	125	7,00E-32	Chlamydiae
UR50:UniRef50_UPI00145F20CAalpha/beta fold hydrolase n=1 Tax=Bifi...	125	7,00E-32	Actinobacteria
UR50:UniRef50_A0A644TNS7 2-succinyl-6-hydroxy-2, 4-cyclohexadiene-...	125	2,00E-31	

UR50:UniRef50_A0A072MVI6 Hydrolase_4 domain-containing protein n=2...	124	2,00E-31	Actinobacteria
UR50:UniRef50_A0A256XMB4 Hydrolase_4 domain-containing protein n=4...	124	2,00E-31	
UR50:UniRef50_E6K0Z8 AB hydrolase-1 domain-containing protein n=6 ...	124	2,00E-31	Bacteroidetes
UR50:UniRef50_A0A2X2RLV4 Dihydrolipoyllysine-residue acetyltransfe...	124	3,00E-31	Bacteroidetes
UR50:UniRef50_A0A3G1KRL6 AB hydrolase-1 domain-containing protein ...	124	4,00E-31	Firmicutes
UR50:UniRef50_A3XN04 Hydrolase of alpha-beta family protein n=2 Ta...	124	7,00E-31	Bacteroidetes
UR50:UniRef50_Q6MCU6 Hydrolase_4 domain-containing protein n=6 Tax...	123	7,00E-31	Chlamydiae
UR50:UniRef50_A0A564TCI22-succinyl-6-hydroxy-2,4-cyclohexadiene-1...	122	8,00E-31	Actinobacteria
UR50:UniRef50_A0A0A6V9N7Alpha/beta hydrolase n=3 Tax=Bacillus Tax...	123	8,00E-31	
UR50:UniRef50_A0A7C1ISM4Alpha/beta hydrolase (Fragment) n=1 Tax=F...	120	1,00E-30	Firmicutes
UR50:UniRef50_S7SRT6Alpha/beta hydrolase family protein n=7 Tax=B...	122	1,00E-30	Firmicutes
UR50:UniRef50_A0A410QEI4Alpha/beta fold hydrolase n=2 Tax=Tissier...	122	1,00E-30	Firmicutes
UR50:UniRef50_UPI0011F069F2alpha/beta hydrolase n=2 Tax=Cellulomo...	122	1,00E-30	
UR50:UniRef50_A0A7C6Z9V6Alpha/beta hydrolase n=3 Tax=Bacteria Tax...	124	1,00E-30	
UR50:UniRef50_A0A1M3CT29 Peptidase_S9 domain-containing protein n=...	122	1,00E-30	Chlamydiae
UR50:UniRef50_S5ZG56 Hydrolase_4 domain-containing protein n=8 Tax...	121	2,00E-30	
UR50:UniRef50_A0A7C2V0M0Alpha/beta fold hydrolase n=2 Tax=TACK gr...	121	2,00E-30	
UR50:UniRef50_UPI00047F6E0Dalpha/beta fold hydrolase n=1 Tax=Dein...	117	2,00E-30	Deinococcus
UR50:UniRef50_A0A0F0LDC52-hydroxy-6-oxononadienedioate/2-hydroxy-...	121	3,00E-30	Actinobacteria
UR50:UniRef50_A0A0X8JGL0 Hydrolase_4 domain-containing protein n=3...	120	5,00E-30	Actinobacteria
UR50:UniRef50_C2CIF9 Hydrolase_4 domain-containing protein n=6 Tax...	120	7,00E-30	Clostridia
UR50:UniRef50_A0A1J4WQ76 Hydrolase_4 domain-containing protein n=3...	120	9,00E-30	
UR50:UniRef50_A0A318S4U1 Hydrolase_4 domain-containing protein n=3...	119	1,00E-29	Deinococcus
UR50:UniRef50_A0A7C2LD26Alpha/beta fold hydrolase n=1 Tax=Thermof...	124	2,00E-29	
UR50:UniRef50_A0A256XSA7 AB hydrolase-1 domain-containing protein ...	119	2,00E-29	

UR50:UniRef50_A0A2G9N4W7 Peptidase_S9 domain-containing protein n=...	119	3,00E-29	
UR50:UniRef50_F8KZH9 Hydrolase_4 domain-containing protein n=3 Tax...	119	3,00E-29	Chlamydiae
UR50:UniRef50_A0A4V4HPV7Alpha/beta fold hydrolase n=1 Tax=Glycomy...	120	5,00E-29	Actinobacteria
UR50:UniRef50_A0A517YUI7Alpha/beta hydrolase family protein n=1 T...	119	5,00E-29	Planctomycetes
UR50:UniRef50_J2I3F4 Hydrolase_4 domain-containing protein n=20 Ta...	118	7,00E-29	Firmicutes
UR50:UniRef50_A0A7C5DQC2Alpha/beta fold hydrolase (Fragment) n=1 ...	120	7,00E-29	
UR50:UniRef50_A0A2M8TDW9Alpha/beta hydrolase n=1 Tax=Clostridium ...	117	9,00E-29	Clostridia
UR50:UniRef50_A0A4P6M108 Aminoacrylate hydrolase RutD n=10 Tax=Ter...	117	9,00E-29	Actinobacteria
UR50:UniRef50_A0A2J0KW78 Peptidase_S9 domain-containing protein n=...	117	1,00E-28	Parcubacteria
UR50:UniRef50_A0A0G0A911 Peptidase_S9 domain-containing protein n=...	117	1,00E-28	
UR50:UniRef50_UPI00096DB779alpha/beta hydrolase n=1 Tax=Paenibaci...	117	1,00E-28	Firmicutes
UR50:UniRef50_UPI000D19F70Dalpha/beta fold hydrolase n=1 Tax=Stre...	115	1,00E-28	Actinobacteria
UR50:UniRef50_A0A3A0CXX4 Peptidase_S9 domain-containing protein n=...	118	1,00E-28	Planctomycetes
UR50:UniRef50_A0A662G586 Hydrolase_4 domain-containing protein n=2...	116	3,00E-28	
UR50:UniRef50_UPI0006931F19alpha/beta fold hydrolase n=1 Tax=Clos...	117	3,00E-28	Clostridia
UR50:UniRef50_A0A7C4VHZ4Alpha/beta fold hydrolase (Fragment) n=1 ...	112	4,00E-28	
UR50:UniRef50_I3E8P1 PGAP1 family protein n=3 Tax=Bacillus TaxID=1...	116	4,00E-28	
UR50:UniRef50_A0A1V5HKM8 2-hydroxy-6-oxo-6-(2'-aminophenyl)hexa-2,...	115	4,00E-28	Actinobacteria
UR50:UniRef50_A0A396KRW0Alpha/beta fold hydrolase n=3 Tax=Terraba...	115	5,00E-28	Actinobacteria
UR50:UniRef50_A0A1G9L876 AB hydrolase-1 domain-containing protein ...	115	5,00E-28	Actinobacteria
UR50:UniRef50_A0A1U7NRK1 Dienelactone hydrolase n=5 Tax=Deinococcu...	115	5,00E-28	Deinococcus
UR50:UniRef50_I9NRE5 Hydrolase_4 domain-containing protein n=1 Tax...	115	7,00E-28	Firmicutes
UR50:UniRef50_C0Z4X2 Hydrolase_4 domain-containing protein n=63 Ta...	115	8,00E-28	
UR50:UniRef50_A0A1I7IGP7 Peptidase_S9 domain-containing protein n=...	114	1,00E-27	Clostridia
UR50:UniRef50_A0A497FIW7 Peptidase_S9 domain-containing protein n=...	114	1,00E-27	

UR50:UniRef50_A0A662Q0B5 Peptidase_S15 domain-containing protein n...	114	2,00E-27	
UR50:UniRef50_C2ER94 Hydrolase_4 domain-containing protein n=1 Tax...	114	2,00E-27	Firmicutes
UR50:UniRef50_A0A380NMF6 Acetoin dehydrogenase E2 subunit dihydrol...	115	2,00E-27	Firmicutes
UR50:UniRef50_R5VL94 Uncharacterized protein n=1 Tax=Clostridium s...	114	2,00E-27	Clostridia
UR50:UniRef50_G9QH89 AB hydrolase-1 domain-containing protein n=15...	114	2,00E-27	Firmicutes
UR50:UniRef50_A0A1M3BBP6 Hydrolase_4 domain-containing protein n=1...	114	2,00E-27	Chlamydiae
UR50:UniRef50_A0A4V2I6X8Alpha/beta hydrolase n=1 Tax=Alteromonas ...	113	5,00E-27	Proteobacteria
UR50:UniRef50_A0A0Q3WN81 Hydrolase_4 domain-containing protein n=5...	112	8,00E-27	Firmicutes
UR50:UniRef50_A0A6N6L3B6Alpha/beta fold hydrolase n=1 Tax=Chlorof...	112	9,00E-27	Chloroflexi
UR50:UniRef50_A0A1H8RZ11 Hydrolase_4 domain-containing protein n=4...	112	1,00E-26	
UR50:UniRef50_A0A6M8SQ21Alpha/beta fold hydrolase n=3 Tax=Deefgea...	111	1,00E-26	Proteobacteria
UR50:UniRef50_A0A1H6I7Y9 Hydrolase_4 domain-containing protein n=3...	112	1,00E-26	
UR50:UniRef50_A0A0J1JD40 Peptidase_S15 domain-containing protein n...	112	2,00E-26	Proteobacteria
UR50:UniRef50_A0A5J6YNP1Alpha/beta fold hydrolase n=2 Tax=Deinoco...	114	2,00E-26	Deinococcus
UR50:UniRef50_A0A1I1JJ50 Hydrolase_4 domain-containing protein n=1...	111	2,00E-26	
UR50:UniRef50_D1QPE8 Antioxidant, AhpC/TSA family n=20 Tax=root Ta...	114	2,00E-26	
UR50:UniRef50_UPI0005C4D4D5alpha/beta hydrolase n=1 Tax=Prevotell...	111	3,00E-26	Bacteroidetes
UR50:UniRef50_A0A089LPB3 DLH domain-containing protein n=14 Tax=Fi...	113	3,00E-26	Firmicutes
UR50:UniRef50_A0A150LL17 Hydrolase_4 domain-containing protein n=2...	110	3,00E-26	Firmicutes
UR50:UniRef50_C3MSB7 Hydrolase of the alpha/beta superfamily n=6 T...	110	5,00E-26	
UR50:UniRef50_A0A1F5Z3K4 Hydrolase_4 domain-containing protein n=1...	110	5,00E-26	
UR50:UniRef50_UPI001177A7F4alpha/beta fold hydrolase n=2 Tax=uncl...	111	6,00E-26	Clostridia
UR50:UniRef50_A0A1H7GTL4 Hydrolase_4 domain-containing protein n=1...	110	6,00E-26	Firmicutes
UR50:UniRef50_UPI00101D386Balpha/beta fold hydrolase n=1 Tax=Bact...	113	6,00E-26	Bacteroidetes
UR50:UniRef50_A0A0E3H183 Feruloyl esterase n=1 Tax=uncultured micr...	110	7,00E-26	

UR50:UniRef50_U2BHA2 Hydrolase, alpha/beta domain protein n=9 Tax=...	109	7,00E-26	Firmicutes
UR50:UniRef50_A0A2D5Z891 Peptidase_S9 domain-containing protein n=...	109	8,00E-26	Bacteroidetes
UR50:UniRef50_A0A101X5F5 Peptidase_S9 domain-containing protein n=...	110	8,00E-26	
UR50:UniRef50_A0A497G9W0 Hydrolase_4 domain-containing protein (Fr...	107	1,00E-25	
UR50:UniRef50_A0A3N5SCD3Alpha/beta fold hydrolase (Fragment) n=1 ...	105	1,00E-25	Chloroflexi
UR50:UniRef50_A0A0M9GU80 Hydrolase_4 domain-containing protein n=3...	109	1,00E-25	Firmicutes
UR50:UniRef50_A0A2D5V1B3 Hydrolase_4 domain-containing protein n=1...	109	1,00E-25	
UR50:UniRef50_A0A133Z6N3 X-Pro dipeptidyl-peptidase n=1 Tax=Bacter...	109	1,00E-25	Bacteroidetes
UR50:UniRef50_UPI00166C434Dalpha/beta fold hydrolase n=2 Tax=Paen...	109	1,00E-25	Firmicutes
UR50:UniRef50_UPI00105DDEB9alpha/beta fold hydrolase n=4 Tax=Cand...	111	1,00E-25	
UR50:UniRef50_U1QU38 Hydrolase_4 domain-containing protein n=11 Ta...	110	2,00E-25	Actinobacteria
UR50:UniRef50_X0V080 Hydrolase_4 domain-containing protein (Fragme...	107	2,00E-25	
UR50:UniRef50_E6K5Q2 Hydrolase_4 domain-containing protein n=15 Ta...	110	2,00E-25	Bacteroidetes
UR50:UniRef50_A0A3D0N7L6 Uncharacterized protein n=1 Tax=Armatimon...	105	3,00E-25	Armatimonadetes
UR50:UniRef50_G6AH16 Hydrolase_4 domain-containing protein n=3 Tax...	109	3,00E-25	Bacteroidetes
UR50:UniRef50_A0A1F7Y214 Hydrolase_4 domain-containing protein n=3...	108	3,00E-25	
UR50:UniRef50_A0A4R1NQQ4 Peptidase_S15 domain-containing protein n...	108	4,00E-25	
UR50:UniRef50_A0A2H6EVT0Alpha/beta hydrolase family protein n=2 T...	107	4,00E-25	
UR50:UniRef50_A0A1M6HZI0 Hydrolase_4 domain-containing protein n=5...	108	4,00E-25	Clostridia
UR50:UniRef50_A0A0V8J792 Peptidase_S9 domain-containing protein n=...	108	4,00E-25	Firmicutes
UR50:UniRef50_A0A3S4VC53 Non-haem bromoperoxidase BPO-A2 n=86 Tax=...	107	5,00E-25	Actinobacteria
UR50:UniRef50_A0A1X7LL25 Hydrolase_4 domain-containing protein n=1...	108	5,00E-25	Proteobacteria
UR50:UniRef50_A0A4P6JQU8Alpha/beta fold hydrolase n=1 Tax=Ktedono...	107	6,00E-25	Chloroflexi
UR50:UniRef50_A0A1H6SYR9 Hydrolase_4 domain-containing protein n=2...	108	6,00E-25	Firmicutes
UR50:UniRef50_UPI00068FCB42alpha/beta fold hydrolase n=1 Tax=Haem...	108	7,00E-25	Proteobacteria

UR50:UniRef50_A0A0R1T798 Alpha beta fold family hydrolase family p...	107	8,00E-25	Firmicutes
UR50:UniRef50_A0A380JFQ6 Cinnamoyl ester hydrolase n=22 Tax=Strept...	107	8,00E-25	Firmicutes
UR50:UniRef50_A0A1H5RRD6 Hydrolase_4 domain-containing protein n=2...	107	9,00E-25	Firmicutes
UR50:UniRef50_A0A0G0K0B6Alpha/beta hydrolase fold protein n=6 Tax...	107	9,00E-25	Bacteroidetes
UR50:UniRef50_A0A255SZ99 Hydrolase_4 domain-containing protein n=3...	108	9,00E-25	Bacteroidetes
UR50:UniRef50_A0A223HZC4Alpha/beta superfamily hydrolase n=1 Tax=...	102	1,00E-24	Firmicutes
UR50:UniRef50_A0A165WGN5 Hydrolase_4 domain-containing protein n=7...	107	1,00E-24	Firmicutes
UR50:UniRef50_A0A3A9C967Alpha/beta fold hydrolase n=1 Tax=bacteri...	107	2,00E-24	
UR50:UniRef50_A0A271JE86 Hydrolase_4 domain-containing protein n=1...	106	2,00E-24	
UR50:UniRef50_A0A1H6F7Y1 Esterase n=1 Tax=Thiotrichales bacterium ...	106	2,00E-24	Proteobacteria
UR50:UniRef50_A0A081C1G4 Peptidase S15 n=4 Tax=Bacteria TaxID=2 Re...	106	2,00E-24	
UR50:UniRef50_A0A4Q5NDK7Alpha/beta hydrolase n=1 Tax=bacterium Ta...	105	2,00E-24	
UR50:UniRef50_A0A2G8DDL3 Peptidase_S15 domain-containing protein n...	107	2,00E-24	Mesotoga
UR50:UniRef50_A0A292YFF2 Permease n=3 Tax=Bacillales TaxID=1385 Re...	106	3,00E-24	Firmicutes
UR50:UniRef50_A0A0G1NYN3 Dienelactone hydrolase n=2 Tax=Microgenom...	105	3,00E-24	
UR50:UniRef50_A0A1I1U6X8 Peptidase_S9 domain-containing protein n=...	105	3,00E-24	Firmicutes
UR50:UniRef50_A0A6M1ZSY0 2-succinyl-6-hydroxy-2, 4-cyclohexadiene-...	105	4,00E-24	Chlamydiae
UR50:UniRef50_R5PAK8 Hydrolase_4 domain-containing protein n=3 Tax...	105	4,00E-24	Bacteroidales
UR50:UniRef50_A0A2X0RBE42-succinyl-6-hydroxy-2,4-cyclohexadiene-1...	105	4,00E-24	
UR50:UniRef50_A0A3N2MZV7Alpha/beta fold hydrolase n=4 Tax=Muribac...	108	6,00E-24	Bacteroidetes
UR50:UniRef50_A0A076IS58Alpha/beta fold hydrolase n=6 Tax=Bactero...	107	6,00E-24	Bacteroidales
UR50:UniRef50_A0A5J5HT44Alpha/beta hydrolase n=2 Tax=Bacillus Tax...	105	6,00E-24	
UR50:UniRef50_A0A353BU96 Peptidase_S9 domain-containing protein n=...	101	7,00E-24	Firmicutes
UR50:UniRef50_A0A6N7XJW8Alpha/beta fold hydrolase n=1 Tax=Clostri...	104	8,00E-24	Clostridia

UR50:UniRef50_A0A370AVS2 Peptidase_S9 domain-containing protein n=...	105	8,00E-24	
UR50:UniRef50_A0A2M8KL77 Hydrolase_4 domain-containing protein n=3...	104	1,00E-23	
UR50:UniRef50_A0A137SUL4 Putative esterase n=1 Tax=Clostridiales b...	107	1,00E-23	Clostridia
UR50:UniRef50_A0A7C5LB81Alpha/beta hydrolase n=1 Tax=Deltaproteob...	103	1,00E-23	Proteobacteria
UR50:UniRef50_A0A0D0SH11 TWA4_scaffold00001, whole genome shotgun ...	104	1,00E-23	Firmicutes
UR50:UniRef50_A0A1M5C420 Peptidase_S9 domain-containing protein n=...	104	1,00E-23	Proteobacteria
UR50:UniRef50_A0A4Y9FM63Alpha/beta hydrolase n=5 Tax=Streptococcu...	104	1,00E-23	Firmicutes
UR50:UniRef50_UPI00168B8E03alpha/beta fold hydrolase n=1 Tax=Baci...	103	2,00E-23	Firmicutes
UR50:UniRef50_A0A0U2W8A5Alpha/beta hydrolase n=2 Tax=Paenibacillu...	103	2,00E-23	Firmicutes
UR50:UniRef50_D9ZEN7 Peptidase_S9 domain-containing protein n=4 Ta...	103	2,00E-23	
UR50:UniRef50_A0A1F9I336 Peptidase_S9 domain-containing protein n=...	103	2,00E-23	
UR50:UniRef50_I2F4G1 LysM domain-containing protein,prolyl oligope...	104	3,00E-23	
UR50:UniRef50_F3P8S0 Carboxymuconolactone decarboxylase family pro...	107	3,00E-23	Actinomyces
UR50:UniRef50_A0A318KX93 Uncharacterized protein YhfF n=2 Tax=Diel...	107	3,00E-23	Firmicutes
UR50:UniRef50_A0A3P3XQ87 Peptidoglycan-binding lysin domain protei...	103	3,00E-23	Firmicutes
UR50:UniRef50_A0A2M7LW84 Hydrolase_4 domain-containing protein n=6...	103	4,00E-23	
UR50:UniRef50_UPI000783B427alpha/beta fold hydrolase n=1 Tax=Mass...	102	4,00E-23	Firmicutes
UR50:UniRef50_A0A1G7LLD5 Hydrolase_4 domain-containing protein n=6...	102	5,00E-23	
UR50:UniRef50_A0A564T726Fermentation/respiration switch protein n...	103	5,00E-23	Actinobacteria
UR50:UniRef50_L1P102 Hydrolase_4 domain-containing protein n=2 Tax...	99.8	5,00E-23	Bacteroidetes
UR50:UniRef50_A0A1H0BRC0 Peptidase_S9 domain-containing protein n=...	102	6,00E-23	Firmicutes
UR50:UniRef50_A0A661IDL4 Hydrolase_4 domain-containing protein n=7...	101	6,00E-23	
UR50:UniRef50_H3NGP5 Hydrolase_4 domain-containing protein n=5 Tax...	102	6,00E-23	Firmicutes
UR50:UniRef50_A0A6M1UEP4Alpha/beta hydrolase n=2 Tax=unclassified...	102	7,00E-23	Firmicutes
UR50:UniRef50_A0A1H9SN66 Peptidase_S9 domain-containing protein n=...	102	7,00E-23	Firmicutes

UR50:UniRef50_A0A6P1AI72 Prolyl oligopeptidase family serine pepti...	102	7,00E-23	
UR50:UniRef50_UPI0006CF9B7Dalpha/beta fold hydrolase n=1 Tax=Thal...	99.8	7,00E-23	Firmicutes
UR50:UniRef50_A0A3E0JMI5Alpha/beta hydrolase (Fragment) n=1 Tax=P...	99.0	7,00E-23	Firmicutes
UR50:UniRef50_A0A2E3QXW6Alpha/beta hydrolase n=1 Tax=Rhodothermac...	103	8,00E-23	Bacteroidetes
UR50:UniRef50_A0A6L3BG93 Hydrolase_4 domain-containing protein n=3...	102	9,00E-23	Firmicutes
UR50:UniRef50_A0A6N9I3X8Alpha/beta fold hydrolase n=2 Tax=Lactoba...	102	9,00E-23	Firmicutes
UR50:UniRef50_A0A5A7RTX7Alpha/beta fold hydrolase n=9 Tax=Thermop...	100	1,00E-22	
UR50:UniRef50_A0A2Z4L6Y5 Peptidase_S9 domain-containing protein n=...	101	1,00E-22	
UR50:UniRef50_A0A7C3Z5F7Alpha/beta hydrolase n=1 Tax=Deltaproteob...	100	1,00E-22	Proteobacteria
UR50:UniRef50_A0A1F6GWG6 Hydrolase_4 domain-containing protein n=8...	101	1,00E-22	Firmicutes
UR50:UniRef50_A0A357APR6 Peptidase_S9 domain-containing protein n=...	102	1,00E-22	Firmicutes
UR50:UniRef50_A0A024KFU3Alpha/beta superfamily hydrolase n=17 Tax...	101	2,00E-22	
UR50:UniRef50_F9ED99 Feruloyl esterase n=10 Tax=Actinomyces TaxID=...	102	2,00E-22	Actinomyces
UR50:UniRef50_UPI0012D8CA25alpha/beta fold hydrolase n=1 Tax=Paen...	100	2,00E-22	Firmicutes
UR50:UniRef50_A0A1G9S4D7 Hydrolase_4 domain-containing protein n=8...	100	2,00E-22	
UR50:UniRef50_A0A0G1H0A8 Carboxylesterase n=3 Tax=Parcubacteria gr...	100	2,00E-22	Parcubacteria
UR50:UniRef50_D9SNU3Alpha/beta superfamily hydrolase n=2 Tax=Clos...	101	2,00E-22	Clostridia
UR50:UniRef50_J4VLU0 Peptidase, S9A/B/C family, catalytic domain p...	101	2,00E-22	Bacteroidetes
UR50:UniRef50_A0A6M2ADF3 Multifunctional-autoprocessing repeats-in...	100	3,00E-22	Chlamydiae
UR50:UniRef50_A0A345Z1H0 Est1E (Fragment) n=52 Tax=Bacteria TaxID=...	100	3,00E-22	
UR50:UniRef50_A0A0U1P777 Hydrolase_4 domain-containing protein n=2...	100	3,00E-22	Proteobacteria
UR50:UniRef50_R5EN90 Hydrolase_4 domain-containing protein n=2 Tax...	100	3,00E-22	Proteobacteria
UR50:UniRef50_W0FQD8 Feruloyl esterase n=1 Tax=uncultured bacteriu...	101	3,00E-22	
UR50:UniRef50_UPI0014029154alpha/beta fold hydrolase n=1 Tax=Subd...	100	3,00E-22	Firmicutes
UR50:UniRef50_UPI00174C1BADalpha/beta fold hydrolase n=1 Tax=Cand...	103	4,00E-22	

UR50:UniRef50_S5XZS6 AB hydrolase-1 domain-containing protein n=16...	100	4,00E-22	Proteobacteria
UR50:UniRef50_UPI000C7C2368alpha/beta fold hydrolase n=1 Tax=Pygm...	100	4,00E-22	
UR50:UniRef50_A0A2G9N5X2 Peptidase_S9 domain-containing protein n=...	100	4,00E-22	
UR50:UniRef50_A0A2D6LJQ3 Peptidase_S9 domain-containing protein n=...	99.8	4,00E-22	
UR50:UniRef50_A0A2H0TBI0 Peptidase_S9 domain-containing protein n=...	100	4,00E-22	
UR50:UniRef50_A0A7C5TGY3Alpha/beta fold hydrolase (Fragment) n=2 ...	96.7	4,00E-22	
UR50:UniRef50_A0A7C4BFQ0Alpha/beta fold hydrolase (Fragment) n=1 ...	99.4	4,00E-22	
UR50:UniRef50_A0A7C3HHR4 Hydrolase_4 domain-containing protein (Fr...	97.8	5,00E-22	Bacteroidetes
UR50:UniRef50_A0A7D5Z3X2Alpha/beta fold hydrolase n=5 Tax=Chromob...	99.8	5,00E-22	Proteobacteria
UR50:UniRef50_UPI001370834Balpha/beta hydrolase n=1 Tax=Clostridi...	100	5,00E-22	Clostridia
UR50:UniRef50_A0A1M5JF38 Peptidase_S9 domain-containing protein n=...	100	5,00E-22	Proteobacteria
UR50:UniRef50_C6LBC1 Acetyl xylan esterase (AXE1) n=11 Tax=Bacteri...	100	5,00E-22	
UR50:UniRef50_U2LY33 Acetyl xylan esterase n=2 Tax=Treponema lecit...	101	5,00E-22	Spirochaetes
UR50:UniRef50_A0A223HZ34Alpha/beta superfamily hydrolase n=1 Tax=...	96.7	6,00E-22	Firmicutes
UR50:UniRef50_UPI0006B67ADEalpha/beta fold hydrolase n=1 Tax=Niam...	100	6,00E-22	Actinobacteria
UR50:UniRef50_A0A3N9NNQ0 Peptidase_S9 domain-containing protein n=...	99.4	7,00E-22	
UR50:UniRef50_A0A1C5ZT52 Prolyl tripeptidyl peptidase n=12 Tax=Clo...	100	7,00E-22	Clostridia
UR50:UniRef50_A0A3S4WJW1 Acetoin dehydrogenase E2 subunit dihydrol...	99.4	7,00E-22	Actinomyces
UR50:UniRef50_A0A0P9DTF9Alpha/beta hydrolase family protein n=1 T...	98.6	8,00E-22	
UR50:UniRef50_M2NDT4 Peptidase_S9 domain-containing protein n=3 Ta...	99.0	8,00E-22	Firmicutes
UR50:UniRef50_I8AKB0 PGAP1 family protein n=1 Tax=Fictibacillus ma...	99.4	9,00E-22	Firmicutes
UR50:UniRef50_E0E1U4 Hydrolase_4 domain-containing protein n=3 Tax...	99.0	1,00E-21	Firmicutes
UR50:UniRef50_Q822R5 Hydrolase_4 domain-containing protein n=71 Ta...	100	1,00E-21	Chlamydiae
UR50:UniRef50_A0A555ZF10Alpha/beta fold hydrolase n=5 Tax=Pantoea...	99.8	1,00E-21	Proteobacteria
UR50:UniRef50_A0A3R8MIT0Alpha/beta fold hydrolase n=1 Tax=Biberst...	99.4	1,00E-21	Proteobacteria

UR50:UniRef50_A0A4R4PJ68Alpha/beta fold hydrolase n=2 Tax=Strepto...	98.2	1,00E-21	Actinobacteria
UR50:UniRef50_A0A329NCT8Alpha/beta fold hydrolase n=19 Tax=Aeroco...	100	1,00E-21	Firmicutes
UR50:UniRef50_A0A1V6GYM0Alpha/beta hydrolase family protein n=1 T...	99.4	2,00E-21	Thermotogae
UR50:UniRef50_A0A1I4HQ83 Peptidase_S9 domain-containing protein n=...	98.6	2,00E-21	Firmicutes
UR50:UniRef50_A0A380K4G1 Cinnamoyl ester hydrolase n=2 Tax=Strepto...	98.6	2,00E-21	Firmicutes
UR50:UniRef50_A0A135YPI0 3-dehydroquinate dehydratase n=5 Tax=Pept...	101	2,00E-21	Firmicutes
UR50:UniRef50_J6HBL6 Peptidase, S9A/B/C family, catalytic domain p...	98.2	2,00E-21	Firmicutes
UR50:UniRef50_A0A0G0PZX8 Hydrolase of the alpha/beta superfamily n...	98.2	2,00E-21	
UR50:UniRef50_UPI0009340A05alpha/beta fold hydrolase n=1 Tax=Lact...	98.2	2,00E-21	Firmicutes
UR50:UniRef50_A0A437SCN9 Hydrolase_4 domain-containing protein n=2...	100	2,00E-21	Firmicutes
UR50:UniRef50_UPI000F7782A8alpha/beta fold hydrolase n=1 Tax=Lact...	99.4	2,00E-21	Firmicutes
UR50:UniRef50_A0A2E0L7X2Alpha/beta hydrolase n=1 Tax=Anaerolineac...	98.6	2,00E-21	Chloroflexi
UR50:UniRef50_UPI0009E6DB92alpha/beta hydrolase n=4 Tax=Leptotric...	98.6	2,00E-21	Fusobacteria
UR50:UniRef50_Q9Z923 Acyltransferase family n=7 Tax=Chlamydia TaxI...	98.2	3,00E-21	Chlamydiae
UR50:UniRef50_A0A0G1I5A7 Hydrolase n=2 Tax=Parcubacteria group Tax...	97.8	3,00E-21	Parcubacteria
UR50:UniRef50_A0A554MFT6 Hydrolase_4 domain-containing protein n=2...	97.4	4,00E-21	Parcubacteria
UR50:UniRef50_UPI0003F95ED9alpha/beta fold hydrolase n=1 Tax=Alic...	98.6	4,00E-21	Alicyclobacillus
UR50:UniRef50_S3XCK4 Hydrolase_4 domain-containing protein n=13 Ta...	98.6	4,00E-21	Actinobacteria
UR50:UniRef50_D3R4M0 Cinnamoyl ester hydrolase n=42 Tax=Bifidobact...	97.8	4,00E-21	Bifidobacterium
UR50:UniRef50_UPI0009DBBE97alpha/beta hydrolase n=1 Tax=Butyrivib...	97.8	4,00E-21	Firmicutes
UR50:UniRef50_A0A259UH65 Putative aminoacrylate hydrolase RutD n=8...	97.4	4,00E-21	Firmicutes
UR50:UniRef50_R5XBI4 Uncharacterized protein n=1 Tax=Anaerotruncus...	98.6	5,00E-21	Firmicutes
UR50:UniRef50_A0A0G1UCW1 Hydrolase_4 domain-containing protein n=3...	97.1	5,00E-21	
UR50:UniRef50_UPI0012B7D3BEalpha/beta hydrolase n=1 Tax=Paenibaci...	97.1	5,00E-21	Firmicutes
UR50:UniRef50_R5QHM6 Feruloyl esterase n=1 Tax=Ruminococcus sp. CA...	98.2	5,00E-21	Firmicutes

UR50:UniRef50_A0A7C4SRC4Alpha/beta fold hydrolase n=1 Tax=Candida...	95.9	5,00E-21	
UR50:UniRef50_A0A6L3TJK6Alpha/beta hydrolase n=2 Tax=Vibrionaceae...	97.4	6,00E-21	Proteobacteria
UR50:UniRef50_A0A3C0IYR8Alpha/beta hydrolase n=3 Tax=Firmicutes b...	97.8	6,00E-21	Firmicutes
UR50:UniRef50_A0A1Y0FS27 Hydrolase_4 domain-containing protein n=1...	97.8	6,00E-21	Proteobacteria
UR50:UniRef50_M8DB53 Hydrolase_4 domain-containing protein n=11 Ta...	97.1	7,00E-21	Firmicutes
UR50:UniRef50_A0A4S3B3M6Alpha/beta fold hydrolase n=2 Tax=Vagococ...	97.8	8,00E-21	Firmicutes
UR50:UniRef50_UPI0009FE83ABalpha/beta fold hydrolase n=1 Tax=Deme...	96.3	9,00E-21	Actinobacteria
UR50:UniRef50_A0A0J1IQ41 Hydrolase_4 domain-containing protein n=6...	96.3	1,00E-20	
UR50:UniRef50_UPI0009F92FE1alpha/beta fold hydrolase n=1 Tax=Alic...	96.7	1,00E-20	Alicyclobacillus
UR50:UniRef50_A6VR29 Cinnamoyl ester hydrolase n=1 Tax=Actinobacil...	96.7	1,00E-20	Proteobacteria
UR50:UniRef50_A0A260EDK6Alpha/beta hydrolase n=1 Tax=Rhodococcus ...	96.3	1,00E-20	Actinobacteria
UR50:UniRef50_A0A1T5IU94 Hydrolase_4 domain-containing protein n=1...	95.5	2,00E-20	Bacteroidetes
UR50:UniRef50_A0A3D2N8D8 Thioredoxin domain-containing protein (Fr...	97.1	2,00E-20	Bacteroidetes
UR50:UniRef50_A0A496Q2A4 Hydrolase_4 domain-containing protein n=3...	95.5	2,00E-20	Verrucomicrobia
UR50:UniRef50_A0A353SAF3 Cinnamoyl ester hydrolase n=2 Tax=Bacteri...	96.3	2,00E-20	
UR50:UniRef50_UPI00160DE3FAalpha/beta fold hydrolase n=1 Tax=Cate...	96.3	3,00E-20	Firmicutes
UR50:UniRef50_I3PVE7 Ferulic acid esterase 3 n=1 Tax=uncultured ba...	94.7	3,00E-20	
UR50:UniRef50_A0A1M4MW73 Putative alpha/beta hydrolase n=4 Tax=Don...	95.1	3,00E-20	Proteobacteria
UR50:UniRef50_C2EMB3 Feruloyl esterase n=53 Tax=Lactobacillus TaxI...	95.9	3,00E-20	Firmicutes
UR50:UniRef50_A0A1D2X1C7 Hydrolase_4 domain-containing protein n=1...	94.7	4,00E-20	Alicyclobacillus
UR50:UniRef50_UPI0004145E31alpha/beta hydrolase n=1 Tax=Ruminococ...	94.7	4,00E-20	Firmicutes
UR50:UniRef50_D1NU52 Hydrolase_4 domain-containing protein n=4 Tax...	95.1	4,00E-20	Bifidobacterium
UR50:UniRef50_UPI00040108C7alpha/beta fold hydrolase n=1 Tax=Alic...	95.1	4,00E-20	Alicyclobacillus
UR50:UniRef50_A0A3B9FYI3Alpha/beta hydrolase n=1 Tax=Erysipelotri...	94.7	4,00E-20	Firmicutes
UR50:UniRef50_A0A0Q5GFR9 AB hydrolase-1 domain-containing protein ...	94.4	4,00E-20	Proteobacteria

UR50:UniRef50_C5ESK4 Hydrolase_4 domain-containing protein n=11 Ta...	94.4	5,00E-20	Clostridiales
UR50:UniRef50_A0A0N0GPE5 Putative aminoacrylate hydrolase RutD n=4...	94.0	6,00E-20	Proteobacteria
UR50:UniRef50_A0A520KX16Alpha/beta fold hydrolase n=4 Tax=Candida...	93.2	6,00E-20	
UR50:UniRef50_UPI0015EF4CE9 hypothetical protein n=1 Tax=Paenactin...	94.0	6,00E-20	Actinomyces
UR50:UniRef50_A0A1F7UVW0 Hydrolase_4 domain-containing protein n=2...	94.0	7,00E-20	Parcubacteria
UR50:UniRef50_A0A1Y4KAL8 Hydrolase_4 domain-containing protein n=3...	95.1	8,00E-20	Actinobacteria
UR50:UniRef50_A0A6B1E4X9Alpha/beta hydrolase n=1 Tax=Chloroflexi ...	95.1	8,00E-20	Chloroflexi
UR50:UniRef50_C5NUM3 Feruloyl esterase n=5 Tax=Terrabacteria group...	94.7	9,00E-20	Actinobacteria
UR50:UniRef50_A0A0L0BGU9 Hydrolase_4 domain-containing protein n=1...	94.0	9,00E-20	Actinobacteria
UR50:UniRef50_A0A1G2U5D4 Hydrolase_4 domain-containing protein n=3...	93.6	9,00E-20	Proteobacteria
UR50:UniRef50_A0A561N4N3 Peptidase_S15 domain-containing protein n...	94.4	1,00E-19	Proteobacteria
UR50:UniRef50_A0A136LZ38Alpha/beta hydrolase family protein n=1 T...	93.2	1,00E-19	
UR50:UniRef50_A0A0V8S178 Hydrolase_4 domain-containing protein n=2...	93.2	1,00E-19	Actinobacteria
UR50:UniRef50_F9VK43 Hydrolase_4 domain-containing protein n=18 Ta...	93.6	1,00E-19	Firmicutes
UR50:UniRef50_A0A3G9JWI1 Cinnamoyl ester hydrolase n=1 Tax=Intesti...	94.0	1,00E-19	
UR50:UniRef50_A0A329LBX6Alpha/beta hydrolase n=1 Tax=Paenibacillu...	93.6	1,00E-19	Firmicutes
UR50:UniRef50_F6LQK6 Feruloyl esterase III n=1 Tax=Cellulosilyticu...	95.1	1,00E-19	Firmicutes
UR50:UniRef50_UPI0003F61EF9alpha/beta fold hydrolase n=2 Tax=Fuso...	93.6	2,00E-19	Fusobacteria
UR50:UniRef50_UPI0008F96E33alpha/beta fold hydrolase n=1 Tax=Trao...	93.2	2,00E-19	
UR50:UniRef50_A0A2N5M6E1Alpha/beta hydrolase n=2 Tax=Peribacillus...	93.2	2,00E-19	Firmicutes
UR50:UniRef50_A0A1H1LNM3 Hydrolase_4 domain-containing protein n=2...	93.2	2,00E-19	Verrucomicrobia
UR50:UniRef50_A0A559NLZ7 Hydrolase_4 domain-containing protein n=3...	92.8	2,00E-19	Proteobacteria
UR50:UniRef50_A0A177XJV8 Hydrolase_4 domain-containing protein n=1...	93.2	2,00E-19	Actinobacteria
UR50:UniRef50_A0A1D7QRA3Alpha/beta superfamily hydrolase n=1 Tax=...	92.8	2,00E-19	Firmicutes
UR50:UniRef50_A0A1F9LWW8 Hydrolase_4 domain-containing protein (Fr...	91.3	2,00E-19	Proteobacteria

UR50:UniRef50_R7CWQ7 Hydrolase_4 domain-containing protein n=17 Ta...	94.0	2,00E-19	Bacteroidetes
UR50:UniRef50_UPI000F794EF8alpha/beta fold hydrolase n=1 Tax=Agri...	93.2	2,00E-19	Firmicutes
UR50:UniRef50_S3JS07 Peptidase_S9 domain-containing protein n=9 Ta...	93.2	2,00E-19	
UR50:UniRef50_A0A1I2U708 Hydrolase_4 domain-containing protein n=1...	92.4	3,00E-19	Firmicutes
UR50:UniRef50_A0A497N1W1 Hydrolase_4 domain-containing protein (Fr...	93.2	3,00E-19	
UR50:UniRef50_UPI00166AE99Falpha/beta hydrolase n=1 Tax=Paenibaci...	92.8	3,00E-19	Firmicutes
UR50:UniRef50_D7CN41 Putative hydrolase n=1 Tax=Syntrophothermus l...	92.4	3,00E-19	Firmicutes
UR50:UniRef50_A0A662FA48 Hydrolase_4 domain-containing protein n=1...	92.4	3,00E-19	
UR50:UniRef50_UPI0015FC81A4alpha/beta fold hydrolase n=1 Tax=Limo...	92.8	3,00E-19	Firmicutes
UR50:UniRef50_A0A202DGJ1 Uncharacterized protein n=1 Tax=archaeon ...	92.0	3,00E-19	
UR50:UniRef50_A0A1H7FMX4 Hydrolase_4 domain-containing protein n=2...	92.0	3,00E-19	
UR50:UniRef50_UPI0011E59630alpha/beta fold hydrolase n=2 Tax=Neis...	92.4	3,00E-19	Proteobacteria
UR50:UniRef50_A0A0R1W5M7 Alpha-beta superfamily hydrolase n=2 Tax=...	92.4	3,00E-19	Firmicutes
UR50:UniRef50_A0A1G9NTZ2 Peptidase_S9 domain-containing protein n=...	92.4	3,00E-19	Actinobacteria
UR50:UniRef50_A0A0M2PHI3 Hydrolase_4 domain-containing protein n=5...	91.7	3,00E-19	
UR50:UniRef50_UPI0013694A57alpha/beta fold hydrolase n=1 Tax=Lact...	91.7	4,00E-19	Firmicutes
UR50:UniRef50_A0A1F9C1G2 Hydrolase_4 domain-containing protein n=6...	91.7	4,00E-19	Proteobacteria
UR50:UniRef50_UPI0004149386alpha/beta hydrolase n=3 Tax=unclassif...	90.9	5,00E-19	Firmicutes
UR50:UniRef50_A0A1F6H6E8 Hydrolase_4 domain-containing protein n=9...	91.3	5,00E-19	
UR50:UniRef50_A0A1E5XPH1 Peptidase_S15 domain-containing protein n...	92.4	5,00E-19	Proteobacteria
UR50:UniRef50_A0A2H0SXA8 Peptidase_S9 domain-containing protein n=...	91.7	5,00E-19	
UR50:UniRef50_A0A4P8L0E3Alpha/beta fold hydrolase n=2 Tax=Desulfo...	92.0	5,00E-19	Proteobacteria
UR50:UniRef50_A0A1Q5PUB6 Hydrolase_4 domain-containing protein n=3...	93.2	6,00E-19	Actinobacteria
UR50:UniRef50_A0A2N0Z197Alpha/beta hydrolase n=2 Tax=Bacillus nea...	91.7	6,00E-19	Firmicutes
UR50:UniRef50_Q74J82 Hydrolase_4 domain-containing protein n=32 Ta...	91.3	6,00E-19	Actinobacteria

UR50:UniRef50_A0A5R8QFL6 Uncharacterized protein n=1 Tax=Firmicute...	90.9	7,00E-19	Firmicutes
UR50:UniRef50_UPI00143C4720alpha/beta fold hydrolase n=1 Tax=Anae...	91.3	7,00E-19	Firmicutes
UR50:UniRef50_A0A3D0XXE5 Hydrolase_4 domain-containing protein n=1...	91.3	7,00E-19	Clostridiales
UR50:UniRef50_A0A2T6DB01 Hydrolase_4 domain-containing protein n=1...	93.2	8,00E-19	Verrucomicrobia
UR50:UniRef50_A0A430JHL9Alpha/beta fold hydrolase n=1 Tax=Paeniba...	94.4	8,00E-19	Firmicutes
UR50:UniRef50_W0FJ07 Cinnamoyl ester hydrolase n=1 Tax=uncultured ...	90.9	8,00E-19	
UR50:UniRef50_A0A2K1P362 Peptidase_S9 domain-containing protein n=...	92.0	9,00E-19	Thermotogae
UR50:UniRef50_A0A074LQC2 Peptidase_S9 domain-containing protein n=...	91.3	9,00E-19	Actinobacteria
UR50:UniRef50_A0A2H0V175 Hydrolase_4 domain-containing protein n=1...	90.5	1,00E-18	
UR50:UniRef50_P94315 CinII n=3 Tax=Lachnospiraceae TaxID=186803 Re...	91.3	1,00E-18	Firmicutes
UR50:UniRef50_A0A2N1SD64 Peptidase_S9 domain-containing protein n=...	91.3	1,00E-18	Spirochaetes
UR50:UniRef50_A0A3D0Y834 Hydrolase_4 domain-containing protein n=1...	91.3	1,00E-18	Clostridiales
UR50:UniRef50_A0A0G0YHJ5 PGAP1 family protein n=1 Tax=candidate di...	90.5	1,00E-18	
UR50:UniRef50_S3KMF3 Hydrolase_4 domain-containing protein n=17 Ta...	91.7	1,00E-18	Spirochaetes
UR50:UniRef50_A0A1F7HDY9 Hydrolase_4 domain-containing protein n=1...	90.5	1,00E-18	
UR50:UniRef50_A0A1F5YRD1 Hydrolase_4 domain-containing protein n=2...	89.7	1,00E-18	
UR50:UniRef50_X1B6J5 Hydrolase_4 domain-containing protein n=1 Tax...	90.1	2,00E-18	metagenome
UR50:UniRef50_A0A0E1XTM6Phospholipase/carboxylesterase n=11 Tax=F...	90.1	2,00E-18	Firmicutes
UR50:UniRef50_UPI0018964F2Aalpha/beta fold hydrolase n=1 Tax=Clos...	91.3	2,00E-18	Clostridia
UR50:UniRef50_A0A3N5X457Alpha/beta fold hydrolase n=2 Tax=Acidoba...	90.5	2,00E-18	Acidobacteria
UR50:UniRef50_A0A350J963Alpha/beta hydrolase n=1 Tax=Clostridiale...	90.9	2,00E-18	Clostridiales
UR50:UniRef50_A0A397S100 Hydrolase_4 domain-containing protein n=1...	89.7	2,00E-18	Tenericutes
UR50:UniRef50_F7V472 Hydrolase_4 domain-containing protein n=2 Tax...	90.9	2,00E-18	Clostridiales
UR50:UniRef50_A0A357FXM6 Uncharacterized protein n=1 Tax=Rhodospir...	90.5	2,00E-18	Proteobacteria
UR50:UniRef50_A0A0M0G2K1 AB hydrolase-1 domain-containing protein ...	90.1	2,00E-18	Actinobacteria

UR50:UniRef50_I8R858 Lysophospholipase L2 n=276 Tax=Firmicutes Tax...	89.7	2,00E-18	Firmicutes
UR50:UniRef50_A0A1F6GXQ6 Hydrolase_4 domain-containing protein n=2...	89.4	3,00E-18	
UR50:UniRef50_A0A1I6KBM2 Uncharacterized protein n=2 Tax=Clostridi...	90.1	3,00E-18	Clostridiales
UR50:UniRef50_A0A1F6JW03 Peptidase_S9 domain-containing protein n=...	89.4	3,00E-18	
UR50:UniRef50_UPI001302B074alpha/beta fold hydrolase n=1 Tax=Neie...	90.5	3,00E-18	
UR50:UniRef50_B9JMY9 Peptidase_S15 domain-containing protein n=34 ...	90.1	4,00E-18	Proteobacteria
UR50:UniRef50_A0A0R1M4F8 Hydrolase_4 domain-containing protein n=4...	89.4	4,00E-18	Firmicutes
UR50:UniRef50_A0A2D6NUQ7 Hydrolase_4 domain-containing protein n=1...	89.4	4,00E-18	
UR50:UniRef50_A0A1G1WQF5 Peptidase_S9 domain-containing protein n=...	89.4	4,00E-18	
UR50:UniRef50_A0A7C3E629Alpha/beta fold hydrolase n=2 Tax=Proteob...	89.0	5,00E-18	Proteobacteria
UR50:UniRef50_J8ZQX3 DLH domain-containing protein n=7 Tax=Bacilla...	89.4	5,00E-18	Firmicutes
UR50:UniRef50_A0A661KJ40 Hydrolase_4 domain-containing protein n=5...	88.6	5,00E-18	Proteobacteria
UR50:UniRef50_B9Y2M8 Hydrolase_4 domain-containing protein n=4 Tax...	90.1	5,00E-18	Firmicutes
UR50:UniRef50_A0A3A4QXA2Alpha/beta hydrolase n=1 Tax=Candidatus A...	89.0	5,00E-18	
UR50:UniRef50_UPI0005094091alpha/beta fold hydrolase n=1 Tax=Haem...	87.8	5,00E-18	Proteobacteria
UR50:UniRef50_A0A3N2D7Y1 Hydrolase_4 domain-containing protein n=3...	90.1	5,00E-18	Actinobacteria
UR50:UniRef50_A0A2H0RIP5 Hydrolase_4 domain-containing protein n=1...	89.0	6,00E-18	
UR50:UniRef50_A0A3D9TET4 Hydrolase_4 domain-containing protein n=1...	89.0	6,00E-18	Actinobacteria
UR50:UniRef50_A0A367GEL2 AB hydrolase-1 domain-containing protein ...	90.1	6,00E-18	
UR50:UniRef50_A0A2J0KVP3 Hydrolase_4 domain-containing protein n=1...	87.0	6,00E-18	Parcubacteria
UR50:UniRef50_A0A2M7V3Q0 Hydrolase_4 domain-containing protein n=1...	88.6	6,00E-18	
UR50:UniRef50_UPI0017489C35alpha/beta fold hydrolase n=2 Tax=Cand...	88.6	8,00E-18	
UR50:UniRef50_A0A259T3W1 Hydrolase_4 domain-containing protein n=7...	88.6	8,00E-18	Firmicutes
UR50:UniRef50_A0A559Q1I7 Hydrolase_4 domain-containing protein n=6...	89.0	9,00E-18	Proteobacteria
UR50:UniRef50_A0A358M881 Uncharacterized protein n=1 Tax=Clostridi...	90.5	9,00E-18	Clostridiales

UR50:UniRef50_A0A1F6ZG60 Uncharacterized protein n=1 Tax=Candidatu...	88.2	9,00E-18	
UR50:UniRef50_A0A3A4KEE1Alpha/beta hydrolase n=1 Tax=Myxococcales...	88.2	1,00E-17	Proteobacteria
UR50:UniRef50_A0A173XYS6 Trifunctional nucleotide phosphoesterase ...	91.3	1,00E-17	
UR50:UniRef50_A0A256ZTN4 Peptidase_S9 domain-containing protein n=...	88.2	1,00E-17	
UR50:UniRef50_A0A4V1ALQ1Alpha/beta fold hydrolase n=1 Tax=Acetila...	87.8	1,00E-17	Firmicutes
UR50:UniRef50_A0A1Y4RKX6 Uncharacterized protein n=1 Tax=Lachnoclo...	90.5	1,00E-17	Clostridia
UR50:UniRef50_R2XTC0 Hydrolase_4 domain-containing protein n=2 Tax...	89.0	1,00E-17	Firmicutes
UR50:UniRef50_R7KXY0 Uncharacterized protein n=2 Tax=environmental...	90.9	1,00E-17	
UR50:UniRef50_A0A6L9HLT7Alpha/beta fold hydrolase n=1 Tax=Lachnos...	86.3	1,00E-17	Firmicutes
UR50:UniRef50_A0A1Q4AZQ5 Hydrolase_4 domain-containing protein n=1...	87.8	1,00E-17	Firmicutes
UR50:UniRef50_A0A1A5I0W9 Hydrolase_4 domain-containing protein n=6...	88.6	1,00E-17	Proteobacteria
UR50:UniRef50_A0A383S8V0 Acetoin dehydrogenase E2 subunit dihydrol...	87.8	1,00E-17	Actinobacteria
UR50:UniRef50_A0A1Q6PVL0 Hydrolase_4 domain-containing protein n=1...	88.2	1,00E-17	Firmicutes
UR50:UniRef50_A0A0R2LSN0 Hydrolase_4 domain-containing protein n=3...	87.8	1,00E-17	Firmicutes
UR50:UniRef50_A0A1I4W7R2 Peptidase_S9 domain-containing protein n=...	88.2	1,00E-17	Bacteroidetes
UR50:UniRef50_M2NG07 Hydrolase_4 domain-containing protein n=3 Tax...	88.2	2,00E-17	Firmicutes
UR50:UniRef50_A0A6G0ZTI9 Lipase 1 n=2 Tax=Andreprevotia TaxID=3972...	87.4	2,00E-17	
UR50:UniRef50_A0A0G0JDF6 Peptidase_S9 domain-containing protein n=...	87.4	2,00E-17	
UR50:UniRef50_A0A387BUD8Alpha/beta fold hydrolase n=2 Tax=Microba...	88.6	2,00E-17	Actinobacteria
UR50:UniRef50_A0A646JSY2Alpha/beta hydrolase n=3 Tax=Lactobacilla...	87.4	2,00E-17	Firmicutes
UR50:UniRef50_A0A151BXR6 AB hydrolase-1 domain-containing protein ...	87.4	2,00E-17	Actinobacteria
UR50:UniRef50_A0A6N9Q4P4Alpha/beta hydrolase n=2 Tax=Chengkuizeng...	87.8	2,00E-17	
UR50:UniRef50_A0A3G8ZMP4 Hydrolase_4 domain-containing protein n=2...	89.0	2,00E-17	Actinobacteria
UR50:UniRef50_A0A351U0D7 Peptidase_S9 domain-containing protein n=...	87.4	2,00E-17	Proteobacteria
UR50:UniRef50_A0A0K9R3E3 Hydrolase_4 domain-containing protein n=1...	87.4	2,00E-17	

UR50:UniRef50_UPI00067B2E5Balpha/beta fold hydrolase n=1 Tax=Olse...	87.8	2,00E-17	Actinobacteria
UR50:UniRef50_A0A0S2W8M7 5'-nucleotidase n=8 Tax=Clostridiales Tax...	90.1	3,00E-17	Clostridiales

Legend Supplementary Table S7: A search against the UniProtKB50 protein sequence data base revealed the top scoring 1000 sequence families with a minimal threshold score of 70 and an E value of 7 x 10-and archaeal phyla, to the extent organisms of origin were unambiguously determined.

Supplementary Table S8: *Tth* MGL sequence/structure relations to other α/β hydrolases

Sequence ID	Protein name	Organism	Phylum	Reference	Score[a]	E value[a]	PDB ID[b,c]	Q score[b]	Rmsd[b]	Seq. identity[b]	Lid[d] type	Lid length[d]	Assembly
I9KU82	Monoacylglycerol lipase	*T. siderophilus*	Firmicutes				7Q4J				HBH	43	Dimer
D3YEX6	Cinnamoyl esterase	*L. johnsonii*	Firmicutes	[14]	117,00	1,00E-31	3S2Z*	0,72	1,18	0,32	HBH	46	Dimer
D2YW37	Feruloyl esterase	*B. proteoclasticus*	Firmicutes	[13]	102,00	1,00E-25	2WTM*	0,68	1,31	0,30	HBH	46	Dimer
D0MHY8	Osmotically inducible protein C	*R. marinus*	Bacteroidetes	[15]	82,00	2,00E-17	5CML	0,44	2,22	0,23	HBH**	48	Dimer
B9JYM4	Hydroxymuconic semialdehyde hydrolase	*A. vitis*	Proteobacteria	unpublished	55,80	9,00E-09	3LLC	0,56	1,88	0,22	HBH	50	Monomer
Q6PE15	Palmitoyl-protein thioesterase A	*M. musculus*	(Vertrebrate)	[16]	51,60	3,00E-07	6NY9	0,52	1,99	0,20	HBH	51	Monomer
Q83AV9	Alpha/beta hydrolase	*C. burnetii*	Proteobacteria	[17]	47,40	4,00E-06	*3TRD*				*no*		*Monomer*
O30361	Xylan esterase	*T. saccharolyticum*	Firmicutes	unpublished	39,30	0,003	3FCY	0,32	2,11	0,20	HB	43	Trimer
Q65EQ1	Carboxylesterase	*B. licheniformis*	Firmicutes	unpublished	38,50	0,005	6NKG				HB	54	Monomer
Q1QEU6	Triacylglycerol lipase	*P. cryohalolentis*	Proteobacteria	unpublished	37,40	0,014	4NS4	0,36	2,03	0,22	HB	54	Monomer

A0A6I8WFT7	Monoacylglycerol lipase	*P. ferrophilus*	Euryarchaeota	unpublished	34,70	0,1	6QE2				HBH	66	Dimer
B0V9K7	Dienelactone hydrolase	*A. baumannii*	Proteobacteria	unpublished	34,70	0,089	4OPM				HB	70	Dimer
A0A6L8NUA5	Bromoperoxidase	*B. anthracis*	Firmicutes	unpublished	33,50	0,23	3FOB				HB	80	Trimer
P82597	Monoacylglycerol lipase	*Bacillus sp.*	Firmicutes	[18]	32,70	0,41	4KE8*	0,45	2,16	0,21	HBH	51	Dimer
O07427	Monoacylglycerol lipase	*M. tuberculosis*	Actinobacteria	[19]	30,40	2,30	6EIC	0,45	1,86	0,18	HBH	70	Trimer
A0A0B5WSQ6	Lysophospholipase	*B. coagulans*	Firmicutes	[20]	28,90	7,7	5O7G*	0,39	2,13	0,15	HB	88	Monomer
J4WAT9	AB hydrolase-1	*B. bassiana*	Ascomycota	[21]			7D79*	0,49	2,00	0,19	HBH	84	Dimer

A BLAST search using the *Tth* MGL sequence (A0A1I1X7Z7) against UniProtKB restricted to sequences with known 3D structures revealed 106 hits. From this pool of sequences, 15 non-redundant validated targets were selected **(Figure 7A)**. These sequences were further analyzed by structural superposition using the PDBeFold server **[10]**. For ten out of fifteen selected hits, PDBeFold produced a reliable structure-based alignment for both catalytic domain segments (**Supplementary wS2**). In addition, an α/β hydrolase from *Beauveria bassiana* (J4WAT9) was included, which was detected in the PDBeFold search but not in the BLAST search **(Supplementary Table S8)**.

[a] Taken from **Supplementary Table S7.**

[b] Taken from PDBeFold output using the structure of *Tth* MGL as template against the PDB.

[c], *, indicates PDB code cited represents multiple structures deposited in PDB of the same sequence.

[d], for further details see **Figure 7A**; **, indicates a non-canonical HBH lid domain (for further details, see text)

References:

1. Royter, M.; Schmidt, M.; Elend, C.; Hobenreich, H.; Schafer, T.; Bornscheuer, U. T.; Antranikian, G., Thermostable lipases from the extreme thermophilic anaerobic bacteria Thermoanaerobacter thermohydrosulfuricus SOL1 and Caldanaerobacter subterraneus subsp. tengcongensis. *Extremophiles* **2009,** *13* (5), 769-83.

2. Rypniewski, W. R.; Holden, H. M.; Rayment, I., Structural consequences of reductive methylation of lysine residues in hen egg white lysozyme: an X-ray analysis at 1.8-A resolution. *Biochemistry* **1993,** *32* (37), 9851-8.

3. Otwinowski, Z.; Minor, W., Processing of X-ray diffraction data collected in oscillation mode. *Method Enzymol* **1997,** *276*, 307-326.

4. Sheldrick, G. M., A short history of SHELX. *Acta Crystallogr A* **2008,** *64* (Pt 1), 112-22.

5. Terwilliger, T. C.; Grosse-Kunstleve, R. W.; Afonine, P. V.; Moriarty, N. W.; Zwart, P. H.; Hung, L.-W.; Read, R. J.; Adams, P. D., Iterative model building, structure refinement and density modification with the PHENIX AutoBuild wizard. *Acta Crystallographica Section D* **2008,** *64* (1), 61-69.

6. Langer, G.; Cohen, S. X.; Lamzin, V. S.; Perrakis, A., Automated macromolecular model building for X-ray crystallography using ARP/wARP version 7. *Nat Protoc* **2008,** *3* (7), 1171-9.

7. Winn, M. D.; Ballard, C. C.; Cowtan, K. D.; Dodson, E. J.; Emsley, P.; Evans, P. R.; Keegan, R. M.; Krissinel, E. B.; Leslie, A. G.; McCoy, A.; McNicholas, S. J.; Murshudov, G. N.; Pannu, N. S.; Potterton, E. A.; Powell, H. R.; Read, R. J.; Vagin, A.; Wilson, K. S., Overview of the CCP4 suite and current developments. *Acta Crystallogr D Biol Crystallogr* **2011,** *67* (Pt 4), 235-42.

8. Emsley, P.; Cowtan, K., Coot: model-building tools for molecular graphics. *Acta Crystallogr D Biol Crystallogr* **2004,** *60* (Pt 12 Pt 1), 2126-32.

9. Afonine, P. V.; Grosse-Kunstleve, R. W.; Echols, N.; Headd, J. J.; Moriarty, N. W.; Mustyakimov, M.; Terwilliger, T. C.; Urzhumtsev, A.; Zwart, P. H.; Adams, P. D., Towards automated crystallographic structure refinement with phenix.refine. *Acta Crystallogr D Biol Crystallogr* **2012,** *68* (Pt 4), 352-67.

10. Krissinel, E.; Henrick, K., Secondary-structure matching (SSM), a new tool for fast protein structure alignment in three dimensions. *Acta Crystallogr D Biol Crystallogr* **2004,** *60* (Pt 12 Pt 1), 2256-68.

11. Lanéelle, M. A.; Spina, L.; Nigou, J.; Lemassu, A.; Daffé, M., Lipid and Lipoarabinomannan Isolation and Characterization. *Methods Mol Biol* **2021,** *2314*, 109-150.

12. Kotov, V.; Mlynek, G.; Vesper, O.; Pletzer, M.; Wald, J.; Teixeira-Duarte, C. M.; Celia, H.; Garcia-Alai, M.; Nussberger, S.; Buchanan, S. K.; Morais-Cabral, J. H.; Loew, C.; Djinovic-Carugo, K.; Marlovits, T. C., In-depth interrogation of protein thermal unfolding data with MoltenProt. *Protein Sci* **2021,** *30* (1), 201-217.

13. Goldstone, D. C.; Villas-Bôas, S. G.; Till, M.; Kelly, W. J.; Attwood, G. T.; Arcus, V. L., Structural and functional characterization of a promiscuous feruloyl esterase (Est1E) from the rumen bacterium Butyrivibrio proteoclasticus. *Proteins* **2010,** *78* (6), 1457-69.

14. Lai, K. K.; Stogios, P. J.; Vu, C.; Xu, X.; Cui, H.; Molloy, S.; Savchenko, A.; Yakunin, A.; Gonzalez, C. F., An inserted α/β subdomain shapes the catalytic pocket of Lactobacillus johnsonii cinnamoyl esterase. *PLoS One* **2011,** *6* (8), e23269.

15. Jensen, M. V.; Horsfall, L. E.; Wardrope, C.; Togneri, P. D.; Marles-Wright, J.; Rosser, S. J., Characterisation of a New Family of Carboxyl Esterases with an OsmC Domain. *PLoS One* **2016,** *11* (11), e0166128.

16. Cao, Y.; Qiu, T.; Kathayat, R. S.; Azizi, S. A.; Thorne, A. K.; Ahn, D.; Fukata, Y.; Fukata, M.; Rice, P. A.; Dickinson, B. C., ABHD10 is an S-depalmitoylase affecting redox homeostasis through peroxiredoxin-5. *Nat Chem Biol* **2019,** *15* (12), 1232-1240.

17. Franklin, M. C.; Cheung, J.; Rudolph, M. J.; Burshteyn, F.; Cassidy, M.; Gary, E.; Hillerich, B.; Yao, Z. K.; Carlier, P. R.; Totrov, M.; Love, J. D., Structural genomics for drug design against the pathogen Coxiella burnetii. *Proteins* **2015,** *83* (12), 2124-36.

18. Rengachari, S.; Aschauer, P.; Schittmayer, M.; Mayer, N.; Gruber, K.; Breinbauer, R.; Birner-Gruenberger, R.; Dreveny, I.; Oberer, M., Conformational plasticity and ligand binding of bacterial monoacylglycerol lipase. *J Biol Chem* **2013,** *288* (43), 31093-104.

19. Aschauer, P.; Zimmermann, R.; Breinbauer, R.; Pavkov-Keller, T.; Oberer, M., The crystal structure of monoacylglycerol lipase from M. tuberculosis reveals the basis for specific inhibition. *Sci Rep* **2018,** *8* (1), 8948.

20. De Vitis, V.; Nakhnoukh, C.; Pinto, A.; Contente, M. L.; Barbiroli, A.; Milani, M.; Bolognesi, M.; Molinari, F.; Gourlay, L. J.; Romano, D., A stereospecific carboxyl esterase from Bacillus coagulans hosting nonlipase activity within a lipase-like fold. *Febs j* **2018,** *285* (5), 903-914.

21. Gao, D. W.; Jamieson, C. S.; Wang, G.; Yan, Y.; Zhou, J.; Houk, K. N.; Tang, Y., A Polyketide Cyclase That Forms Medium-Ring Lactones. *J Am Chem Soc* **2021,** *143* (1), 80-84.

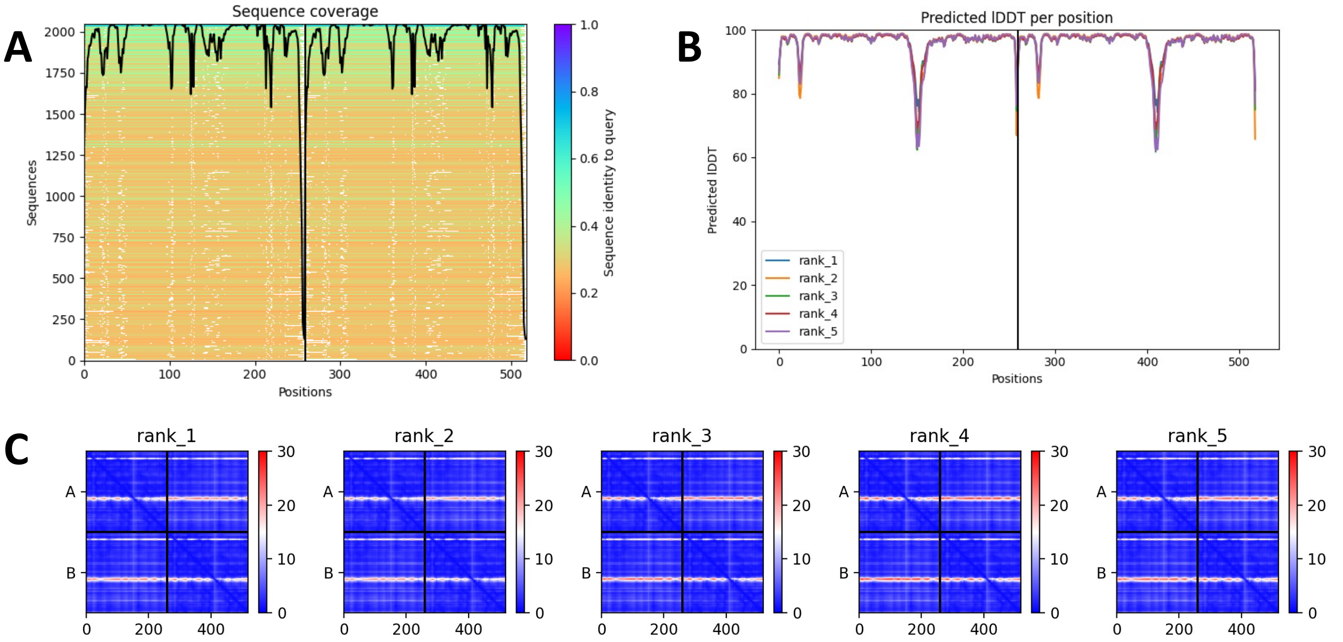

Alpha Fold 2 predicted structures of dimeric *Tth* MGL. The overall root mean square deviations of the five top predicted structures with the experimental *Tth* MGL structures are in the range of 0.4-0.5 Å. The majority of the *Tth* dimer interface specific interactions **(Figure 2C)** are not recovered in the predicted structures. In addition, any information on protein-ligand interactions (**Figure 3**) is missing in the predicted models. The vertical and horizontal lines shown in the plots indicate the border between the first and second sequence chains (A, B) of the predicted models. **A**, Sequence coverage of the predicted models; **B,** Local Distance Difference Test, indicating a major peak within the sequence segment of the *Tth* MGL lid domain; **C,** Distance matrices of the top five ranking models, indicating the highest level of uncertainty at the sequence segment of the *Tth* MGL lid domain.

Supplementary Figure S1

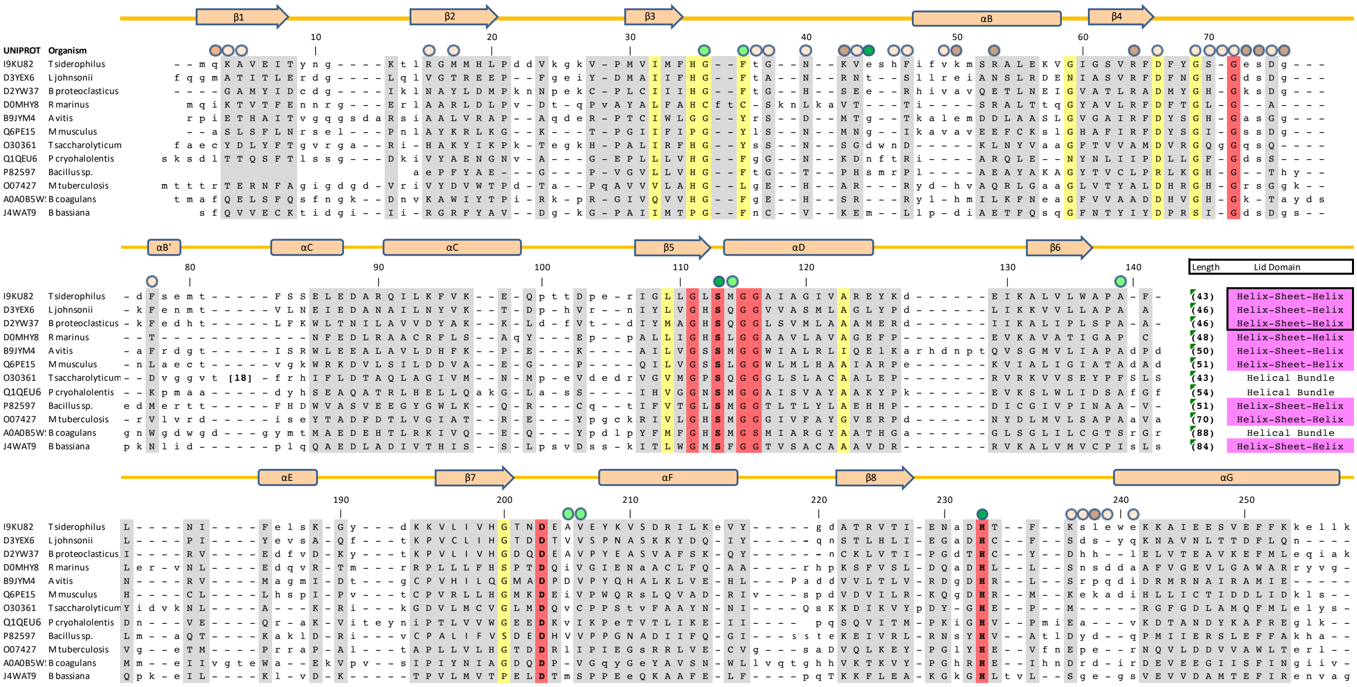
β1
β2
β3
αB
β4
αB'
αC
αC
β5
αD
β6
αE
β7
αF
β8
αG
UNIPROT
Organism
I9KU82 T siderophilus
D3YEX6 L johnsonii
D2YW37 B proteoclasticus
D0MHY8 R marinus
B9JYM4 A vitis
Q6PE15 M musculus
O30361 T saccharolyticum
Q1QEU6 P cryohalolentis
P82597 Bacillus sp.
O07427 M tuberculosis
A0A0B5W! B coagulans
J4WAT9 B bassiana
Length
Lid Domain
(43) Helix-Sheet-Helix
(46) Helix-Sheet-Helix
(46) Helix-Sheet-Helix
(48) Helix-Sheet-Helix
(50) Helix-Sheet-Helix
(51) Helix-Sheet-Helix
(43) Helical Bundle
(54) Helical Bundle
(51) Helix-Sheet-Helix
(70) Helix-Sheet-Helix
(88) Helical Bundle
(84) Helix-Sheet-Helix

Alignment of 12 CD sequences, for which an overall structure-based alignment was possible. UNIPROT codes and organisms of aligned sequences are indicated to the left. Structurally aligned residues are shown in capital letters and respective aligned positions are shaded in grey; other residues are in small letters. As a structure-based alignment of the lid domain segment, inserted into the N-terminal and C-terminal part of each CD sequence, was not possible due to high level of sequence and structural diversity, instead the length and type of lid domains of all chosen esterase/lipases are indicated. HBH-type lid domains with structural relations to the *Tth* MGL lid domain are colored in magenta. Sequence numbers indicated in 10-residues intervals on top of the alignment refer to the *Tth* MGL sequence. Helices and β-strands, indicated by cylinders and arrows, respectively, are taken from the *Tth* MGL coordinates. The coloring codes of these secondary structural elements are as in **Figure 2**. Long insertions of single sequences are shown by numbers, indicating the length of the inserted sequence. Conserved residue positions are highlighted in red (invariant) or yellow (highly conserved). Residues involved in ligand interactions (glycerol, C18 mono-acyl) in the *Tth* MGL structure without PMSF are indicated by green circles on top of the alignment: hydrogen bond interactions, dark green; other interactions, light green. Residues involved in *Tth* MGL dimer interactions are indicated by orange circles: hydrogen bond interactions, dark orange; other interactions, light orange.

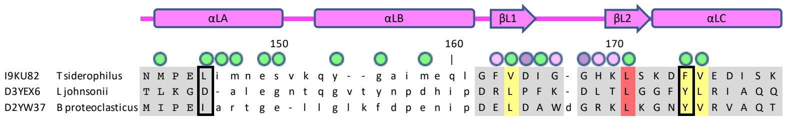
αLA
αLB
βL1
βL2
αLC
150
160
170
I9KU82 T siderophilus
D3YEX6 L johnsonii
D2YW37 B proteoclasticus

Alignment of the HBH lid domains of three two sequences closely related to *Tth* MGL, for which a structure-based alignment was possible. The color codes are as for panel A, except residues involved into lid domain dimer interface interactions are highlighted with magenta circles according to the color codes from **Figure 2** on top of the alignment. Residues with changed properties for active site ligand binding are boxed.

Supplementary Figure S2

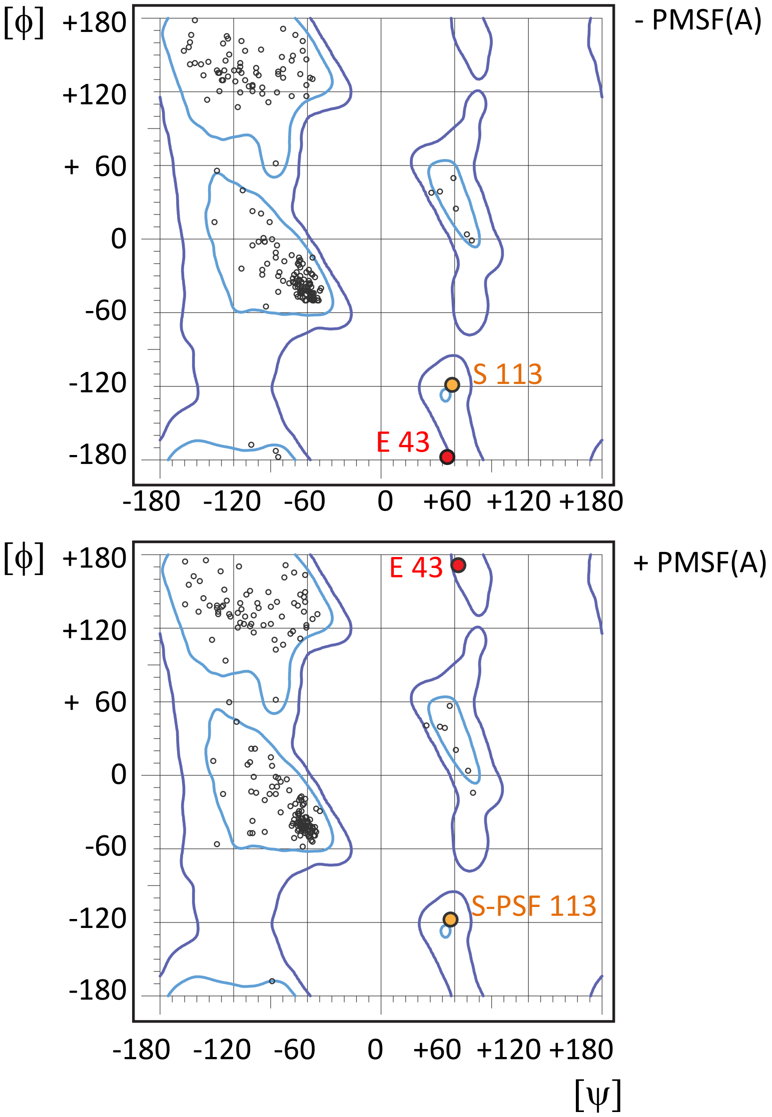

Ramachandran plot of *Tth* MGL structures, in the absence and presence of PMSF. In both structures, Glu43 and Ser113 have unusual dihedral angles, due to functional reasons (for details, see text).

Supplementary Figure S3

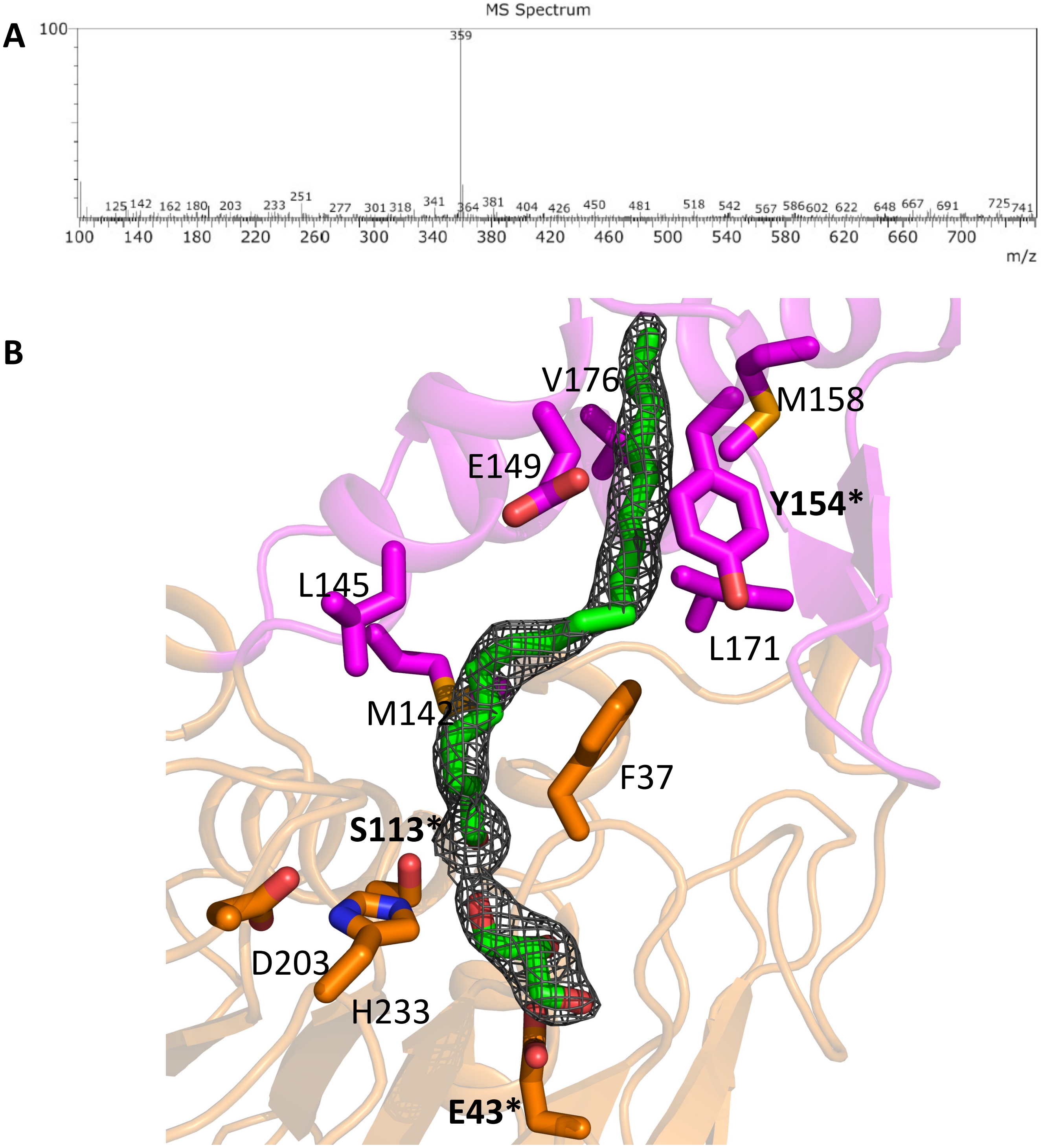

Evidence for the presence of active site-bound C18 monoacylester intermediate and glycerol in the *Tth* MGL structure without PMSF. A, Reverse phase chromatography analysis of bound ligands in *Tth* MGL crystals in the absence of PMSF**. B,** *2Fo-Fc* omit electron density map at 1 σ contour level. *Tth* MGL residues that are involved in binding to C18 monoacylester intermediate and glycerol are shown and labeled (*cf*. **Figure 3A**).

Supplementary Figure S4

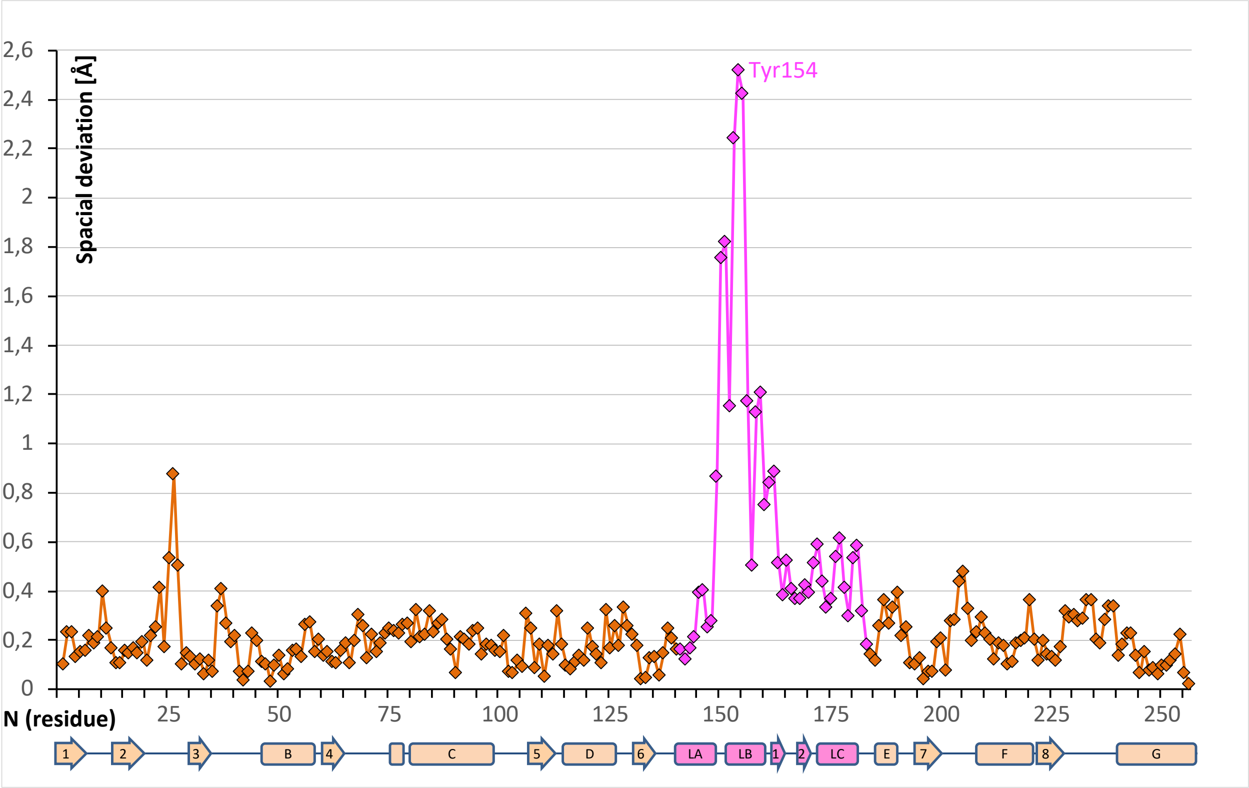

Dynamic substrate tunnel opening in the *Tth* MGL lid domain (*cf*. **Figure 3D-E**). Spatial differences of the Cα positions of the *Tth* MGL structures, with and without PMSF. Color codes are as in **Figure 2.** The approximate positions of secondary structural elements are indicated **(Figure 2A, Supplementary Figure S2)**. The comparison indicates peak movements of lid domain residues next to the tunnel opener Tyr154.

Supplementary Figure S5

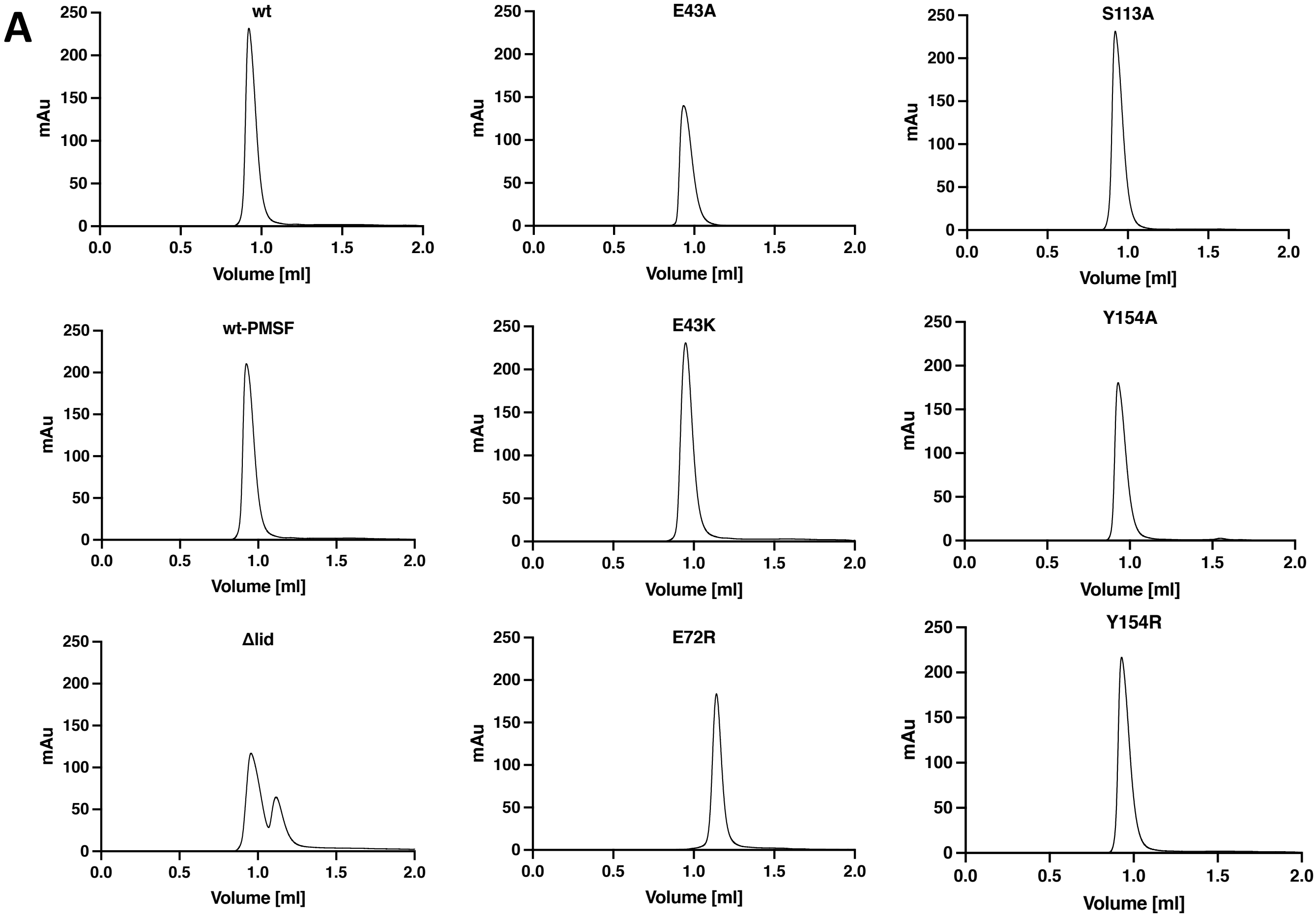

Analytic SEC profiles of all *Tth* MGL variants investigated. The respective elution profiles – except the ΔLid and E72R mutants – were interpreted as showing a dimeric state of the enzyme.

Supplementary Figure S6

A

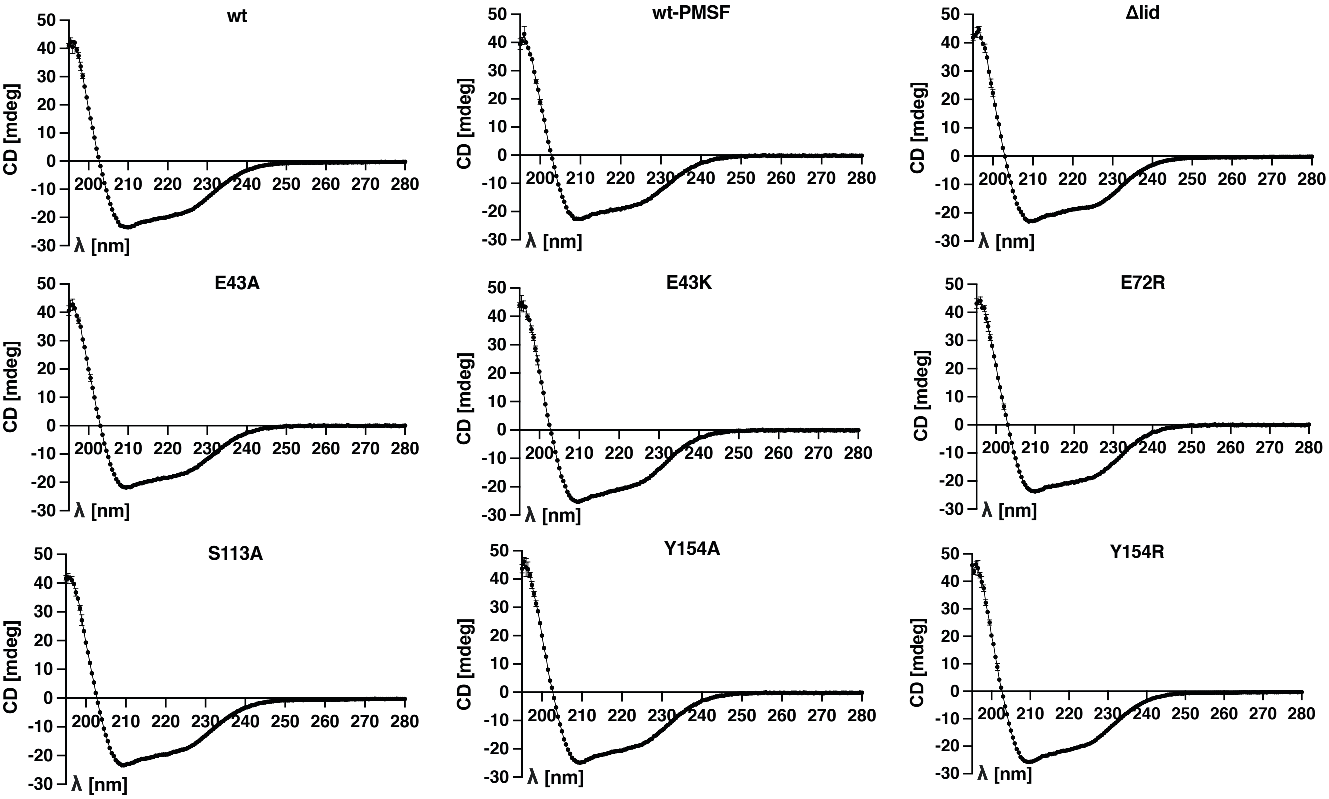

CD spectra for all MGL *Tth* variants investigated, showing no significant deviations from wt *Tth* MGL.

Supplementary Figure S7

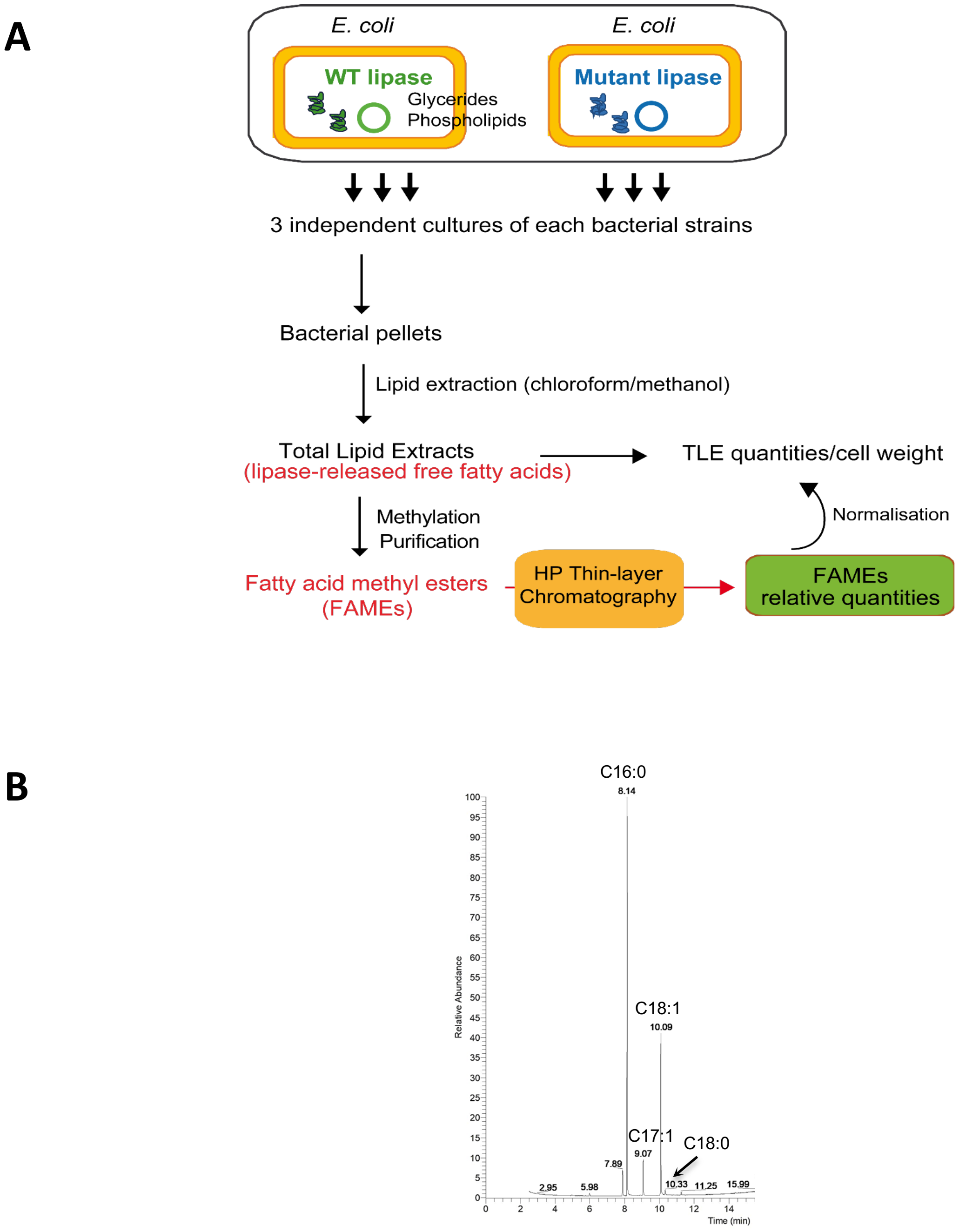
A
E. coli
E. coli
WT lipase
Glycerides
Phospholipids
Mutant lipase
3 independent cultures of each bacterial strains
Bacterial pellets
Lipid extraction (chloroform/methanol)
Total Lipid Extracts
(lipase-released free fatty acids)
TLE quantities/cell weight
Methylation
Purification
Normalisation
Fatty acid methyl esters
(FAMEs)
HP Thin-layer
Chromatography
FAMEs
relative quantities
B
C16:0
8.14
C18:1
10.09
C17:1
9.07
C18:0
7.89
2.95
5.98
10.33
11.25
15.99
Relative Abundance
Time (min)
0
2
4
6
8
10
12
14
0
5
10
15
20
25
30
35
40
45
50
55
60
65
70
75
80
85
90
95
100

A, Schematic workflow of sample preparation and lipid cell-based data analysis. *E. coli* cultures were transformed with *Tth* MGL variants, induced with IPTG for 60 min. Bacterial pellets were used to prepare total lipid extracts (TLE) following CHCl3/CH3OH extraction). Lipid extracts were methylated to yield Fatty Acid Methyl Esters (FAMEs), further purified though florisil columns and the resulting enriched FAMEs were analyzed by high-pressure thin-layer chromatography (HPTLC) and quantified. Plate visualization was realized using primuline dye and scanning. Fluorescence associated with FAME bands was quantified, and normalization to TLE and bacterial mass was performed to correct for variations across samples. **B,** representative gas chromatogram used for FAME analysis.

Supplementary Figure S8

A

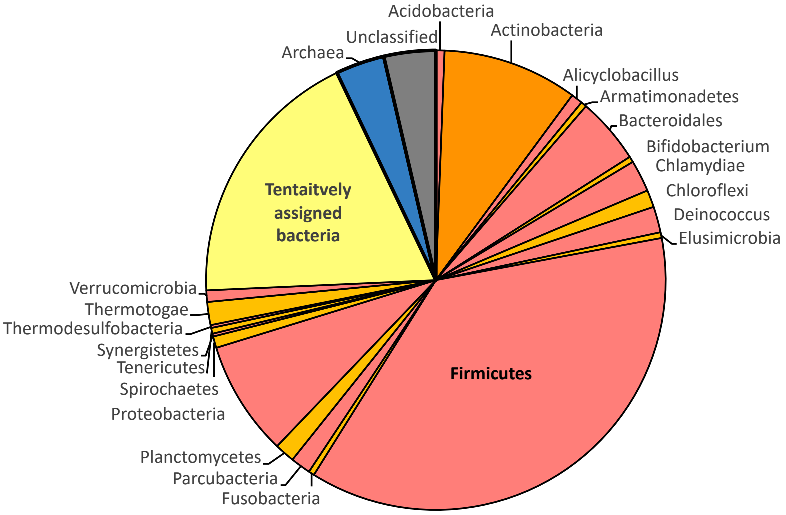

Taxonomic analysis of most closely related 496 sequence groups as defined in UniprotKB50, indicating that all related sequences (to the extent unambiguously assigned) are either of bacterial or archaeal origin. The statistics for different bacterial phyla are shown in alphabetic order and in alternating colors (red, orange). Statistics of unclassified or tentatively assigned bacterial sequences are shown in yellow, archaeal sequences in blue, and unclassified sequences are in grey. The complete list of sequence groups is in **Supplementary Table S7.**

B

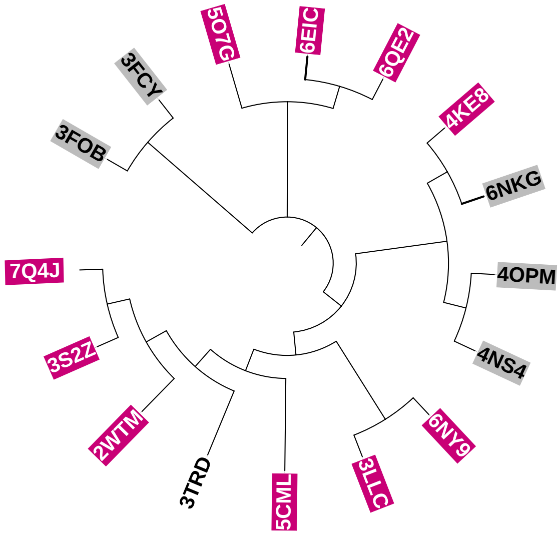

Phylogenetic tree presentation of sequences with known 3D structures and distant relations to *Tth* MGL, indicating the respective PDB ID codes (*cf*. **Supplementary Table S8**). Sequences containing a HBH lid domain are highlighted in pink **(*cf.* Figure 7),** other sequences with helical lid domains are in grey. The precise phylogenetic distances are not reliable because of only distant relations and hence have no meaning in this presentation. Conditions for target selection: a) presence of a complete α/β hydrolase catalytic triad (Ser113, Asp203, His233 in the *Tth* MGL sequence) to discard any false-positive hits with unrelated function, b) coverage of both the N-terminal and C-terminal segments of the *Tth* MGL domain with the lid domain inserted in the resulting pairwise sequence alignments.

Supplementary Figure S9

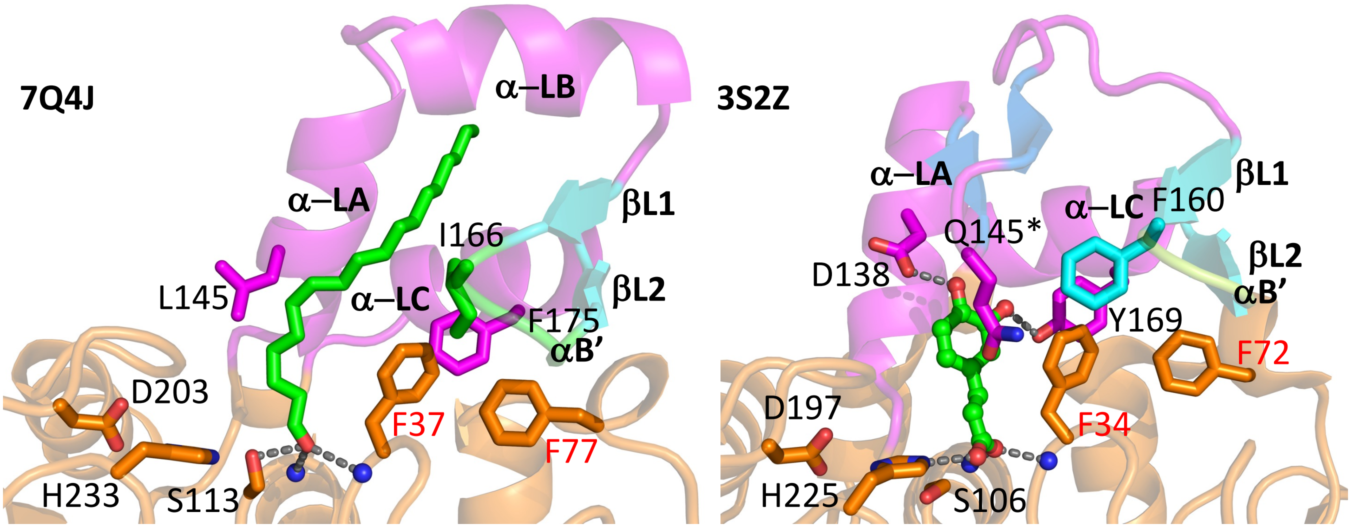
7Q4J
α–LB
α–LA
βL1
I166
L145
α–LC
βL2
F175
αB’
D203
F37
F77
H233
S113
3S2Z
βL1
α–LA
α–LC
F160
Q145*
βL2
D138
αB’
Y169
F72
D197
F34
H225
S106

Structural comparison of the ligand bound HBH lid domains and active site area for *Tth* MGL in the presence of C18 monoacyl (left) and the esterase from *L. johnsonii* (PDB code: 3S2Z) in the presence of ferulate (right), indicating different substrate specificities. Two residues critical for specific hydrogen bond interactions with ferulate in structure of the esterase from *L. johnsonii* (Asp138, Tyr169) are substituted by hydrophobic residues in *Tth* MGL (equivalent residues Leu145, Phe175). Other key residues with critical roles for substrate binding are also shown. In the structure of the esterase from *L. johnsonii,* an additional N-terminal lid β-sheet is formed (colored in blue) that hovers over the CD active site. At the end of the short turn connecting the two β-strands, there is a highly exposed residue, which is Gln145 in this structure. Residues that are part of the conserved HGF motif (residues 35-37 in *Tth* MGL, residues 32-34 in the *L. johnsonii esterase*) and less conserved FSE/D motif (residues 77-79 in *Tth* MGL, residues 70-72 in in the *L. johnsonii esterase*) are labeled in red **(Supplementary Figure S2).**

Supplementary Figure S10